UNIVERSIDADE ESTADUAL DE CAMPINAS

FACULDADE DE ENGENHARIA MECÂNICA

E INSTITUTO DE GEOCIÊNCIAS

ISABELA MAGALHÃES DE OLIVEIRA

WELL REPRESENTATION IN SIMULATION MODELS OF NATURALLY FRACTURED RESERVOIRS CONSIDERING THE IMPACT OF DFN UPSCALING

REPRESENTAÇÃO DE POÇOS EM MODELOS DE SIMULAÇÃO DE RESERVATÓRIOS NATURALMENTE FRATURADOS CONSIDERANDO O IMPACTO DA TRASFERÊNCIA DE ESCALA DE UMA REDE DISCRETA DE FRATURAS

CAMPINAS

[2021]

ISABELA MAGALHÃES DE OLIVEIRA

WELL REPRESENTATION IN SIMULATION MODELS OF NATURALLY FRACTURED RESERVOIRS CONSIDERING THE IMPACT OF DFN UPSCALING
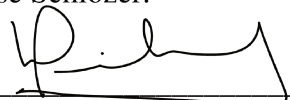
REPRESENTAÇÃO DE POÇOS EM MODELOS DE SIMULAÇÃO DE RESERVATÓRIOS NATURALMENTE FRATURADOS CONSIDERANDO O IMPACTO DA TRASFERÊNCIA DE ESCALA DE UMA REDE DISCRETA DE FRATURAS

Dissertation presented to the Mechanical Engineering Faculty and Geosciences Institute of the University of Campinas in partial fulfillment of the requirements for the degree of Master's in Petroleum Sciences and Engineering in the area of Reservoir and Management.

Dissertação de Mestrado apresentada à Faculdade de Engenharia Mecânica e Instituto de Geociências da Universidade Estadual de Campinas como parte dos requisitos exigidos para obtenção do título de Mestra em Ciências e Engenharia de Petróleo, na área de Reservatórios e Gestão.

Orientador: Prof. Dr. Denis José Schiozer

Este exemplar corresponde à versão final da Dissertação defendida pelo aluno Isabela Magalhães de Oliveira e orientada pelo Prof. Dr. Denis José Schiozer.

_____
Assinatura do Orientador

CAMPINAS

[2021]

Ficha catalográfica
Universidade Estadual de Campinas
Biblioteca da Área de Engenharia e Arquitetura
Rose Meire da Silva - CRB 8/5974

OL4w

Oliveira, Isabela Magalhães de, 1994-
Well representation in simulation models of naturally fractured reservoirs considering the impact of DFN upscaling / Isabela Magalhães de Oliveira. – Campinas, SP : [s.n.], 2021.

Orientador: Denis José Schiozer.
Dissertação (mestrado) – Universidade Estadual de Campinas, Faculdade de Engenharia Mecânica.
Em regime multiunidades com: Instituto de Geociências.

1. Reservatórios de petróleo. 2. Reservatórios de petróleo. 3. Métodos de simulação. 4. Reservatórios. 5. Engenharia do petróleo. 6. Reservatórios (Simulação). I. Schiozer, Denis José, 1963-. II. Universidade Estadual de Campinas. Faculdade de Engenharia Mecânica. III. Título.

Informações para Biblioteca Digital

Título em outro idioma: Representação de poços em modelos de simulação de reservatórios naturalmente fraturados considerando o impacto da transferência de escala de uma rede discreta de fraturas
Palavras-chave em inglês:
Petroleum Reservoirs
Reservoirs – Fracture
Simulation methods
Reservoirs
Petroleum engineering
Reservoirs (Simulation)
Área de concentração: Reservatórios e Gestão
Titulação: Mestra em Ciências e Engenharia de Petróleo
Banca examinadora:
Denis José Schiozer [Orientador]
Frances Vivien Abbots Guardiola
Manuel Gomes Correia
Data de defesa: 24-02-2021
Programa de Pós-Graduação: Ciências e Engenharia de Petróleo

Identificação e informações acadêmicas do(a) aluno(a)

- ORCID do autor: https://orcid.org/0000-0002-1295-3509
- Currículo Lattes do autor: http://lattes.cnpq.br/5441933646450558

UNIVERSIDADE ESTADUAL DE CAMPINAS

FACULDADE DE ENGENHARIA MECÂNICA

E INSTITUTO DE GEOCIÊNCIAS

DISSERTAÇÃO DE MESTRADO ACADÊMICO

WELL REPRESENTATION IN SIMULATION MODELS OF NATURALLY FRACTURED RESERVOIRS CONSIDERING THE IMPACT OF DFN UPSCALING

REPRESENTAÇÃO DE POÇOS EM MODELOS DE SIMULAÇÃO DE RESERVATÓRIOS NATURALMENTE FRATURADOS CONSIDERANDO O IMPACTO DA TRASFERÊNCIA DE ESCALA DE UMA REDE DISCRETA DE FRATURAS

Autor: Isabela Magalhães de Oliveira
Orientador: Prof. Dr. Denis José Schiozer

A Banca Examinadora composta pelos membros abaixo aprovou esta Dissertação:

Prof. Dr. Denis José Schiozer, Presidente
FEM - Unicamp

Dr. Manuel Gomes Correia
FEM/Cepetro - Unicamp

Dra. Frances Vivien Abbots Guardiola
Technology Manager (Carbonate IOR R&D Program) - Shell Brasil

A ata dessa defesa com as respectivas assinaturas dos membros encontra-se no processo de vida acadêmica do aluno.

Campinas, 24 de fevereiro de 2021.

DEDICATION

I dedicate this dissertation to my precious family and to God my lovely Father.

(Eu dedico esta dissertação à minha preciosa família e a Deus meu Pai Amado).

ACKNOWLEDGEMENTS

Portuguese version

Em primeiro lugar, sou grata a Deus, que me inspirou o desejo de fazer este mestrado e que providenciou tudo o que era necessário para eu finalizar este trabalho.

Gostaria de agradecer aos meus pais, Janine e Geraldo, e ao meu irmão Arthur Magalhães, os quais tem me apoiado nas minhas decisões profissionais. Às minhas famílias Honório e Magalhães, eu jamais esquecerei a ajuda e o apoio que me deram durante esses anos. Amo todos vocês.

Ao meu amado noivo, Arthur Pastore, que dedicou tanto tempo e atenção em cada momento que eu precisava. Gostaria também de agradecer a família Lima por todo apoio e carinho que me deram nesse tempo.

Ao meu orientador, Dr. Denis Schiozer, pela atenção, apoio e paciência. Eu pude aprender muito e fico muito grata pela assistência e pela oportunidade que recebi.

Ao grupo UNISIM, em especial aos pesquisadores Dr. Gonçalo Oliveira, Dr. Célio Maschio, Dr. Manuel Correia e Dr. Alexandre de Lima que deram uma contribuição significativa para este trabalho. Aos funcionários de administração e tecnologia Guilherme Tonin, Paulo Soares, Daniel Carvalho e Thiago Feliciano. Aos meus amigos do DEP e do projeto SIMFRAC, especialmente Alice, Obata, Letícia Sirqueira, Henrique Treptow, Geltom Junior, Fernanda Gois, Vinicius Casanova e Kelly Quispe.

Aos meus irmãos e irmãs do Grupo de Oração Universitário (GOU) Beraká e da Pastoral Universitária. É lindo de observar como me ajudaram a conciliar a fé e a razão durante esse mestrado. Gratidão.

Aos meus amigos em Aracaju e no Movimento Escalada, por todas as orações e apoio.

Agradeço também a Shell por esta oportunidade de pesquisa e pelas valiosas contribuições. Eu gostaria de citar Dra. Frances Abbots, que me ajudou no projeto SIMFRAC com muita atenção e carinho.

Por fim, gostaria de agradecer à Energi Simulation e à CAPES pelo apoio financeiro. Este estudo foi financiado em parte pela Coordenação de Aperfeiçoamento de Pessoal de Nível Superior - Brasil (CAPES) - Código de Financiamento 001 (88882.434988/2019-01). Também sou grata à Schlumberger e ao CMG pelas licenças de software e suporte técnico.

"Behold, I am the handmaid of the Lord; let it be to me according to your word."

"Eis aqui a serva do Senhor, faça-se em mim segundo a vossa palavra."

Luke 1:38

RESUMO

O estudo de reservatórios naturalmente fraturados (*naturally fractured reservoirs* – NFR) é complexo e revela muitos desafios na modelagem e simulação de reservatórios, incentivando o uso de técnicas não convencionais. O uso da transferência de escala de Rede de Fraturas Discretas (*discrete fractured network* – DFN) para construir modelos de simulação de dupla permeabilidade (DK) tem sido um dos processos aplicados. Os principais objetivos deste trabalho são (1) estudar o impacto dos métodos de transferência de escala de DFN em novos poços alocados no modelo e (2) desenvolver uma proposta de representação de poços em modelos de simulação de NFR. Três métodos de transferência de escala em três modelos de fidelidade (alta, média-alta e média) e o conceito de Unidade Característica de Fluxo (*characteristic flow unit* – CFU) foram utilizados. Os métodos de transferência de escala aplicados foram Oda, Oda corrigido e numérico com quatro condições de contorno. O trabalho possuiu três etapas principais: (1) avaliar as diferenças nos parâmetros estáticos e dinâmicos do poço ao alterar o método de transferência de escala e a escala de fidelidade, (2) testar metodologias de calibração de poço em uma malha de média fidelidade, considerando as conclusões dos resultados anteriores e (3) testar diferentes métodos de transferência de escala em uma escala de campo para avaliar o impacto na previsão de produção do campo. Os principais resultados para a primeira etapa sugeriram maior variabilidade dos dados dinâmicos na escala de média fidelidade e teve o método de Oda como o mais sensível à mudança de escala de dimensão de bloco. Já a combinação da escala de alta fidelidade com o método numérico (pressão linear) forneceu uma menor variabilidade na taxa de fluxo e BHP dos poços, o que levou ao uso deste modelo como o caso de referência para os testes da segunda etapa. Dentre as metodologias testadas na segunda etapa, a calibração dos poços foi obtida com a substituição do índice de poço (*well index* – WI) nos sistemas de matriz e fratura pelo WI do modelo de referência. Os testes em escala de campo mostraram impacto significativo do método de transferência de escala de DFN no curto tempo de previsão de produção, e diminuiu o impacto ao longo do tempo. Os resultados mostram que as fases de desenvolvimento e gerenciamento do reservatório podem ser significativamente afetadas se as incertezas causadas pelos métodos de transferência de escala de DFN não forem consideradas ao se alocar novos poços em modelos DK. A proposta de representação de poço deste trabalho, a qual utiliza um WI baseado no método numérico, mostrou resultados promissores para reduzir o impacto dos métodos de transferência de escala de DFN na previsão de produção e injeção de poços em modelos de média fidelidade. Este trabalho apresenta um estudo de possível representação de poço para modelos de simulação de reservatórios naturalmente fraturados, proporcionando, para casos de campos reais, uma melhor representação da previsão de produção e injeção relacionada a inclusão de falhas e fraturas através de métodos de transferência de escala de DFNs.

Palavras-Chave: modelo de poço, transferência de escala de DFN, dimensão de malha, reservatórios naturalmente fraturados, índice de poço, modelos de simulação de dupla permeabilidade, CFU

ABSTRACT

The study of naturally fractured reservoirs (NFR) is complex and has many challenges in reservoir modeling and simulation, requiring non-conventional techniques. The use of Discrete Fracture Networks (DFN) to build dual permeability (DK) simulation models has been one of the processes applied. The main objectives of this work are (1) to evaluate the impact of DFN upscaling methods on new wells placed in the model and (2) develop a proposal for well-representation for new wells in simulation models of NFR. Three DFN permeability-upscaling methods at three model fidelities (high, medium-high, and medium fidelity) and the concept of Characteristic Flow Unit (CFU) were used. The upscaling methods applied were the Oda, Oda Corrected and Flow-based with four boundary conditions. The work was focused in three main steps: (1) to observe the differences in static and dynamic well parameters when changing the upscaling method and fidelity scales; (2) to test well calibration methodologies in a coarse grid by considering the previous step conclusions, and (3) to test the different DFN upscaling methods at a field scale to evaluate the impact on predicted field production. The main results for the first step suggested more uncertainty of well dynamic data in medium fidelity models and showed that the Oda method is the most sensitive to the grid-block scale change. Otherwise, combining the high-fidelity scale with the flow-based upscaling (linear pressure) tended to provide less variation in well flow rate and BHP, which led to the use of this model as the reference case for the second step analysis. Among the tested methodologies, the producer and injector well calibration was achieved with the substitution of their well index (WI) in the matrix and fracture systems by the reference model's WI. The field scale application showed a significant impact of the DFN upscaling method in the short-term production forecast, decreasing in impact as the production time increases. The results show that if the DFN permeability upscaling method variabilities are not considered when placing new wells in DK models, the reservoir development and management phase can be significantly affected. The proposed well representation utilizing a WI based on the flow-based method showed promising results to reduce the impact of DFN upscaling methods in the well's production and injection forecast for medium-fidelity models. This work presents an investigation of a possible well-representation approach for simulation models of naturally fractured reservoirs, providing for real field cases a better representation of injection and production forecast related to fault and fracture inclusion, when utilizing DFN permeability-upscaling methods.

Key Words: well model; DFN upscaling; grid block size; naturally fractured reservoirs; well index; dual permeability simulation models; CFU.

LIST OF FIGURES

LIST OF TABLES

NOMENCLATURE

2D	Two dimension
3D	Three dimension
b	Fracture aperture
ANP	Agência Nacional de Petróleo
bbl	Barrels
BHI	Bottom Hole Images
BHP	Bottom Hole Pressure
boe/d	Barrel of oil equivalent per day
CFU	Characteristic Flow Unit
CP	Constant Pressure boundary condition
D	Fracture Spacing
DFM	Discrete Fracture and Matrix
DFN	Discrete Fracture Network
DK	Dual-permeability model
DP	Dual-porosity model
eCI	Extended Connectivity Index
EDFM	Embedded Discrete Fracture Modeling
FB	Flow based method
F^{mf}	Transmissibility factor
FZI	Flow Zone Indexes
HFM	High-Fidelity Model
IBPOS	Image Based Periodic Object Simulation
K_f	Fracture Permeability
Ki	Fracture Permeability (X direction)
Ky	Fracture Permeability (Y direction)
Kz	Fracture Permeability (Z direction)
LFM	Low Fidelity Model
LGR	Local Grid Refinement
LP	Linear Pressure boundary condition
MFM	Medium Fidelity Model
MHFM	Medium-High Fidelity Model
MINC	Multiple Interacting Continua

NF	No Flow boundary condition
NFR	Naturally Fractured Reservoir
ODAC	Oda Corrected method
P32	fracture density (m^{-1})
P_{block}	Well block pressure
PD	Periodic boundary condition
PI	Productivity or Injectivity Index
PLT	Production Logging Tools
PTA	Pressure Transient Analysis
PVT	Pressure, Volume, Temperature
q	Flow Rate
RD	Relative Difference
r_e	Effective radius
RFT	Repeat Formation Testers
RRT	Reservoir Rock Type
SP	Single-porosity model
STW	Surface Water Rate
wfrac	well fraction
WI	Well Index
σ	sigma factor
K	Absolute Permeability

TABLE OF CONTENTS

1 INTRODUCTION

Naturally Fractured Reservoirs (NFR) are those which the natural fractures cause a positive or negative impact on the reservoir flow by increasing the reservoir permeability, porosity, or anisotropy (Lima, 2013; Nelson, 2001). NFRs are usually divided into four types, and the type definition is a challenge due to the difficult characterization of the multiscale heterogeneities (Nelson, 2001). However, despite the challenges, NFRs have been an investment target of the petroleum industry as half of the worldwide petroleum reserves are concentrated in carbonate reservoirs, and most of them are naturally fractured (Ahmed-Elfeel and Geiger, 2012; Correia, 2014).

The occurrence of multiscale heterogeneities in NFRs, as faults, fractures, vugs, and karsts, cause a significant challenge in NFR modeling and simulation due to the presence of geological uncertainties and scale variation (Amiry, 2014; Cazarin, 2015). Consequently, the conventional modeling and simulation techniques are not always suitable to perform reliable reservoir flow predictions. For example, for an NFR type three of which "fractures assist permeability in an already producible reservoir" (Nelson, 2001), the flow inside the matrix and fracture systems should be considered, and single-porosity simulation models are limited for this application. Deterministic fracture modeling, for instance, it is not ideal in reservoirs with significant uncertainties of fracture aperture, density, direction, or permeability (Nelson, 2001).

Considering these conventional modeling and simulation limitations, the need for non-conventional techniques has increased. The use of Discrete Fracture Networks (DFN) to build dual-permeability (DK) simulation models have been some of these non-conventional methodologies. DFN upscaling and DK models can also be associated with probabilistic approaches to incorporate the NFR uncertainties and provide a more reliable production forecast. However, probabilistic approaches usually demand fast medium-fidelity simulation models (the recommended scale for simulation studies), and it is difficult to represent the multiscale heterogeneities in this scale, demanding efficient upscaling processes.

The DFN porosity upscaling is volumetric, and the permeability upscaling is calculated through different methods. The usual DFN permeability upscaling methodologies available in commercial software are the Oda (1985) and the Flow-based (FB) method. The Oda method is broadly used due to its fast processing, but it is not accurate for non-connected and non-dense fracture networks (Pires, 2016). On the other hand, the Flow-based method is considered more precise as it considers the connectivity of fractures; however, it has the limitation of being

boundary condition sensitive and time-demanding (Correia, 2014). Moreover, the software Petrel has proposed the Oda corrected method, which aims "to be as close as possible to Flow-based permeability upscaling method, but faster and taking into account the whole fracture network" (Schlumberger, 2018).

Despite the variability of DFN permeability upscaling methods, some limitations are reported in the literature. Two main issues are the variability of the permeability results when changing the method, making it difficult to find an adequate upscaling method for a specific case, and the dependency of each method on the grid-scale, changing the outcome according to the grid cell dimension (Ahmed-Elfeel and Geiger, 2012; Decroux, 2012).

These two limitations make the well study in DK models of NFR more complex, as not only the geological matrix uncertainties are present during modeling and simulation. As mentioned, fractured uncertainties can arise from the characterization phase, the DFN upscaling method, and the grid-scale. Consequently, the well model is affected by these uncertainties as it depends on the fracture permeability and fidelity scale of the well block. These two variables are included in the well model by the well-index (WI) parameter, a geometric factor responsible to connect the reservoir's heterogeneities to the well model (Ribeiro, 2010). Thus, erroneous fracture parameters included in the WI after the DFN upscaling may impact the estimation of well flow rate and bottom hole pressure (BHP) during the production forecast, increasing the necessity of a well calibration process.

The WI depends on the effective well radius (r_e), and different equations of r_e have been proposed by the literature, specifying a variety of well models. The objective of those models is to find a correlation so that the high-pressure gradient in the wellbore does not jeopardize the calibration of the simulated well flow rate and BHP with the history data. As example, there is the Peaceman's (1983) proposal, commonly used in commercial software simulators (Ribeiro, 2010). An important highlight of these works is that by modifying the geometric part of the well model, a calibration of the dynamic data can be achieved.

Another methodology used in well calibration is the Local Grid Refinement (LGR) technique. Even if it increases the simulation time and requires more computational effort, some works have been reported success in the well dynamic data calibration as the pressure gradient close to the wellbore is better represented, making the radial flow more precisely simulated (Panja et al., 2013; Correia et al., 2018).

1.1   Motivation

The study of wells in NFR simulation models constructed with DFN upscaling methods is relevant to ensure a correct calculation of productivity data. Sanjombi (2004) emphasizes that during an upscaling process it is necessary to do a special treatment in the well blocks as these blocks cause a direct impact in the simulation results. Furthermore, Correia et al. (2012) concluded that erroneous well index values can be yielded if the near-well region is not considered in the DFN upscaling analysis.

The DFN upscaling can be a useful tool in the study of NFR. However, its uncertainties can cause a significant impact on wells Productivity Index (PI), as the well index is dependent on fracture system properties. Additionally, even if LGR has been an approach used in wells calibration, applying the DFN upscaling in high fidelity models does not necessarily provide the most precise results (Decroux, 2012).

A variety of authors have been searching about the DFN upscaling dependency on grid scale and on different methodologies (Wang et al., 2008; Ahmed-Elfeel and Geiger, 2012; Correia et al., 2012; Decroux, 2012; Tueckmantel et al., 2013; Pires, 2016; Haridy et al., 2019), by showing how the fracture effective permeability and the reservoir flux and pressure can change through the tests. Nevertheless, a deeper understanding about the DFN upscaling impact on the well behavior is not described.

The narrow understanding of how the well productivity and injectivity are affected by the DFN upscaling method can cause a negative impact on the reservoir development phase, since the production and injection forecast of new wells is exclusively dependent on well's location heterogeneities. If faults and fractures are not properly included in an NFR simulation model through the DFN upscaling, and no production data is available to perform a calibration process, the reservoir development phase uncertainty is increased as the new wells productivity can have an erroneous value. Hence, as mentioned by Decroux (2012): "even if a very accurate geological model has been built, the estimation of the recovery factor for a given production scenario can be wrong if the effective properties are improperly calculated."

1.2   Objectives

The main objectives of this work are (1) the evaluation of the impact of DFN upscaling methods on new wells and (2) the development of a methodology to improve the representation of new wells in simulation models of naturally fractured reservoirs.

Four specific objectives will guide the fulfillment of the two main objectives:

1) Methodology to detect the fidelity scales which are the least and the most impacted by the variation of the DFN upscaling method utilizing a synthetic case;

2) Methodology to detect the DFN upscaling methods which cause the lower and higher variability in well flow rate and BHP through different grid scales utilizing a synthetic case;

3) Propose a methodology to reduce the variability of wells flow rates and BHP related to the impact of DFN upscaling methods by providing a well representation proposal for new wells in medium fidelity models, utilizing a synthetic case;

4) Evaluate the impact that the DFN upscaling methods cause in a NFR field production for a medium-fidelity model.

1.3 Organization

This work is organized into seven chapters. Chapter 1 focuses on an overview of NFR dual-continuum models and its implications on well behavior study when using DFN upscaling methods, besides this work motivation and objectives. Chapter 2 has the theoretical background necessary to understand the proposed methodology and the discussed results. Chapter 3 covers a literature review about DFN upscaling techniques and well calibration in simulation models of NFR, showing how the present work is included in the current studies about these topics. Chapter 4 presents the proposed general and specific methodology to achieve these work objectives and the case study adopted for the methodology application. Chapter 5 has the main results and discussion of all methodology topics such as the well calibration tests and the well representation proposal for new wells in medium-fidelity models, besides the NFR field scale application. Finally, chapter 6 has the main conclusions and future work suggestions.

2   THERORETICAL BACKGROUND

This chapter provides the necessary theoretical background for the comprehension of this work development, covering concepts about Naturally Fractured Reservoirs (NFR), NFR modeling and simulation approaches, and well models.

2.1   Naturally Fractured Reservoirs (NFR)

The definition of a naturally fractured reservoir is not limited to a reservoir with natural fractures. Defining an NFR implies that the existing fractures cause a positive or negative impact on the reservoir flow by increasing the reservoir permeability, porosity, or anisotropy (Lima, 2013; Nelson, 2001). Another important aspect is that half of the worldwide petroleum reserves is concentrated in carbonate reservoirs, and most of these reservoirs are naturally fractured, making the NFRs an investment target of the petroleum industry (Ahmed-Elfeel and Geiger, 2012; Correia, 2014).

The main cited petrophysical characteristic of an NFR is the presence of multiscale heterogeneities, but their classification can vary according to the study's purpose. Since this work is related to reservoir engineering, multiscale heterogeneities are classified as complex geological features that affect the recovery of fluids into the reservoir, occurring in a different range of scales (Alpay, 1972).

Although those structures are in a multiscale scenario, there is not a standard nomenclature for the heterogeneities' scale range in the literature. According to Fanchi (2006), "features that affect fluid flow have a huge range of length scales, from pore throats with sizes down to less than 10 nm to large-scale faults that can be tens of kilometers in length," making the division of scale's ranges a challenge. However, some authors have published some proposals. Alpay (1972) divides the different scales into three domains: microscopic (pore to pore-scale), macroscopic (inter-well region or intra-formational), and megascopic (field-wide or regional). Other scale range classifications can be found in Correia (2014).

Considering the heterogeneities types, it is important to mention that not all multiscale heterogeneities are described in this chapter, but the main structures found in NFRs, as faults, fractures, vugs, karsts, and fracture corridors. They are detailed in the next paragraphs.

Fault and fracture definitions are broad and can change according to the area of study, varying in geomechanics, geology, or reservoir engineering. As this work focus on petroleum reservoirs, it is used the following definitions. Faults are deformation zones which occurred in response to shear stresses (Fanchi, 2006), and according to Nelson (2001), "a reservoir fracture

is a naturally occurring macroscopic planar discontinuity in rock due to deformation or physical diagenesis." Both faults and fractures can act as permeable channels for the flux or as barriers (Lima, 2013; Fanchi, 2006).

Some faults are classified as seismic or sub-seismic and are usually included in the microscopic or macroscopic scale as they have a wide variation in its length. Seismic faults are the structures identified through seismic resolution, and sub-seismic faults are the ones not detected by seismic maps, being a challenge in faults characterization (De Lima et al., 2019). Correia (2014) considers sub-seismic faults as objects with no more than 200m.

The natural fractures can be classified into four types: tectonic, regional, contractional, and surface-related fractures (Nelson, 2001). The tectonic fractures can be present in the micro or macroscopic scale and its origin is related to a local tectonic event, being formed from surface forces. Consequently, they can be related to networks formed by faults or folds. The regional fractures or "joints" are developed in large areas and have little orientation variation. Differing from tectonic fractures, they have a simple geometry and large spacing (Figure 2.1). According to Nelson (2001), the contractional fractures are "a collection of tension or extension fractures associated with a general bulk volume reduction throughout the rock." These fractures are originated from internal forces (body forces) and can produce hydrocarbons when under the right diagenetic and depositional conditions, since they do not have a dependency on trapping occurrence. Finally, the surface-related fractures are often generated from body forces and they are a diverse class of fractures which development occurs "during unloading, release of stored stress and strain, creation of free surfaces or unsupported boundaries, and weathering in general" (Nelson, 2001).

Figure 2.1: example of regional fractures in the western Sinai of Egypt. A pen is included for scale measure (Nelson, 2001)

Diffuse fractures or background fractures (Lima, 2013) are also an important heterogeneity in NFRs. According to Richard et al. (2017), they are "small scale bed bounded fractures," and Correia (2014) classify these fractures with a scale of no more than 10m. They do not necessarily cause an impact on the flux, but they should be considered during the reservoir characterization phase (De Lima et al., 2019).

Fracture corridors or fracture swarms (Figure 2.2) are a cluster of quasi-parallel fractures gathered in high quantity, may varying from hundreds to ten thousand fractures (Singh et al., 2008; Lima, 2013). Their dimensions can widely vary (Singh et al., 2008), and they impact the fluid flow by causing anisotropies in the system (De Lima et al., 2019).
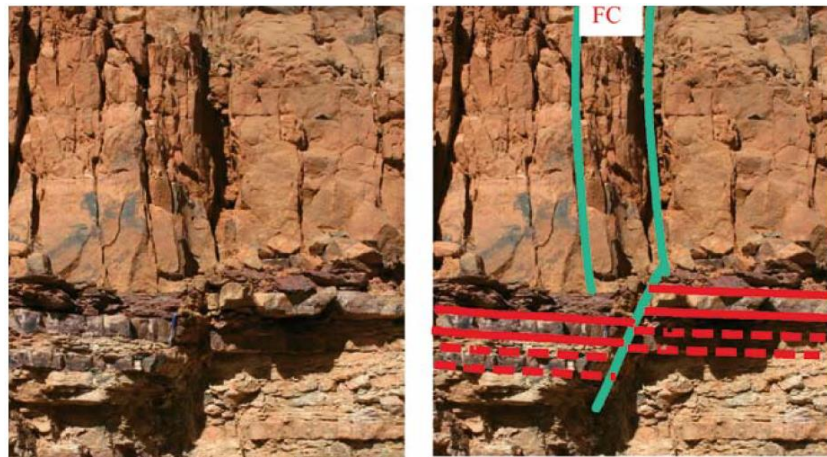
Figure 2.2: example of a fracture corridor developed in the top of a small fault (Singh et al., 2008)

The multiscale fractures can allow the generation of secondary porosity as karsts and vugs, through the percolation of basin fluids which causes silicification, dolomitization and/or dissolution processes (Cazarin, 2015).

According to Araújo et al. (2021), "vugs are microscale voids with equidimensional shape and small aspect ratios." Therefore, they are included in the microscopic scale, Correia (2014) considers isolated vugs' dimensions with a measure of less than 50cm. Nelson (2001) associates the formation of vugs with the percolation of fluids around a fracture plane in a matrix of low permeability.

For the karst definition, there is a wide and conflicting source of descriptions (Trice, 2005). For this work, karsts are the result of the chemical dissolution of the porosity and permeability of geological systems in micro or macroscopic scales, and in surface or subsurface areas (Ledsaak, 2016; Araújo et al., 2021). Therefore, they can be a result of vuggy fractures (Nelson, 2001). Karsts are usually divided into two main groups according to their origin: epigenic or hypogenic karsts. The epigenic type is originated from meteoritic waters flowing in

the near-surface and causing the dissolution in the rock. Epigenic karst can form epigenic caves, which are the ancestors of paleocaves reservoirs around the world. Paleokarst can be defined as an inactive karst system, and caves as a "natural underground opening in rock that is large enough for human entry" (Ledsaak, 2016). The second group is the hypogenic karsts, which are formed by ascending hydrothermal fluids without correlation with the overlying surface (Ledsaak, 2016; Araújo et al., 2021). An important aspect of hypogenic karsts is their potential to originate reservoir rocks (Cazarin, 2015). Figure 2.3 has an example of an analogue hypogenic karst system.

Figure 2.3: Toca da Boa Vista karst system defined as a hypogenic karst analogue (Cazarin et al., 2016)

Considering the primary recovery mechanisms of an NFR and its flux behavior during production, it is well-known that NFRs have a quite different behavior of conventional reservoirs. According to Saafeld (2016), these differences are due to the distinct hydrodynamic properties between matrix and fracture. During the primary recovery, the pressure drop expands the fluids inside the matrix system and the fluids are conducted to the fracture system (Saafeld, 2016). The natural depletion is directly influenced by the system compressibility and its duration depends on the difference between the initial pressure of the reservoir and the bubble pressure of the stored fluid (Lima, 2013; Saafeld, 2016). The flux behavior in NFR is usually characterized with high flow rates, which leads to an early breakthrough and rapid production declines. Therefore, NFRs tends to be a short-lived reservoir with low ultimate recovery factor (Allan and Sun, 2003; Decroux, 2012).

Rock wettability is an important characteristic during NFR recovery processes, particularly during waterflooding. The wettability of the rock in naturally fractured reservoirs tends to be intermediate to oil-wet (Soler, 2019). This characteristic makes the injected water during a waterflooding process rapidly override the fracture, decreasing the sweep efficiency.

For water-wet rocks the capillary imbibition is significant for the hydrocarbon recovery (Correia et al., 2016; Saafeld, 2016). Therefore, as shown in Soler's (2019) results, the water-wet rocks tend to have a higher oil recovery factor during different water injection rates if compared to the intermediate and oil-wet scenarios.

The classification of NFRs is challenging due to the presence of multiscale heterogeneities. A commonly used classification is proposed by Nelson (2001), who divides NFRs into four types according to the contribution of the matrix and fracture systems in the reservoir's permeability and porosity (Figure 2.4). Overall, Nelson's (2001) proposal infers about the positive or negative contribution of the fracture system in the reservoir quality.
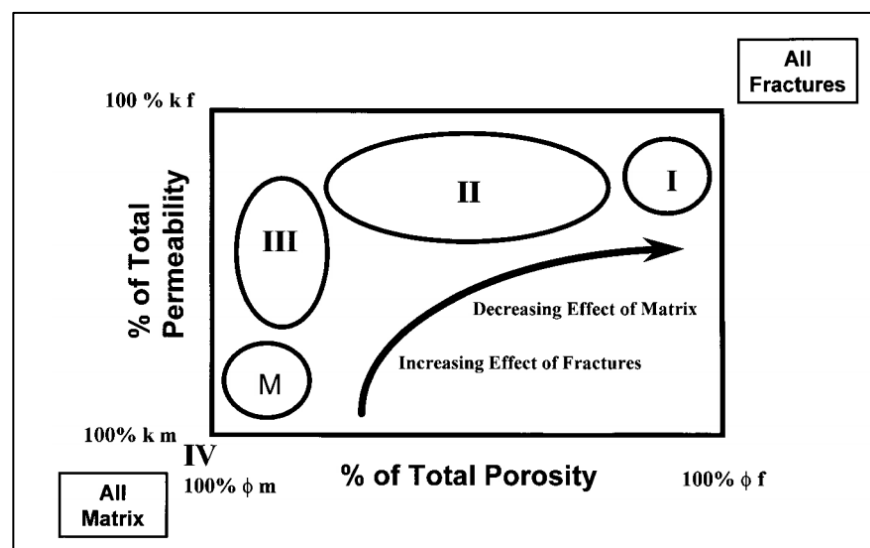
Figure 2.4: cross plot of the four types of NFRs according to the contribution of fractures and matrix in the reservoir total porosity and total permeability (Nelson, 2001)

A summary of the four types definition and highlights are described below:

- **Type 1:** Fractures supply the essential porosity and permeability of the reservoir. A reservoir of this type can have a large drainage area per well but a rapid decline curve. Besides the existence of an impermeable matrix (Correia, 2014).

- **Type 2:** Fractures supply the essential permeability of the reservoir. Consequently, the matrix provides essential porosity or storage volume. Type 2 of NFR can develop rocks with low permeability but if the interaction between matrix and fracture porosity is poor, the secondary recovery may have a terrible performance.

- **Type 3:** Fractures supply the permeability in an already productive reservoir. Therefore, the matrix already has the capacity to produce fluids (Correia, 2014). This reservoir type has a positive aspect of being capable of high sustained well rates but can have a high anisotropic permeability.

- **Type 4:** <u>Fractures create significant reservoir anisotropy acting as barriers and do not provide any additional porosity or permeability to the reservoir</u>. This is the NFR type that does not have positive contributions for the flux and one of its drawbacks is the highly variable recovery factor across the field.

The NFR classification is possible to be done after the reservoir characterization when it is determined the fracture system characteristics and the interaction between the matrix and fracture, which is an essential parameter in Nelson's (2001) proposal. However, the multiscale heterogeneities have many geologic uncertainties, making their characterization a considerable challenge (Cazarin, 2015). These uncertainties are present in the fractures size, connectivity, orientation, distribution, and conductivity, making the gathering of reliable data a difficult task. Furthermore, the NFR modeling and simulation phases are also challenging due to the high computational costs required in large carbonate fields, in complex fracture networks, or during the utilization of probabilistic approaches (Amiry, 2014).

Examples of relevant NFRs are the pre-salt carbonate reservoirs in Brazil. The formation of these reservoirs is related to the conditions of high salinity and low energy provided by the salt layer. This led to the appearance of bacteria colonies, which its secretion together with the precipitation of carbonate salts, formed the pre-salt carbonate reservoirs (Medina, 2012). According to De Lima et al. (2019), the "Brazilian Pre-salt reservoirs have permeable matrix with some anisotropy caused by fractures and fault corridors," and they can have other multiscale heterogeneities such as karsts and vugs.

2.2 NFR characterization

The reservoir characterization phase is the quantitative and three-dimensional determination of the limit, volume, heterogeneities, and distribution of the rock and fluid properties of the reservoir (Passarela, 2012). The main objective of this phase is to provide the necessary data to execute reservoir modeling and simulation. However, the presence of geological uncertainties in the multiscale heterogeneities introduces considerable challenges in NFR characterization. That is why Richard et al. (2017) emphasize the importance of quality control of the interpreted data, as different conclusions about the same multiscale heterogeneity can be described through different data sources.

A successful characterization is a result of a multidisciplinary data analysis from geology, geophysics, and reservoir engineering. The geologic data usually comes from core analysis and sedimentological and stratigraphic interpretations of the studied area. The

geophysical data come from well-logs and seismic maps, and reservoir engineering can analyze the PVT (pressure, volume, and temperature) and production data (Passarela, 2012).

The NFR characterization should have three main objectives: fracture network characterization, quantification of their impact on the flux, and the analysis of the interaction between matrix and fracture. Therefore, the geological matrix characterization with its petrophysical and texture properties is also performed during the NFR characterization, but in this section the focus is on the multiscale heterogeneities characterization.

Characterize the NFR heterogeneities implies the determination, in different scales, of their physical morphology, distribution, and petrophysical properties such as porosity, permeability, fluid saturation, and expected recovery factor (Nelson, 2001). Other properties defined through the fracture network characterization are the fractures spacing, aperture, orientation, connectivity, and density (Saafeld, 2016).

The source data utilized in the multiscale heterogeneities characterization are divided into two main groups: static and dynamic data. The static group includes seismic maps, cores, Bottom Hole Images (BHI), geomechanics data, well logs, and outcrops, and the dynamic data includes pressure data (static pressure and Repeat Formation Testers (RFTs)), production data, and well tests as the Production Logging Tools (PLT) (Lima, 2013; Ateeq et al., 2017).

Static and dynamic data can assist the characterization of different multiscale heterogeneity types. 3D seismic maps can be used in the characterization of seismic and sub-seismic faults and fracture corridors. Whole-core samples can allow fracture absolute permeability calculation, fracture permeability anisotropy analysis, the determination of fluid saturation in fractures, and relative permeability tests. Core analysis assists the determination of fractures' types, their density, and their impact on the flux. BHI can be used to characterize fracture scales (micro to macroscopic), their distribution, and some properties as orientation and density. According to Ateeq et al. (2017), the geomechanics data is useful in the analysis of the "response of fractures to the present day in-situ stress conditions," and well logs assist the description of fracture's occurrence and distribution through the wellbore. Regarding the dynamic data, PLT analysis can quantify the impact that fractures cause on the flux, production data can reveal the presence of conductive fractures, and pressure data can assist the measurement of fracture permeability, and the quality of fractures' connectivity and compartmentalization (Nelson, 2001; Lima, 2013; Correia, 2014; Ringrose and Bentley, 2015; Saafeld, 2016; Ateeq et al., 2017).

During the fracture characterization, fractures can be divided into fracture sets. According to Decroux (2012), "these sets represent families of fractures which share a similar orientation (characterized by the dip and the azimuth), length, aperture, and permeability."

Moreover, specific methodologies can be applied during characterization. Sign et al. (2008) have details about fracture corridors characterization, Ledsaak (2016) has a deep explanation about karst and paleokarst characterization, and De Lima et al. (2019) propose a methodology for sub-seismic fault characterization.

Considering the interaction between matrix and fracture, it can be defined from core, well logs, and well tests analysis. These data assist the determination of matrix permeability and fractures spacing, which are the necessary properties to analyze the communication between the matrix and fracture network (Saafeld, 2016).

To have a reliable reservoir flow prediction, an efficient methodology of NFR characterization that successfully integrates all available data should be adopted. Different workflows of NFR characterization, modeling, and simulation are available in the literature (Elsaid et al., 2007; Benko et al., 2012; Boro et al., 2014; Bigi et al., 2015; Felici et al., 2016; Richard et al., 2017). Figure 2.5 has an example of fracture network characterization, modeling, and simulation workflow, with a summary of the cited static and dynamic data.

The use of conceptual models, as demonstrated in Figure 2.5, can support the understanding of the data acquired during the characterization. They are models that represent, with simplicity, the heterogeneities characterized in the reservoir, being a support for further reservoir modeling (Ateeq et al., 2017). According to Ledsaak (2016), the utilization of these models can "in turn be utilized to improve interpretation of available seismic-, well- and production data." Another example of a conceptual model is in Figure 2.6.
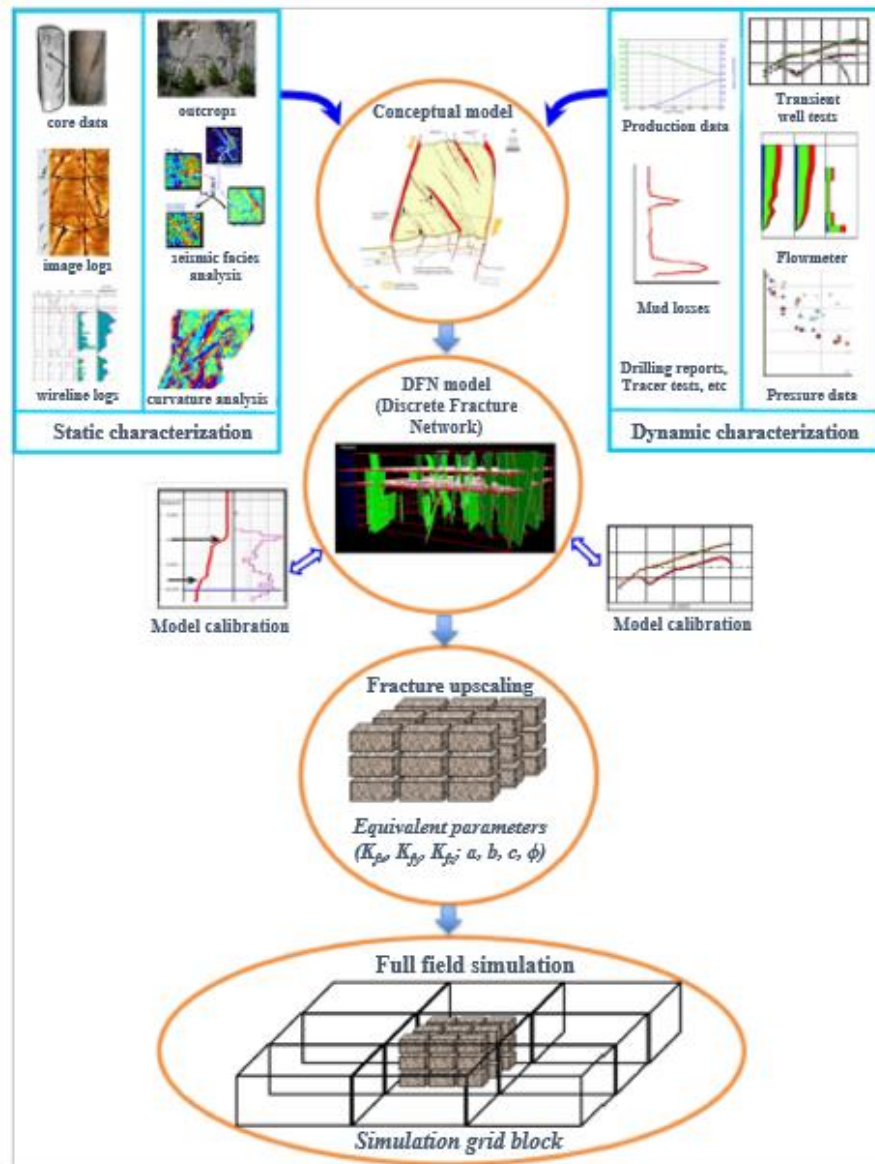
Figure 2.5: workflow example of characterization, modeling, and simulation of the fracture system in an NFR (modified from Ateeq et al., 2017)
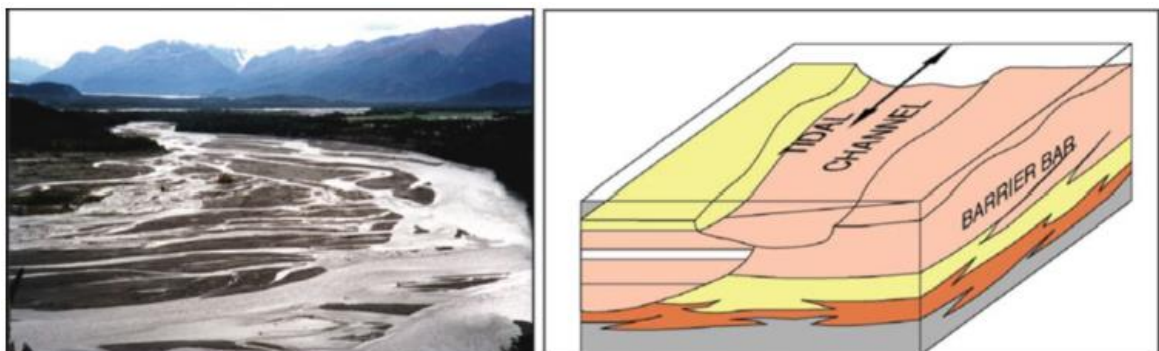
Figure 2.6: conceptual model of a reservoir analogue (Ringrose & Bentley, 2015)

2.3   NFR modeling

The NFR modeling phase occurs after the characterization of the reservoir and it is defined as the representation of the matrix and fracture network by gathering all the static and dynamic data interpreted during characterization. The purpose of reservoir modeling can vary with the study's objective. Ringrose and Bentley (2015) discuss two main purposes:

1) To provide a 3D digital representation of the hydrocarbon reservoir.

2) To build fit-for-purpose models by constructing and maintaining a field database.

The first option is an "all-purpose" model that can be used for reservoir visualization, oil volume calculations, well placement studies, or production forecasting through reservoir simulation. Different from the first option, fit-for-purpose models are modeled according to a well-defined objective, focusing on answering a specific question, and not necessarily are a full-reservoir representation. Moreover, the fit-for-purpose modeling can be stochastic, generating a set of models which incorporates the uncertainties of the multiscale heterogeneities of an NFR.

Regardless of the modeling purpose, it is important to mention that the characterization and modeling phases are not a unique realization before the reservoir simulation. They may continue during the reservoir development phase, as data of new wells and production history are available (Saafeld, 2016).

As defined, NFR modeling has a direct dependency on the NFR characterization; thus, a well-developed characterization is essential for a successful NFR modeling, mostly because other uncertainties will be present in the modeling phase. The two main challenges are the representation of the multiscale heterogeneities in the defined grid-scale and the consideration of their geological uncertainty. The first challenge can be overcome by the utilization of upscaling methods and calibration methodologies, and the second issue can be managed by executing stochastic modeling (Passarela, 2012). According to Amiry (2014), other challenges are the limited amount of information and the scale variation in the characterized data.

Different methods are used for the multiscale heterogeneities modeling. As examples, there are the Discrete Fracture Network (DFN), implicit fracture network, the Discrete Fracture and Matrix modeling (DFM), and Embedded Discrete Fracture Modeling (EDFM) (Ahmed-Elfeel and Geiger, 2012; Lima, 2013; Dong et al., 2019). Moreover, if some small-scale fractures and vugs cause an impact on the flux, they may be implicitly included in the matrix system (Correia, 2014).

2.3.1 Discrete Fracture Network (DFN)

A DFN is a fracture modeling method that explicitly represents the fractures in 3D by using the properties obtained in the reservoir characterization phase (Bigi et al., 2015). Figure 2.7 has an example of a full-field DFN. Moreover, the DFN can be associated to any grid dimension (Figure 2.8) and can have a variety of fracture sets.
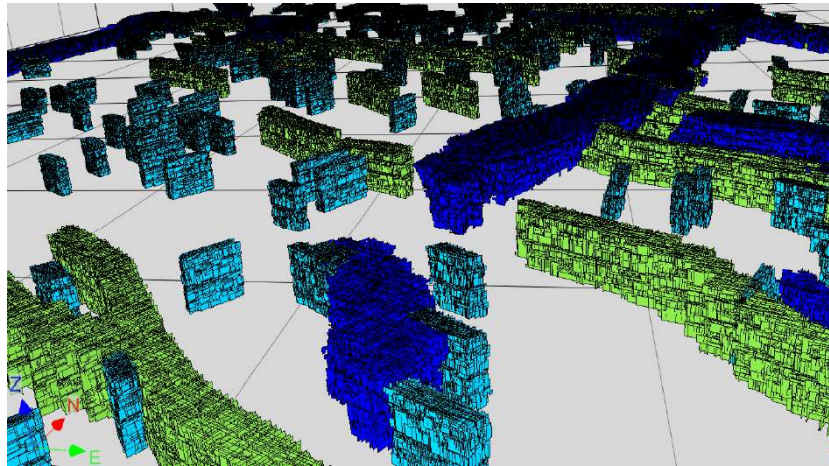
Figure 2.7: full-field DFN example, the background grid has 5km of scale (Richard et al., 2017)
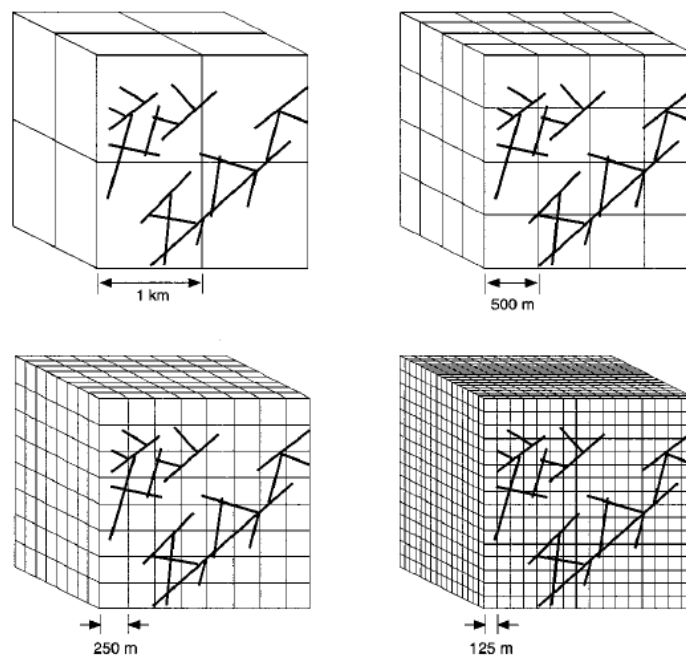
Figure 2.8: illustration of a DFN associated to different grid scales (modified from Dershowitz et al., 2000)

The necessary fracture data to build a DFN include the length, aperture, orientation, density, and intrinsic permeability. Since the fracture network has geological uncertainties and not all properties are possible to be characterized, the fracture sets are usually built with probability laws as power, log-normal, exponential, and normal distributions (Decroux, 2012).

Moreover, for the orientation, there are the Fisher, Bringham, and Kent's model. The fracture representation can vary from ellipses or rectangles, depending on the selected software. As example, Boro et al. (2014) have a complete description of the utilized DFN inputs as example.

The main limitation of a DFN is its low capacity to represent exactly what is observed in the characterization phase (Richard et al., 2017). To honor what is observed, a high quantity of heterogeneities should be built, demanding a high computational effort. Consequently, the DFN is difficult to be used in full-field or large field applications. Another limitation is the lack of information about the input parameters (Amiry, 2014).

In the literature, some procedures are utilized to estimate the values of fracture properties that are not fully characterized. The following paragraphs describe some techniques utilized in the fracture density, aperture, and permeability estimation.

The fracture density is usually referred by the P32 index, which is the cumulative fracture area per unit of volume. It can be obtained from bottom hole image (BHI) analysis or from correlations utilizing the P10 and P21 indexes. Bigi et al. (2015) have a description of this calculation, and Table 2.1 has a summary of the fracture density indexes that may be used in the DFN modeling.

Table 2.1: summary of the fracture density indexes (adapted from Beicip Franlab, 2019)

DIMENSION OF FRACTURE	DIMENSION OF MEASUREMENT		
	1 Length	2 Area	3 Volume
0: number of fractures	**P10** Number of fractures per length (m^{-1})	**P20** Number of fractures per surface unit (m^{-2})	**P30** Number of fractures per volume unit (m^{-3})
1: length		**P21** Cumulative fracture length per surface unit (m^{-1})	**P31** Cumulative fracture length per volume unit (m^{-2})
2: Area		**P22** Fracture area per cumulative surface unit (%)	**P32** Cumulative fracture area per volume unit (m^{-1})
3: Volume			**P33** Fracture volume per volume unit (=fracture porosity) (%)

The fracture aperture is one of the most challenging parameters to be measured and is usually estimated from pressure data (Ringrose and Bentley, 2015). However, data from

outcrop analogues can assist the understanding of the fracture's fluid flow and provide some aperture values for DFN modeling, but the differences in burial depth and diagenetic conditions should be considered (Miranda et al., 2018; Massaro et al., 2018).

The fracture intrinsic permeability can be estimated from the cubic law (Equation (2.1). This law is derived from the Poiseuille's law for a parallel-plate geometry (Equation (2.2) and Figure 2.9), as it shows that the fracture flow is proportional to the cube of the aperture (Ringrose and Bentley, 2015).

$$K_{if} = \frac{b^2}{C * 12} \tag{2.1}$$

where K_{if} is the intrinsic fracture permeability (mD), b is the fracture aperture (m), and C is a conversion factor of 1 mD = 10^{-15} m^2 (Bigi et al., 2015).

$$q = \frac{w \times b^3}{12\mu} \frac{\Delta P}{L} \tag{2.2}$$

where q is the volumetric flow rate, **w** is the fracture width, b is the fracture aperture, **μ** the fluid viscosity, $\Delta \boldsymbol{P}/\boldsymbol{L}$ the pressure gradient (Ringrose and Bentley, 2015).
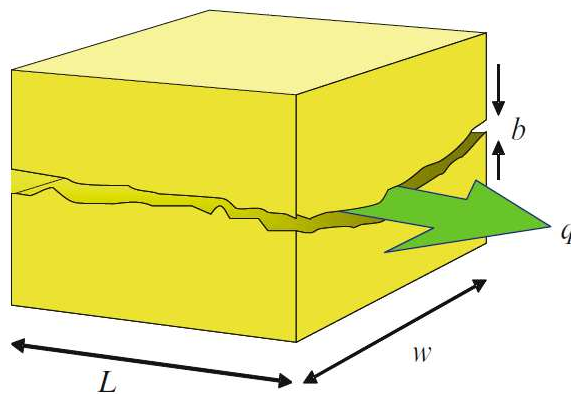
Figure 2.9: fluid flow inside a pair of fractures, where w is the fracture width, b the fracture aperture, and L the fracture length (Ringrose and Bentley, 2015)

Furthermore, correlations among fracture parameters can be adopted to estimate other properties as fracture spacing and porosity. Nelson (2001) describes a couple of correlations, Figure 2.10 has an example among fracture spacing, aperture, and permeability.
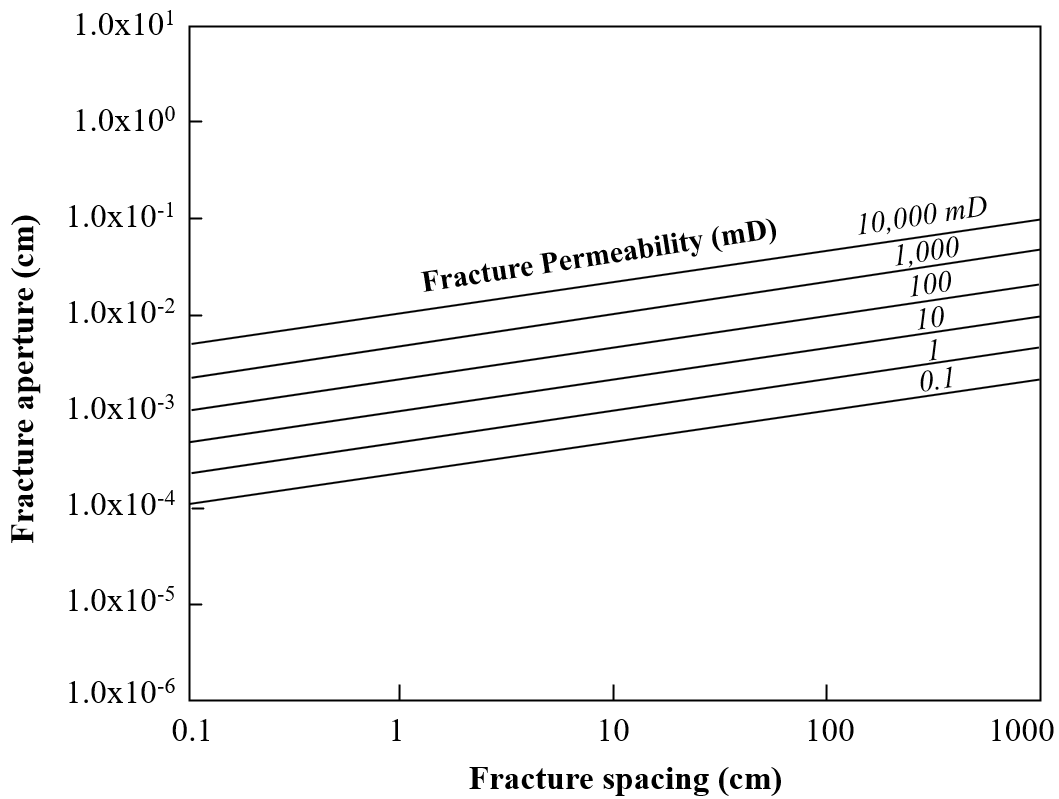
Figure 2.10: fracture permeability as a function of fracture aperture and fracture spacing (modified from Nelson, 2001)

For reservoir engineering, the DFN should at least represent the dynamic behavior of the wells, even if the fractures are not perfectly modeled due to computational limitation. Therefore, the calibration of the DFN is utilized to validate the DFN (Decroux, 2012). This procedure can be done before or after the upscaling process utilizing well tests as Pressure Transient Analysis (PTA) (Saafeld, 2016; Lima, 2013). Lamine et al. (2017) have a complete workflow on DFN calibration utilizing PTA.

However, the DFN calibration can be hampered not only by the geological uncertainties from the characterization phase but also by the upscaling procedure. Consequently, a well-executed characterization does not guarantee that the fracture network is well represented in the simulation model (Ahmed-Elfeel and Geiger, 2012). The next section highlights the limitations of the DFN upscaling process and its definition.

2.3.2 DFN upscaling

The DFN upscaling is the process responsible to calculate the fracture grid properties from the discrete fracture objects. The grid data resulted from the DFN upscaling process is used as input in the construction of dual-continuum simulation models, these grid data are the

fracture spacing, fracture effective permeability, and fracture effective porosity. Figure 2.11 has a representation of the DFN upscaling outcomes of permeability and porosity for a carbonate fractured reservoir analogue. It is important to mention that each fracture effective property is calculated in each grid cell, and the DFN can be upscaled to any 3D grid, as illustrated in Figure 2.8.
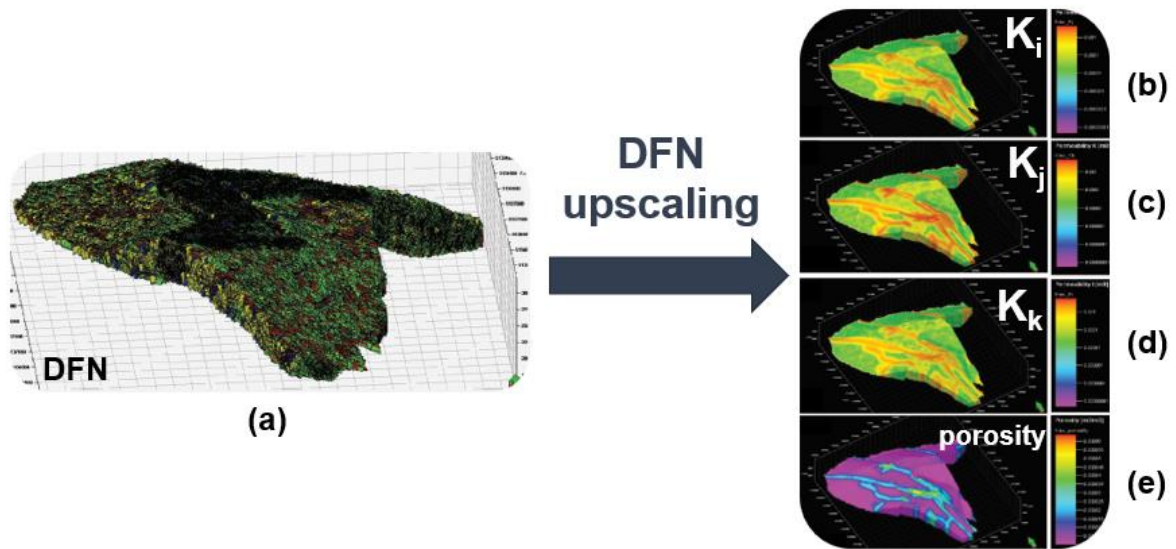
Figure 2.11: representation of the DFN upscaling outcomes for the Latemar carbonate platform, where (a) represents the DFN model; (b), (c) and (d) are the results for the fracture effective permeability grid in three directions; and (e) is the fracture effective porosity grid. The general 3D grid used to perform the upscaling is not illustrated (modified from Bigi et al., 2015)

The DFN porosity upscaling is volumetric, supposing that the fractures have an empty space (Decroux, 2012). Equation (2.3) has the effective porosity equation for each grid cell.

$$Grid\ cell\ effective\ porosity = \frac{Fractures\ volume}{Block\ volume} \qquad (2.3)$$

The fracture spacing (or matrix block size) is the distance between fractures in each direction, representing the matrix block length in dual-continuum models (Figure 2.16). The fracture spacing values in each grid cell (a, b, and c) are used to compose the transmissibility factor in the dual-continuum simulation models (Equation (2.10)), and it shows how it is the interaction between matrix and fracture systems throughout the reservoir.

According to Amiry (2014), the fracture spacing corresponds to the fracture intensity distribution calculated in the characterization phase. According to the same author, this distribution is calculated with statistical laws and is defined as "the number of fractures per unit length of a simple line," an example is in Figure 2.12.
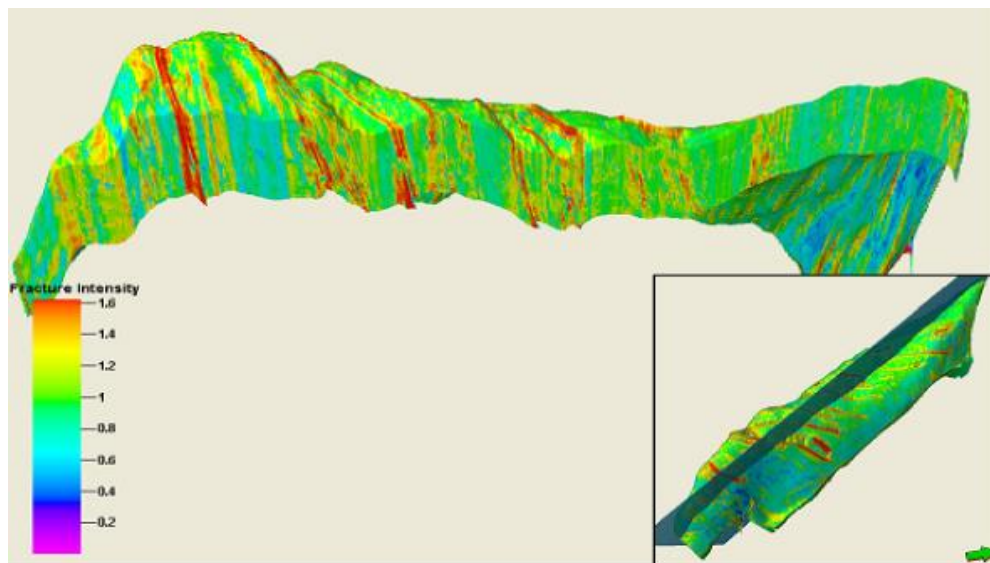
Figure 2.12: example of a fracture intensity distribution in a 3D reservoir model (Amiry, 2014)

The fracture effective permeability is different from the fracture intrinsic permeability defined in the NFR characterization and modeling phase, since the effective permeability is an anisotropic property (Figure 2.11) and the intrinsic permeability is isotropic. Consequently, the effective permeability is usually represented by a tensor (Figure 2.13) to consider the fracture anisotropy. This tensor is formed from Darcy's law theory, as the permeability terms are a consequence of the pressure gradient applied in each direction. For example, the K_{xz} term in Figure 2.13 represents the flow in the x-direction due to a pressure gradient applied in the z-direction (Decroux, 2012; Ringrose and Bentley, 2015).

During the numerical simulation, the "cross-flow" terms (K_{xy}, K_{xz}, and K_{yz}) are usually neglected and only the diagonal tensor is considered (Figure 2.13). To reduce the error caused by this simplification, the grid should be aligned with the fracture network, so the "cross-flow" terms are as small as possible (Decroux, 2012). However, this alignment is a challenging task as the direction of the fracture sets can change through the grid blocks, as discussed by Ghahfarokhi (2017).

Full permeability tensor

$$k_{eff} = \begin{bmatrix} k_{xx} & k_{xy} & k_{xz} \\ k_{yx} & k_{yy} & k_{yz} \\ k_{zx} & k_{zy} & k_{zz} \end{bmatrix}$$

Permeable medium

Coordinates

Diagonal permeability tensor

$$k_{eff} = \begin{bmatrix} k_{xx} & 0 & 0 \\ 0 & k_{yy} & 0 \\ 0 & 0 & k_{zz} \end{bmatrix}$$
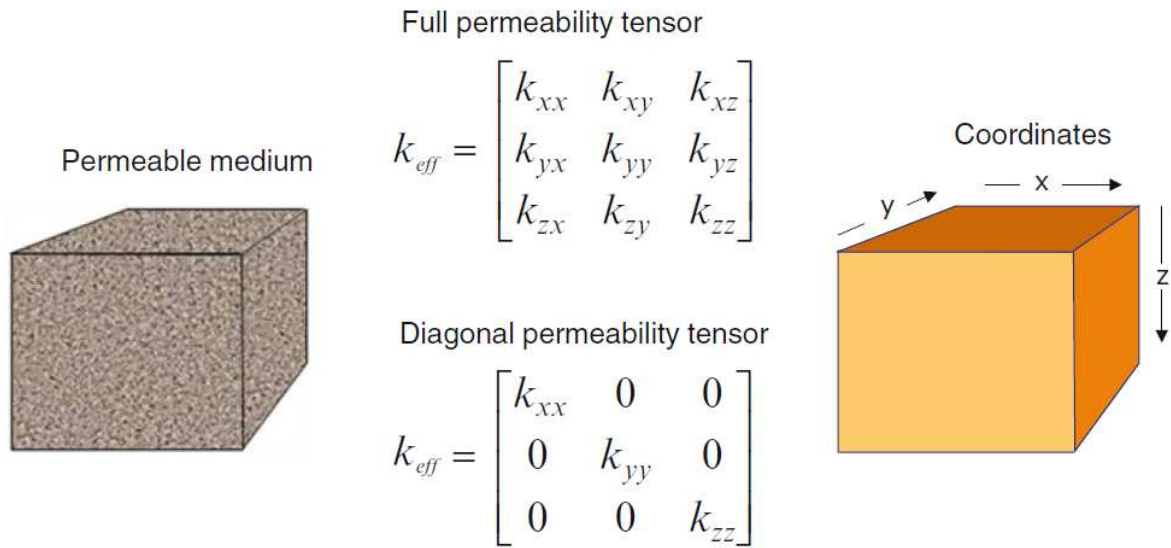
Figure 2.13: effective permeability (K_eff) full tensor and diagonal tensor representation (Ringrose and Bentley, 2015)

The fracture effective permeability calculation is done with different methods and it is usually sensitive to the method change, producing different permeability values when changing the methodology (Ahmed-Elfeel and Geiger, 2012). The Oda (1985) and the Flow-based methods are the most common in commercial software.

The Oda (1985) method proposes an analytical calculation of the effective permeability, being an adaptation of Snow's (1969) equations by extending their use in implicit fracture networks (Decroux, 2012). Equation (2.4) has the effective permeability tensor proposed by Oda (1985) for a general DFN. It is observed that it depends on fractures aperture, orientation, and size (Ghahfarokhi, 2017). The full equation development and their application in implicit fracture networks can be found in Decroux (2012) and Ahmed-Elfeel and Geiger (2012).

$$k_{ij} = \frac{1}{V_{block}} \sum_f b^{(f)} A^{(f)} k^{(f)} \left(\delta_{ij} - n_i^{(f)} n_j^{(f)} \right) \qquad (2.4)$$

where k_{ij} is the effective permeability tensor (same unit as $k^{(f)}$), V_{block} is the block volume (in m³), $b^{(f)}$ is the fracture aperture (in m), $A^{(f)}$ is fracture area (in m²), $k^{(f)}$ is the fracture permeability (in any unit), δ_{ij} is the Kroneker delta (used to normalize the fracture orientation relative to the grid block geometry (Ahmed-Elfeel and Geiger, 2012)), and $n_i^{(f)}$ is the fracture orientation (Decroux, 2012).

For being an analytical method, Oda (1985) has fast processing, but it considers the fracture with an infinite length, producing non-existent connectivity. Besides, as it mainly

considers the geometry of the fractures, it always computes positive permeability values even if no connectivity exists among the fractures (Ahmed-Elfeel and Geiger, 2012). Consequently, this is a method not accurate for non-connected and non-dense fracture networks.

According to Decroux (2012), Lough et al. (1997) was the first to calculate the fracture permeability tensor from a DFN utilizing the flow-based (FB) method. The FB is usually cited as the most precise method as it considers the connectivity of the fractures by preserving the DFN geometry in each grid cell. This method simulates a single-phase flow inside each grid block by imposing pressure on two faces and a boundary condition in the other sides, and it uses Darcy's law to calculate the fracture permeability tensor (Ahmed-Elfeel and Geiger, 2012; Decroux, 2012). Figure 2.14 has the four possible types of boundary conditions: no flow, linear pressure, constant pressure, and periodic (inlet velocity is equal to outlet velocity).
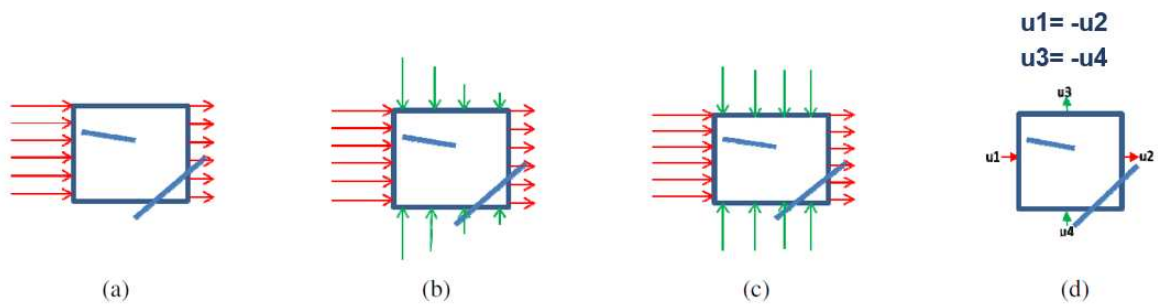
Figure 2.14: four types of boundary conditions in the application of the flow-based method: (a) no side flow, (b) linear pressure, (c) constant pressure, (d) periodic boundaries (modified from Ahmed-Elfeel and Geiger, 2012)

Despite the accuracy of the FB method, three main limitations can be cited: the sensitivity to the boundary condition, the high computational cost, and the time demand. Thus, the change in the boundary condition may result in different values of fracture permeability, the computational resources may not run a FB upscaling, and the processing time is higher than the Oda method.

Table 2.2 has examples of the time expended to run Oda and FB methods when varying the grid dimension for the same DFN. The machine has an Intel Xeon E3 1225 @ 3.30 GHz with 16 GB RAM. It is possible to observe that the FB may not be feasible to be used in models with a high quantity of cells or with an expressive cell refinement. However, the time and computational resources required are also dependent on the number of fractures in the DFN, as described by Haridy et al. (2019).

Table 2.2: comparison of the upscaling time of the Oda and FB methods applied in different grid dimensions for the same DFN. Machine description: Intel Xeon E3 1225 @ 3.30 GHz with 16 GB RAM

Model dimension (m)	1000x1000x20	600x600x20	500x500x20	400x400x20	
Cell dimension (m)	5x5x1	5x5x1	5x5x1	5x5x1	5x5x2
Number of cells	800,000	288,000	200,000	128,000	64,000
Oda time	Minutes	Seconds	Seconds	Seconds	Seconds
FB time	2 weeks	2-5 days	4-5 days	2-3 days	1 day
FB status (% of computed cells)	Incomplete (3%)	Incomplete (35%)	Incomplete (50%)	Incomplete (80%)	Complete

Moreover, the software Petrel has proposed the Oda corrected (ODAC) method, which aims "to be as close as possible to Flow-based permeability upscaling method, but faster and taking into account the whole fracture network" (Schlumberger, 2018). The main idea is to multiply the Oda output by a ratio which considers an extended connectivity index and the fractures length (Equation (2.5) and (2.6)). The extended connectivity index (eCI) depends on the average number of intersections between fractures and on the number of intersections between fractures and cell boundaries, and L depends on the grid cell geometry and the fracture length.

$$K_{Odac} = K_{Oda} * ratio \qquad\qquad (2.5)$$

where K_{Odac} is the fracture permeability resulted for the ODAC method, K_{Oda} refers to the fracture permeability obtained with the Oda method, and the ratio is described by Equation (2.6).

$$ratio = f(eCI, L) \qquad\qquad (2.6)$$

where eCI is the extended connectivity index and L is the ratio between the cell geometry and the fracture length.

The determination of the eCI is a challenge in the ODAC calculation and some authors have been proposing different methodologies to achieve an accurate eCI, as proposes Haridy et al. (2019).

Finally, it is important to mention that the application of the DFN upscaling in different grid scales tends to change the fracture permeability outcome. Besides, applying the DFN

upscaling in high fidelity models does not necessarily provide the most precise results, as it is expected in conventional simulation models (Decroux, 2012).

2.4 NFR simulation

A well-developed characterization and modeling of the multiscale heterogeneities are essential to accurately represent their impact in reservoir flux during simulation (Lima, 2013). However, the choice of the simulation model type should be appropriate for each NFR to make an adequate representation of these heterogeneities. For example, the identification of connected fractures and the strong impact of matrix capillary continuity indicate the necessity of dual-continuum models instead of single-porosity simulators (Bourbiaux et al., 2010).

Before the modeling and simulation processes start, there is the grid-scale selection, when different model fidelity scales are chosen accordingly to the study's objective. For example, the high-fidelity model (HFM) focuses on a high precision representation of the reservoir heterogeneities, fluids condition, and drive mechanisms, but it usually demands a high computational time. Besides the high-fidelity model, there are the medium-high (MHFM), medium (MFM), and low fidelity models (LFM). The precision and simulation time decrease as the model fidelity decreases. Table 2.3 has the summary of the fidelity model classification from an internal publication of Unisim online (Avansi et al., 2020). It is important to mention that medium-fidelity models are considered the scale usually used by industry in probabilistic approaches.

Table 2.3: default fidelity model classification (adapted from Avansi et al., 2020)

Model	Abbreviation	Characteristic
High fidelity	HFM	computational expensive and high accuracy
Medium-high fidelity	MHFM	medium running time and accuracy
Medium fidelity	MFM	suitable running time and accuracy
Low fidelity	LFM	fast to run and less accurate

The main challenges in the NFR simulation are the representation of the heterogeneities flux and the management of the simulation time. Bourbiaux et al. (2010) have a methodology to select the flow modeling method for a fractured reservoir (Figure 2.15). About the simulation time, this is an important parameter when selecting the fidelity scale. For example, a full field may require days of simulation when using high-fidelity models, which jeopardize the use of probabilistic approaches and the inclusion of the NFR's uncertainties in the simulation studies.
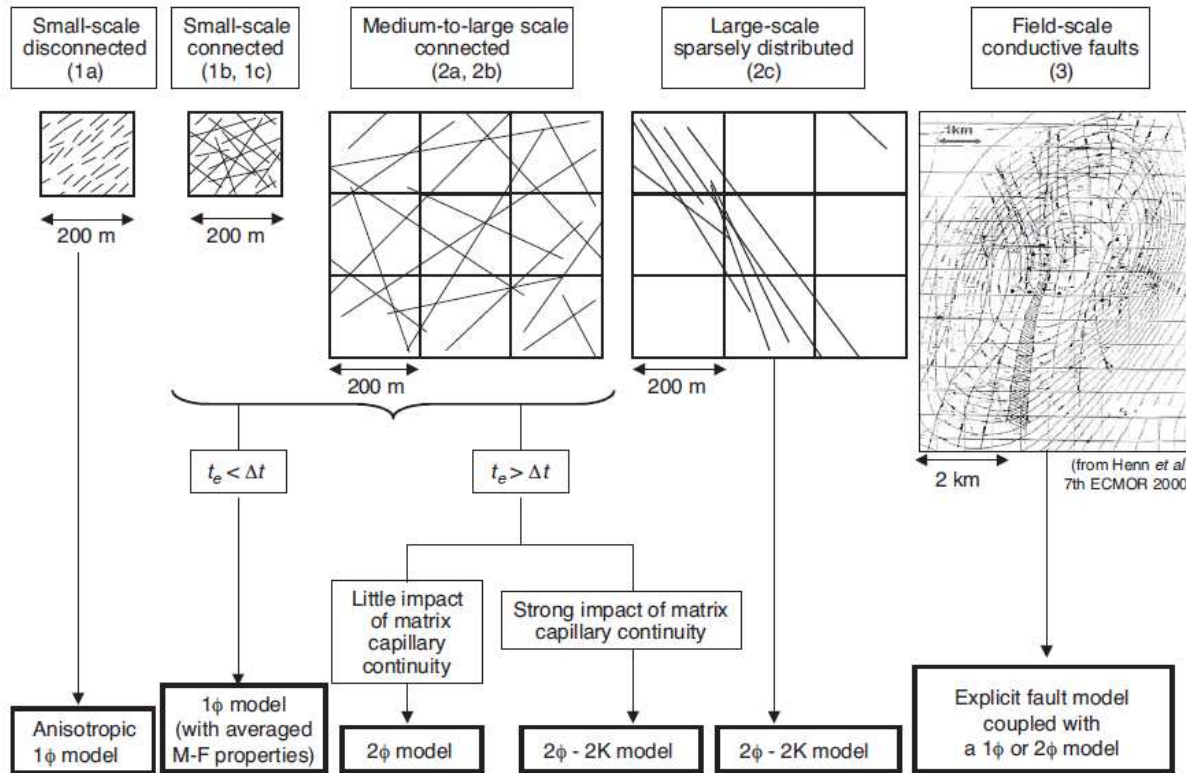
Figure 2.15: methodology for the selection of the flow modeling method for a fractured reservoir (Bourbiaux et al., 2010)

In NFRs, the use of the Characteristic Flow Unit (CFU) concept can facilitate the reservoir flux behavior understanding and reduce the simulation time. According to Mahjour et al. (2019), CFU is a region of the reservoir that have similar petrophysical features and are horizontally homogenous, and different methodologies can be adopted to define a CFU, as the use of neural networks and Flow Zone Indexes (FZI).

For NFRs, four types of flux simulators available in commercial software may be used. They are the explicit discrete fractures, single continuum, dual continuum, and discrete-fracture networks. The explicit discrete fractures represent the shape and size of the fracture in grid cells. The single continuum may be referred as the single-porosity model, and it uses pseudo relative permeability and pseudo capillary curves to represent the fractured medium. The dual continuum models can be classified as dual-porosity (DP) and dual-permeability (DK) models, possibly utilizing the multiple interacting continua (MINC) and subdomain methods. Finally, the discrete fracture network utilizes the finite element method to build the fracture network geometry, and the matrix can be represented by triangular elements, the use of DFN for simulation is the application of this method when the matrix is not represented (Lima, 2013).

2.4.1   Dual-continuum models: DP and DK

The dual-continuum models are characterized by the presence of a fracture and a matrix system connected by a transmissibility parameter. These models represent the fractures implicitly, by not directly considering their shape, size, and orientation (Berre et al., 2018). Therefore, the necessary input grids for the fracture system are the effective permeability, effective porosity, and fracture spacing, the same DFN upscaling output.

The idea of dual continuum was firstly idealized by Barenblatt et al. (1960) and was introduced in the petroleum industry by Warren and Root (1963) who developed the sugar cube concept (Lima, 2013). The Warren and Root (1963) model (Figure 2.16) is an idealized fracture reservoir that has the matrix blocks surrounded by orthogonal fractures. This idea creates a sugar cube pattern, where each cube is separated by a fracture and has its dimension according to the matrix block size (fracture spacing).

(a,b,c)= equivalent matrix block size

(k_x, k_y, k_z)= effective fracture permeability
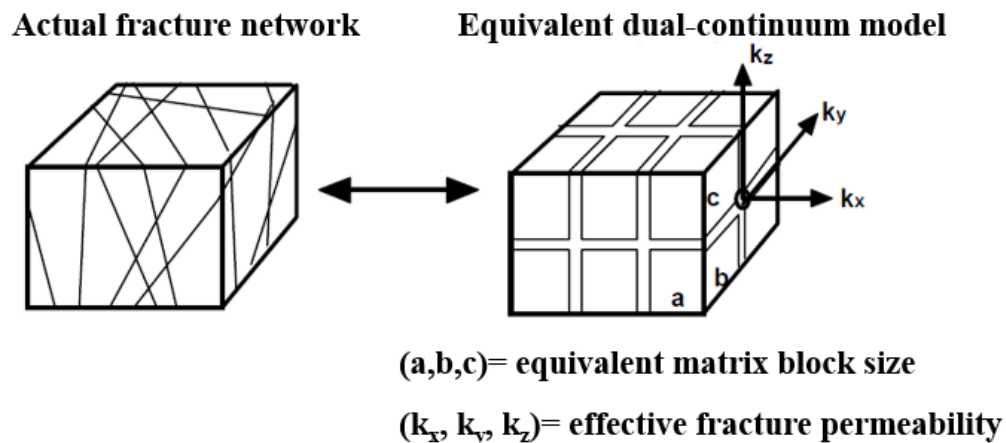
Figure 2.16: sugar cube concept of Warren and Root (1963) (modified from Sabathier et al., 1998)

The block size is not dependent of the grid size. As illustrated in Figure 2.17, each grid cell can have a variety of matrix blocks, and the fracture and matrix grids are superposed grids, interacting with each other by the transmissibility factor.

Initially, the dual-continuum models proposed by Warren and Root (1963) did not consider the fluid transfer between matrix blocks. The fluid occurs only through fractures, characterizing a single-permeability model with the matrix as the fluid storage. This is the definition of the dual-porosity (DP) model. The dual permeability (DK) is an extension of the DP model, by considering the flow through the matrix system beyond the fracture system. Figure 2.18 has the representation of this difference between DP and DK models.
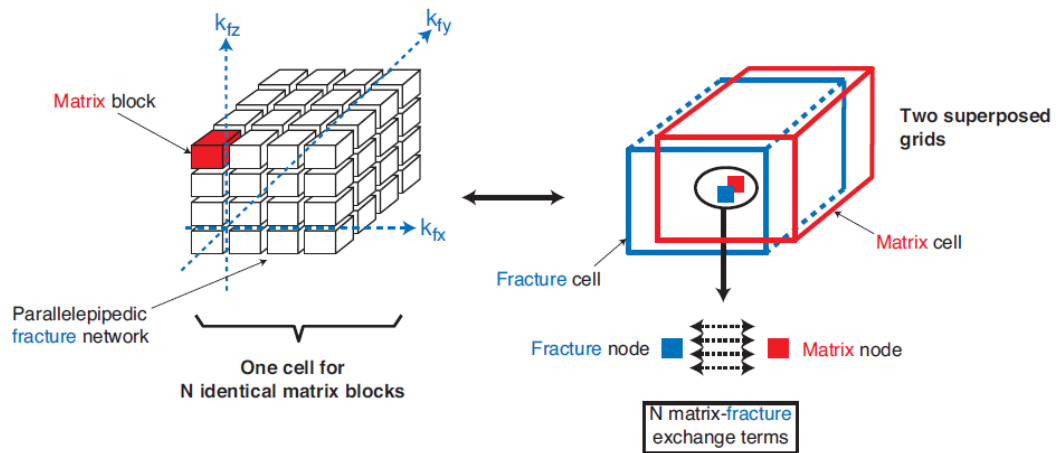
Figure 2.17: dual-continuum grid illustration. Each cell represents a grid block (Lemonnier and Bourbiaux, 2010)
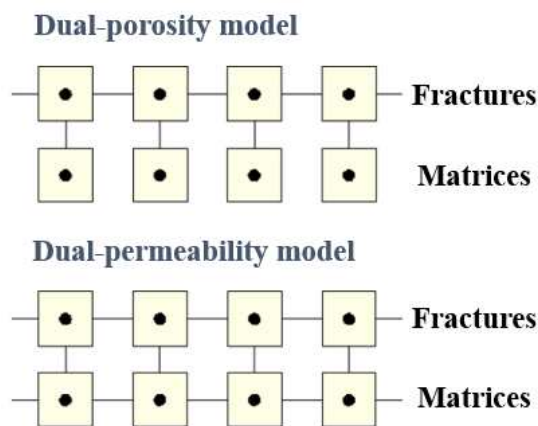
Figure 2.18: DP and DK models representation (modified from CMG, 2019)

The mathematical formulation for the mass balance equation of a DP model is described in Equations (2.7) and (2.8) for the fracture and matrix systems, respectively. In the DK model, the matrix-matrix flow term is added to Equation (2.8), resulting in Equation (2.9) for the matrix system. Additional equations for some items described in the mass balance equations are in Lemonnier and Bourbiaux (2010).

The following equations are for a unit volume of the reservoir for each component $\boldsymbol{k}$, including water (Lemonnier and Bourbiaux, 2010):

$$\frac{\partial}{\partial t}\left[\phi^f \sum_p \left(\rho_p^f C_{kp}^f S_p^f\right)\right] + div\left[\sum_p \rho_p^f C_{kp}^f \vec{u}_p^f + \vec{J}_{kp}^f\right] + \sum_p \left(\rho_p^f C_{kp}^f Q_p^f\right) - F_{kp}^{mf} = 0 \qquad (2.7)$$

$$\frac{\partial}{\partial t}\left[\phi^m \sum_p (\rho_p^m C_{kp}^m S_p^m)\right] + \sum_p (\rho_p^m C_{kp}^m Q_p^m) + F_{kp}^{mf} = 0 \tag{2.8}$$

$$\frac{\partial}{\partial t}\left[\phi^m \sum_p (\rho_p^m C_{kp}^m S_p^m)\right] + div\left[\sum_p \rho_p^m C_{kp}^m \vec{u}_p^m + \vec{J}_{kp}^m\right] + \sum_p (\rho_p^m C_{kp}^m Q_p^m) + F_{kp}^{mf} = 0 \tag{2.9}$$

where:

- The superscript f refers to the fracture system, the superscript m refers to the matrix system, and the subscript p refers to the phase
- ϕ^f and ϕ^m are the fracture and matrix porosity
- F_{kp}^{mf} is the matrix-fracture mass flow rate (or transmissibility factor) of component k in phase p per unit bulk volume of the reservoir
- Considering $M = f, m$:
  - C_{kp}^M and S_p^M are the mass fraction of component k in phase p and the saturation of phase p
  - ρ_p^M is the density of phase p in the medium M
  - $\vec{u}_p^M$ is the velocity of phase p in medium M. It is usually calculated from the Darcy´s law utilizing the upscaled permeability
  - $\vec{J}_{kp}^M$ is the molecular diffusion and dispersion flux of component k in phase p in medium M
  - Q_p^M is the volumetric injection/production rate of phase p in medium M. The rate is positive in production and negative in injection

Warren and Root (1963) rewrote the transmissibility factor F^{mf} of Barenblatt et al. (1960) by considering the matrix block dimension (Equation (2.10)). The sigma factor (σ) is a geometric parameter which depends on the matrix block size. A variety of models for σ have been proposed in substitution of the Warren and Root (1963) equation (Equation (2.11) and (2.12)). The Gilman and Kazemi (1983) proposal consider a multiphase flow and the capillary and gravity forces, being another option available in commercial software (Equation (2.13)).

$$F^{mf} = -\sigma K^m \frac{\rho}{\mu} (p^f - p^m) \tag{2.10}$$

where F^{mf} is the transmissibility factor between matrix and fracture systems, σ the sigma factor, K^m the matrix permeability, ρ the fluid density, μ the fluid viscosity, p^f and p^m the fracture and matrix pressure (Lemonnier and Bourbiaux, 2010).

$$\sigma = \frac{4N(N+2)}{l^2} \tag{2.11}$$

where N is the normal sets of fractures (or the number of flow dimensions) varying from 1 to 3, and l is the characteristic dimension of heterogeneous region. If the matrix block sides are $x = a$, $y = b$, and $z = c$, l can be defined by the surface volume ratio. Equation (2.12) has an example for l when N is equal to 3 (Warren and Root, 1963):

$$l = \frac{2abc}{ab + bc + ac} \; for \; N = 3 \tag{2.12}$$

$$(\sigma k)_{GK} = 4 \left(\frac{k_{mx}}{a^2} + \frac{k_{my}}{b^2} + \frac{k_{mz}}{c^2} \right) V_b \tag{2.13}$$

where $(\sigma k)_{GK}$ is the sigma factor of Gilman-Kazemi multiplied by the matrix permeability for an anisotropic case; k_{mx}, k_{my}, and k_{mz} are the matrix effective permeability along x, y, and z directions; a, b, and c are the matrix block size; and V_b is the block volume (Gilman and Kazemi, 1983).

The dual-continuum models are a simplification of a real NFR, having limitations in describing the heterogeneities' properties, as permeability and connectivity (Ouenes and Hartley, 2000). Therefore, the parameters included in DP and DK models should be carefully defined.

2.4.2 Well model

In the numerical simulation, the well is a source or an outlet of fluids, having the well model responsible to connect the near well region to the reservoir. The objective of this model is to find a correlation so that the high-pressure gradient between the reservoir and the wellbore does not jeopardize the calculation of the simulated well flow rate and BHP, since there is a significant difference between the grid block dimension and the well radius (Ribeiro, 2010). The well model considered in this work for producer and injector wells is in Equation (2.14) for dual-continuum models, where the flow rate and BHP are dependent on the well block pressure and the productivity or injectivity index (PI).

$$q_l = \left(\sum_{i=1}^{n} PI_i(P_{blocki} - BHP)\right)_{matrix} + \left(\sum_{i=1}^{n} PI_i(P_{blocki} - BHP)\right)_{fracture} \quad (2.14)$$

where q_l is a phase total flow rate considering n well grid blocks for each system (matrix and fracture), PI_i is the productivity or injectivity index, P_{blocki} the well block pressure, and BHP the bottom-hole pressure (CMG, 2019).

The PI is the well capacity to produce or inject liquids and is calculated separately for both matrix and fracture systems. It depends on the well index (WI) and the phase mobility. Equation (2.15) has the description of PI and Equation (2.16) has the definition of phase mobility, which is the fluid relative permeability divided by the fluid viscosity.

$$PI_{si} = WI_{si} * phase\ mobility_{si} \quad (2.15)$$

where PI_{si} is the productivity or injectivity index for the system s (matrix or fracture) for each well grid block i and WI_{si} is the well index (CMG, 2019).

$$Phase\ mobility = \frac{K_r}{\mu} \quad (2.16)$$

where K_r is the fluid relative permeability and μ is the fluid viscosity (CMG, 2019).

The WI is the parameter responsible to connect the reservoir heterogeneities to the well model and is influenced by the grid-scale and by the system permeability properties (Equation (2.17)) (Ribeiro, 2010). The WI is calculated separately for the matrix and fracture systems in dual-continuum models, and it is constant in each well block layer, having its parameters unchanged during the simulation. Therefore, as the production starts, PI changes only with the phase mobility.

$$WI_{si} = \frac{2\pi \times K_{si} \times h_i \times wfrac}{ln\left(\frac{r_{ei}}{r_w}\right) + skin} \quad (2.17)$$

where, WI_{si} is the well index for the system s (matrix or fracture) for each well grid block i, K_{si} the well block absolute permeability, h_i the grid block thickness, $wfrac$ the well fraction (it determines the fraction of the well included in the well block), r_w the wellbore radius, and r_{ei} the well block effective well radius (CMG, 2019).

The WI depends on the effective well radius (r_e), and different equations of r_e have been proposed by the literature, specifying a variety of well models. The r_e corresponds to the radio which the well block pressure is the same of the well flowing pressure (Peaceman, 1978). In other words, it means the radio of the well control volume (Ribeiro, 2010). The model available in commercial software are usually the Peaceman (1983) proposal. Equation (2.18) has this model for a radial flux and for an anisotropic medium. This model can be used in 2D or 3D models.

$$r_{e_i} = 0.28 \left(\frac{\sqrt{d_i{}^2 k_j + d_j{}^2 k_i}}{\sqrt{k_i} + \sqrt{k_j}} \right) \tag{2.18}$$

where d_i and d_j are the grid block lengths, and k_i and k_j are the well block permeability, both in x and y directions respectively (Peaceman, 1983).

3 LITERATURE REVIEW

The objective of this chapter is to describe some relevant works related to DFN upscaling techniques and well calibration, showing how the present work is included in the cited studies.

3.1 DFN upscaling techniques

Effective fracture properties are calculated through different approaches, and the methods used in the DFN upscaling processes are not exclusive to DFN application. However, this section has techniques applied to DFN structures only.

Decroux (2012) has a critical literature review about the former references related to DFN upscaling, DP/DK models, and NFRs. This section of the literature review is focused on works with methodologies and conclusions that directly contribute to this work, executing a comparison among the methods Oda, Flow-based, and Oda corrected.

Starting by describing works that compare Oda and Flow-based methods, Correia et al. (2012) have the objective to improve the well productivity accuracy by proposing a conjunction of well-refinement with conventional fracture upscaling technique. They use a carbonate fractured reservoir for the model characterization, defining constant matrix petrophysical properties and a DFN with sub-seismic faults and diffuse fractures, three cases are built. A DP simulation model in a fine grid (cell dimension of 5x5x5m) is used for the reference case and DP coarse models with and without well-refinement are used for comparison, all models utilize the Oda method for the fracture upscaling and are in 3D dimension. Moreover, the Flow-based method is tested in the coarse conventional grid (without refinement) and validation of the reference model is performed by comparing it with a DFN simulation utilizing SP models (2D dimension).

The results are processed for field dynamic data and field water saturation maps. They achieve their objective by demonstrating a better performance of the hybrid grids (with well-refinement) when having lower fracture intensity. However, the Flow-based application (without refinement) yields a similar result to the reference case. They concluded that the Oda method is appropriate only for high-dense and connected fracture networks and that the Flow-based is more accurate despite being CPU time expensive. They also noticed that the Oda is sensitive to the grid block size.

Ahmed-Elfeel and Geiger (2012) aim to assess the uncertainties caused by different DFN upscaling methods. Their motivation is the negative impact that those methods and their

grid dependency can cause on the oil recovery prediction of an NFR. They use a real reservoir dataset to build synthetic cases, with the objective to analyze the scale dependency of DFN upscaling methods (Oda and FB) and to demonstrate the impact of the DFN upscaling on final reservoir simulation results. They compare Oda with FB (linear pressure, constant pressure, and periodic) results in static and dynamic analysis:

- **Static analysis:** they do a variation in the fracture length and fracture intensity in two grid block sizes (a fine grid block of 30x30m and a coarse grid block of 120x120m). They observe that an increase in fracture connectivity (by increasing the fracture length and/or the fracture intensity) produces an increase in the similarities of the fracture permeability between the Oda and FB method, having more impact of the fracture intensity (P32) in the coarser grid.

- **Dynamic analysis:** they test two DFNs with high fracture connectivity (similar fracture permeability between Oda and FB) in the same block sizes of the previous tests. They simulate in an SP model and the upscaling changes occur in a sector model around the producer well (2000 ft of diameter). The results show less sensitivity of the grid change and the DFN method in the DFN with higher connectivity. However, the Oda results tend to have a higher well production rate than the FB results, even if the fracture permeabilities are similar.

Their main conclusions are that the choice of the grid-scale and the DFN upscaling method has a significant impact on the oil recovery estimates. Therefore, the uncertainty in this process can mask the geological uncertainties. However, the degree of the impact depends on the DFN connectivity. They also propose a calibration methodology which is discussed in the next section (section 3.2).

Decroux (2012) compare different fracture permeability upscaling methods to test their accuracy. They test the Oda, the FB (no flow and linear pressure), and a type of numerical method called IBPOS (Image Based Periodic Object Simulation). Two DFN structures are created in two-dimension with constant fracture properties each. The DFNs are simulated explicitly for the reference case and later they are upscaled with the cited upscaling methods to compose simulation models of type 1 of NFR (Figure 2.4) in Nelson's classification (the matrix medium is set with zero permeability). The simulation models with "effective properties" are considered as "single-medium" models and have a "well zone" with homogenous porosity and permeability values to increase the connectivity of the wells with the fractured medium (Figure 3.1). They use two different grids for comparison (one with 81 cells and the other with 729 cells).
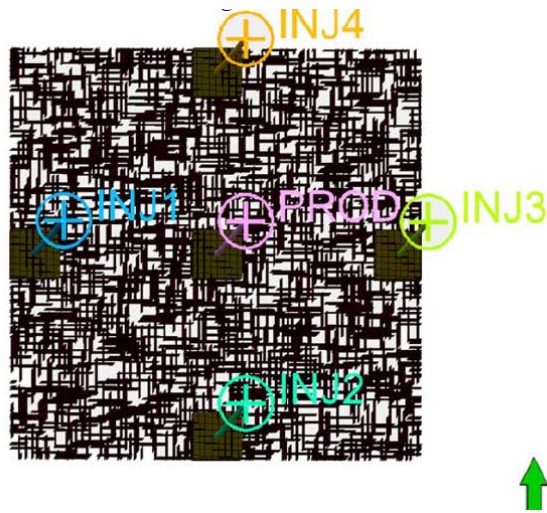
Figure 3.1: production strategy with the "well zone" for the homogenous model (Decroux, 2012)

The static and dynamic results and discussion are:

- **Static results (fracture permeability analysis considering the mean, standard deviation, and histograms in both directions)**: they show that generally, the Oda yields the biggest fracture permeability and the IBPOS the lowest, but between the FB boundary conditions, the no-flow gives the lowest permeability values. By reducing the grid cell dimension, they observe an increase in the fracture permeability standard deviation, maintenance of the mean value for the Oda method, and a similarity between the FB boundary condition results.

- **Dynamic results (oil and water production rate)**: the highest rates are achieved with the model built with the Oda method, and the lowest rates are achieved with the IBPOS and no flow methods. The best matches with the reference case are for these last two methods, this is explained by the very low connectivity of the fracture network, showing that the Oda method is not appropriate in this case. The results for the Oda method between the two tested grids are similar, and this is explained by their same fracture permeability mean. Similar results for water and oil rates are observed for the linear and no flow for the thinnest scale, as they also have similar fracture permeability in this grid. However, the authors affirm that reducing the grid-scale does not guarantee a more accurate flow rate result, as it can lead to an overestimation of the fracture connectivity (Figure 3.2).
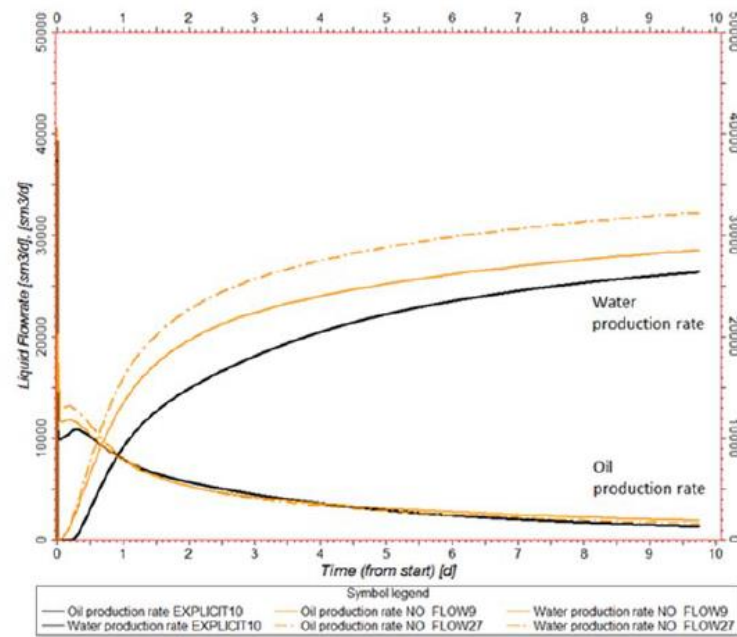
Figure 3.2: liquid rate for the heterogeneous model with the no flow method for the thinnest grid (solid orange line) and for the coarse grid (dashed orange line) and for the reference case (black line) (Decroux, 2012)

In another test, the authors compare the cited methods with DFM models results, but this is not the focus of this literature review.

Tueckmantel et al. (2013) propose a methodology to capture the DFN connectivity before applying the conventional DFN upscaling methods. They cite the advantages and disadvantages of the Oda and FB methods, highlighting that none of them can capture the fracture network connectivity properly if used in the DFN for the entire field. Moreover, as Ahmed-Elfeel and Geiger (2012), they cite the necessity to minimize the impact of these methods on the simulation of fluid flow, well rates, and reservoir development decisions.

The upscaling methods tested are the Oda and FB (they do not specify the boundary conditions). After the DFN modeling, they perform a cluster analysis (Figure 3.3), where the blue color represents fractures without connectivity and the other colors represent fractures with connectivity (each color is a cluster of homogenous fractures). Their results show that the Oda method considers all network connected, generating inexistent connectivity in blue areas of Figure 3.3. On the other hand, the FB results underestimate the size of the cluster with connectivity. Therefore, the authors propose an upscaling with the Oda method just in the clustered areas and a separated upscaling of the background fractures, which could be incorporated in the simulation model as a multiplier in the matrix medium. Finally, they do a comparison of the final model (with the proposed modifications) with the input DFN to assure that the fracture connectivity is well represented.
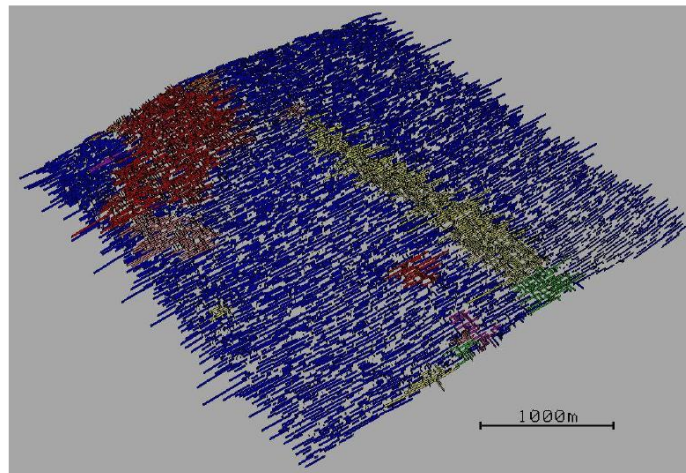
Figure 3.3: DFN with the cluster analysis. The DFN has two perpendicular sets of fractures. The fractures in blue have no connectivity with other fracture and fractures with other colors are connected to fractures of their color (Tueckmantel et al., 2013)

Pires (2016) and Haridy et al. (2019) also discuss the Oda Corrected method besides Oda and/or FB. Pires (2016) proposes a methodology to compare different upscaling methods (for matrix grid and DFN) to calibrate a coarse model according to a reference case, obtaining the most appropriate upscaling methods. The reservoir model is the Benchmark UNISIM-II, a synthetic fractured carbonate reservoir. However, only a region of the Unisim-II is used according to Figure 3.4. The CFU concept is used and two CFUs are defined, one with a Super-K layer and other without. The selected parameters for validation are permeability histograms, water cut, reservoir pressure, recovery factor, and oil rate. Diverse matrix upscaling techniques are tested for the porosity, permeability, and net to gross. For the DFN, the Oda and Oda Corrected methods are compared. The calibration of the dynamic properties is obtained through the Corey coefficients for the relative permeability.

The selected upscaling methods for both CFUs are the harmonic-arithmetic mean for the matrix permeability and the Oda Corrected for the fracture permeability. The Oda and Oda corrected did not have many different results (for static and dynamic parameters), however, the ODAC had a faster upscaling and provided a better match with the reference case. Pires (2016) also concluded that the upscaling study per CFU assisted the well completion layers selection.

Haridy et al. (2019) have the main objectives to study and compare the performance of different DFN permeability upscaling methods in different connectivity scenarios. Their data set are from the Teapot Dome field, and the DFN upscaling methods are the Oda, FB (linear pressure boundary condition), and Oda Corrected. They build different DFN scenarios, performing two sensitivity analyses focused on the fracture length and fracture intensity. The first sensitivity analysis has the objective to validate the ODAC method by comparing it to the

FB method. This first test also includes a connectivity analysis for all permeability results of the DFN upscaling methods. The second sensitivity analysis compares ODAC with Oda method utilizing 2 sets of DFN realizations (one varying the fracture intensity and the other varying the fracture length). Finally, the dynamic performance of Oda and ODAC are measured in a dual-porosity simulation model. The grid description is in Table 3.1.
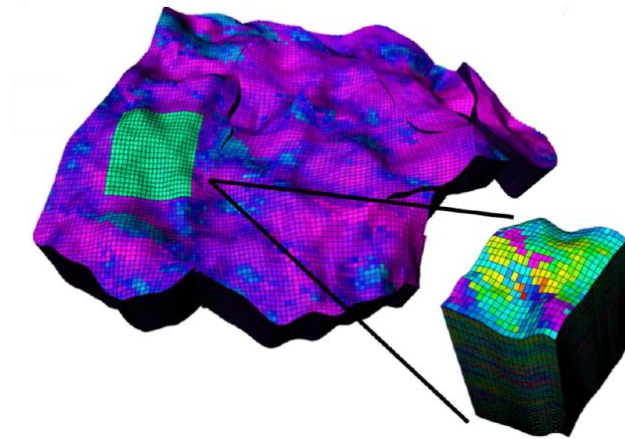
Figure 3.4: Unisim-II sector utilized in the tests (Pires, 2016)

Table 3.1: grid characteristic utilized in Haridy et al. (2019)

	X	Y	Z
Number of cells	39	91	18
Grid size (m)	73.3	83.7	7.4

The main results obtained by Haridy et al. (2019) are summarized as follows:

- **ODAC validation (comparison with FB)**:
  - Effect of fracture intensity (analysis of the fracture permeability): for low connectivity, ODAC and FB have differences in order of magnitudes, but for certain connectivity, they have similar values.
  - Effect of fracture length (analysis of the fracture permeability): a bigger similarity between FB and ODAC is observed in the higher fracture intensity scenario. The ODAC permeability increases as the fracture length increases. However, for the FB, the permeability loses the fracture length dependency from a certain value, and ODAC do not capture this behavior accurately.

- **ODAC comparison with Oda**:
  - Effect of fracture intensity and fracture length: the agreement between methods increases with the fracture intensity. This is a result of an increase in the connectivity, which causes a decrease in the correction factor of the ODAC. The

agreement between methods also increases with the fracture length. Moreover, for the vertical permeability, both methods have equal results for all intensity scenarios (in the vertical direction the fractures have a high length ratio, which leads to the elimination of the correction factor for length and intensity in the ODAC).

○ <u>Dynamic behavior in different fracture intensity scenarios (production rate and water cut)</u>: Oda underestimates the water cut, as it has a fixed anisotropy ratio (Kv/Kh) for not account the fracture length changes (it considers all fractures with infinite length). In opposite, ODAC has a bigger anisotropy ratio and it can capture the channeling effects that are common in NFRs.

According to the percolation threshold, which is "the minimum connectivity at which a fracture network can permit flow," the recommendations of Haridy et al. (2019) for the appropriate DFN upscaling methods in the studied case are:

- <u>For values below the percolation threshold (fracture intensity below 0.01 1/ft)</u>: FB
- <u>Moderate fracture intensity (0.05-0.11/ft):</u> ODAC
- <u>Fracture intensities higher than 0.1/ft:</u> any method can be used

The impact of the grid-scale in the DFN upscaling methods is concluded by some of the cited literature, as Correia et al. (2012), Decroux (2012), and Ahmed-Elfeel and Geiger (2012). Wang (2008) and Ghahfarokhi (2017) also discuss this issue. Wang (2008) affirms that the permeability upscaling results have a strong dependency on the grid block size, besides the dependency on fracture geometry and on the simulator type (SP, DP, or DK). Ghahfarokhi (2017) study the grid orientation dependency on the ODAC method and concludes that this dependency occurs for different fracture orientation scenarios. The grid size and grid orientation dependency lead to one of the motivation topics of this work, that the application of the DFN upscaling in high fidelity models does not necessarily provide the most precise results.

3.2   Well calibration in simulation models of NFR

This section is focused on describing methodologies used in the well calibration of NFR simulation models. The methods are modifications in the Well Index (WI), utilization of Local Grid Refinement technique (LGR), and utilization of well-test data.

Ding et al. (2006) propose a near-well DFN upscaling procedure to increase the accuracy of the well productivity in NFRs. The proposed methodology is based on a single-phase pseudo-steady-state-flow solution simulated in the near-well region in a DFN model. The

single-phase flow equations are analogous to the work of Barenblatt et al. (1960), but they are applied directly in the fracture network to calculate the effective fracture permeability. The upscaling method is combined with a well modeling approach to better represent the flow around the well. The WI utilized in the fractured medium for a well block $\boldsymbol{O}$ is in Equation (3.1).

$$WI_{f,O} = \frac{Q_O}{P_O - P_{w,O}}$$ (3.1)

where $\boldsymbol{WI_{f,O}}$ is the well index for the fracture in the wellblock O, $\boldsymbol{Q_O}$ is the well flow rate calculated from the DFN model, $\boldsymbol{P_O}$ is the average fracture pressure in the wellblock, and $\boldsymbol{P_{w,O}}$ is the wellbore pressure.

Finally, they incorporate the calculated effective fracture permeability and well indices in a dual-porosity simulation model, for validation in three different fracture networks and grid-block scenarios. They compare the proposed method with a DFN simulation, used as a reference case, and with a conventional DP model constructed with the FB method (linear pressure boundary condition) with Peaceman's formula (Equation (2.18)). The error among the three models is compared using PI values, pressure curves, and pressure derivative curves. The proposed methodology has a significant match with the reference model in the long term for all validations, but not in short terms for two validations.

To increase the accuracy of the flow prediction due to the impact of the different DFN upscaling approaches and its dependency on the grid block size, Ahmed-Elfeel and Geiger (2012) propose a Discrete Fracture and Matrix (DFM) modeling to find an optimum combination of grid block size and DFN upscaling method. The methodology workflow is in Figure 3.5. They do not account for the matrix permeability and use an SP simulation model for a DFN constructed with data of a fracture onshore reservoir.

The results of the combination of DFN upscaling methods, grid block sizes, and conventional grid upscaling are analyzed and compared to a DFM model used as a reference. Their results indicate that the use of DFM models can assist the analysis of the DFN grid-scale dependency and can indicate the optimum grid-scale and DFN upscaling method. Overall, for the studied cases, the Oda method overestimated the results when compared to the DFM, and the FB method is more likely to be grid-sensitive in the open boundary conditions (linear pressure, constant pressure, and periodic). The concern about the application of this methodology is the high computational cost of a DFM model, which jeopardizes its use in

commercial software and full-field applications. They mitigate this issue by using steady-state single-phase simulation in a sector scale.
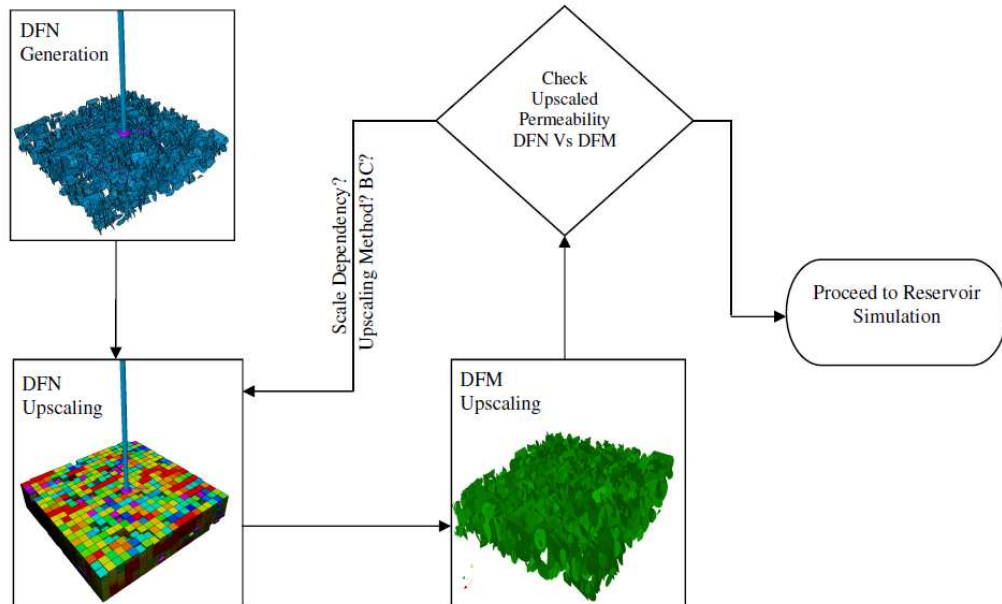
Figure 3.5: methodology workflow proposed by Ahmed-Elfeel and Geiger (2012)

As cited in the previous section, the results obtained by Correia et al. (2012) show that the application of the near-well refinement combined with the Oda method can improve the accuracy of the well productivity index calculation in fracture networks (with high fracture aperture variability or lower fracture intensity). They also affirm that conventional grids (medium-fidelity models) may produce the wrong well index when the fractures do not cross the near-well location, showing the relevance of the grid refinement around the well.

Furthermore, the same authors developed a work in 2018 (Correia et al., 2018) integrating the LGR technique in high permeability layers ("super-k" layers) besides the well locations. They associate the LGR with upscaling techniques to better represent highly laminated and fractured reservoirs in the flow simulation. They compare a coarse grid with a high-fidelity model used as reference, UNISIM-II-R benchmark, and study single-porosity (SP) and dual-continuum models. They use the flow-based method as an upscaling procedure for the SP model and the Oda method in the dual-continuum cases.

In their conclusions, for the SP case, they discuss that the LGR applied after the upscaling process produces worst results than when it is used before the upscaling. Besides, the grid corners of the reference model should be aligned with the coarse model to produce better results. The LGR in the location of the wells and in the "super-k" layers produced better results. For the dual-continuum tests, the LGR could not be applied with DFN upscaling methods due

to geostatistical software limitations. However, their tests could conclude that the Oda method is only applicable for highly connected DFNs.

Finally, a well calibration could also be achieved by the calibration of the discrete fracture network. Lamine et al. (2017) perform the calibration of the DFN around the well location utilizing PTA data tests, reducing the uncertainty of the fracture data to utilize the calibrated DFN in forecast simulation.

3.3 Final remarks

This section has the objective to connect the present work with the discussed references. The cited works affirm that there are differences among DFN permeability-upscaling outputs and the associated grid-scale, demonstrating that these differences should be evaluated to reduce the impact in the reservoir production forecast. This conclusion shows the relevance of this dissertation, as this is the main objective of this study. Besides, the successful use of well calibration methodologies in NFR simulation models provides a background to the execution of the proposed methodology.

Additionally, this dissertation considers some aspects that are not simultaneously included in the cited literature and should be deeply studied. This work utilizes a 3D reservoir, considering the NFR heterogeneity in the vertical direction. Real data and fracture uncertainty are utilized, incorporating a higher heterogeneity to the NFR model. The integration of the matrix influence in the flux by utilizing a DP or DK model makes it possible to represent different types of NFR reservoirs according to Nelson's (2001) classification. The well representation proposal focuses on well geometric parameters modification, not requiring long time simulation results, and utilizes a calibration that considers DFN upscaling methods available in commercial software.

Moreover, the cited works do not focus on the analysis of the impact of DFN upscaling methods in well behavior. Motivating the present work to deeply study the well productivity and injectivity behavior, which can directly contribute to the development phase of the reservoir, not depending on the history matching process, DFN validation, or dynamic data availability, as observed in the cited references.

4 METHODOLOGY

This chapter aims to describe the steps of the methodology divided into three main sections: general methodology, specific methodology, and field tests. The first contains the main steps to increase the representation of new wells in simulation models of NFR. The second section describes specific implementations used in this work to develop the general methodology, fulfilling the main objectives of this work. A third section focusses on describe the field scale application to study the impact of the DFN upscaling methods in the field production. Finally, a fourth section has the case studies adopted to execute the methodology and the field scale application.

4.1 General methodology

The general methodology (Figure 4.1) describes the basic steps to construct, simulate, interpret, and calibrate the well performance in a dual continuum simulation model considering the Characteristic Flow Unit (CFU) concept.
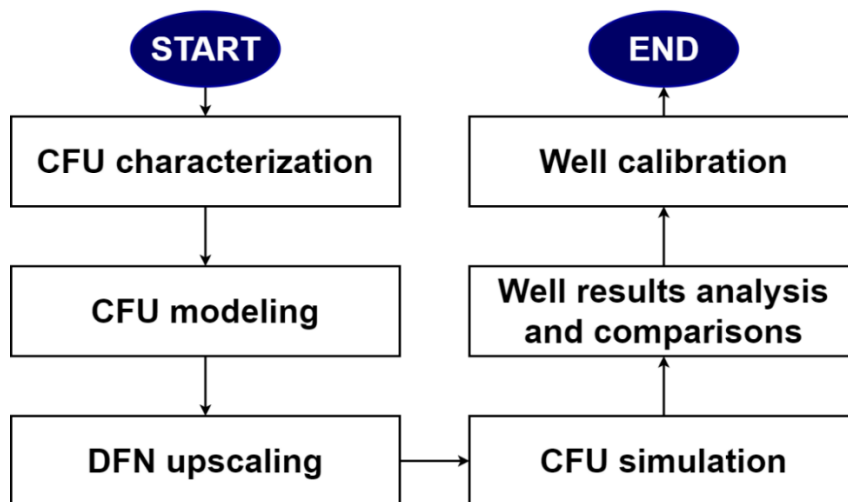
Figure 4.1: general Methodology Workflow

4.1.1 CFU characterization

As the objective of this work is to build a representative NFR CFU, the CFU characterization is done synthetically with properties from the literature and real data due to lack of information.

This step is based on the following CFU information:

- Classification of the CFU type according to Nelson's (2001) classification

- Geological matrix petrophysics of porosity and permeability for the reservoir rock types (RRT)
- Multiscale heterogeneities characterization:
  - Definition of heterogeneities types: faults, fractures, vugs or karsts.
  - Characterization of heterogeneities properties: length, orientation, density, aperture, and intrinsic permeability.

4.1.2 CFU modeling

The CFU modeling step is responsible for the 3D construction of the geological matrix grid and the fracture network.

For the matrix grid modeling, firstly it is selected the fidelity grid-scale. Then, a simple and cartesian grid is built with the characterized matrix petrophysics.

The Discrete Fracture Network (DFN) technique is used to model the fracture network utilizing the characterized multiscale heterogeneities. The DFN fracture sets are modeled deterministically or stochastically according to the property's uncertainties.

4.1.3 DFN upscaling

The DFN upscaling step provides the fracture grid values of effective permeability, fracture spacing (block sizes), and porosity for the dual-continuum simulation model. Therefore, the upscaling is performed in the same fidelity grid scale of the matrix.

The permeability upscaling is executed with a variety of methods, and only the diagonal permeability tensor is utilized in the simulation model input. The porosity upscaling is done utilizing Equation (2.3), and the block size is calculated with statistical laws.

4.1.4 CFU simulation

For this step, simulation models are built for each fidelity scale with each DFN upscaling method, utilizing the matrix and fracture properties resulted from the "CFU modeling" and "DFN upscaling" steps. The following parameters are also defined:

- Dual-continuum model type (DP or DK) according to CFU classification
- Sigma factor equation
- Simulator type: black oil or compositional
- Reservoir initial conditions of pressure and saturation
- Reservoir rock and fluid data
- Well types and well boundary conditions

- Production strategy

4.2 Specific methodology

According to the main and specific objectives of this work, the specific methodology considers three main particularities:

1) Utilization of the same constant geological matrix properties for all tested cases to concentrate the attention in the effect of heterogeneities, isolating the effect of fracture upscaling (CFU characterization step).

2) Variation of the fidelity scale (CFU modeling step), to fulfill the first and the second specific objectives.

3) Variation of DFN permeability-upscaling methods for a unique DFN (DFN upscaling step), to fulfill the first and the second specific objective.

The next sections describe in detail each one of these implementations and the last two steps of the general methodology workflow (Figure 4.1).

4.2.1 Matrix constant properties calculation

From the reservoir characterization phase, different rock types in the reservoir are defined. For the matrix constant properties calculation, it is proposed the selection of one RRT followed by the construction of porosity and permeability histograms utilizing well-log data of the selected RRT. Lastly, the constant value of porosity and permeability are approximations of the most frequent value in each histogram.

4.2.2 Model fidelities scales

For the same model dimension of 600x600x12m, three fidelity scales are used for the tests (Figure 4.2 has an illustration of them):

- **High-fidelity model (HFM)**: the thinnest grid possible to run a flow-based upscaling for the available computational resources;

- **Medium-high fidelity model (MHFM)**: a possible dimension adopted by the geologists in the reservoir-modeling phase;

- **Medium fidelity model (MFM)**: considered here the scale usually used in reservoir simulation studies in real-field applications, as it has suitable running time and accuracy. This is the scale adopted for the well calibration step.
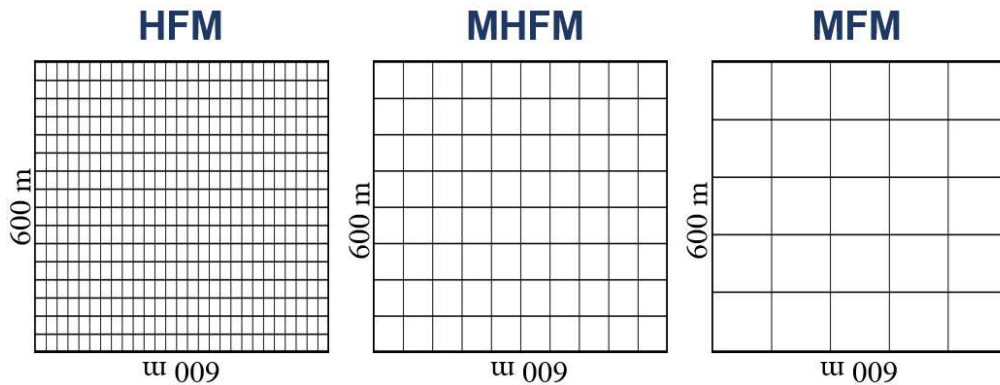
Figure 4.2: illustration of the three fidelity scales and the model dimension

4.2.3   DFN upscaling methods

Three DFN permeability-upscaling methods are tested: Oda, Oda corrected (ODAC), and Flow-based (FB) with four boundary conditions. Each FB boundary condition is referred as LP (linear pressure), CP (constant pressure), NF (no flow), and PD (periodic).

4.2.4   Well results analysis and comparisons

In this step, the objective is to identify what method and what scale cause the least and the most impact on well behavior. Since the simulation models are built for all three fidelity scales and all six DFN upscaling methods, a total of eighteen simulation models are used.

The nomenclature for each model is the CFU number, followed by the scale fidelity abbreviation, and finished with the DFN upscaling method. For example, an MFM built with the FB method (PD boundary condition) for a random CFUX is referred as CFUX MFM PD.

The analysis uses static and dynamic parameters of producer and injector wells:

- **Static parameters:** well block fracture effective permeability and well index (WI)
- **Dynamic parameters:** flow rate and bottom hole pressure (BHP)

These parameters are analyzed in two comparison sets, one (1) to observe the impact of the method change through the same scale, and other (2) to observe the scale-change sensitivity within each method. Comparison (1) considers the fracture effective permeability, flow rate, and BHP, and comparison (2) considers the dynamic parameters. A schematic picture of these comparisons is in Figure 4.3. To perform these comparisons, some considerations of each parameter are done to have a representative value of them in each well.
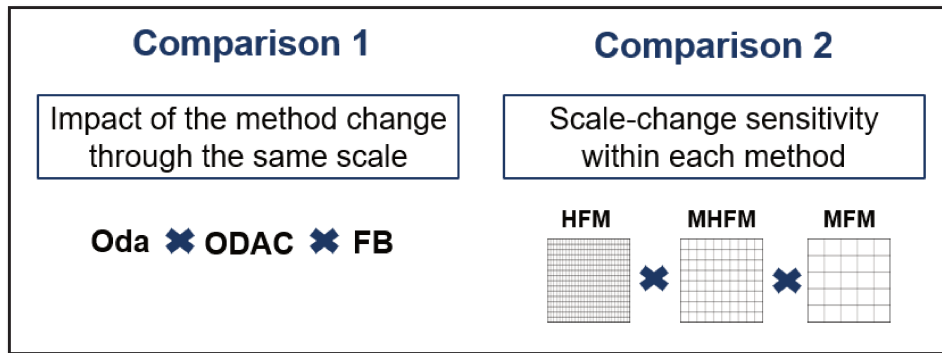
Figure 4.3: illustration of Comparison (1) and (2) analysis

The utilized flow rate and BHP data are the values of the first registered seconds of production when it is possible to analyze the influence of the well block heterogeneities. As the production starts, changes in pressure and phase saturations cause a variation on fluids mobility and consequently on PI values (Equations (2.15) and (2.16)). Nevertheless, before the simulation starts, the simulator considers a pre-calculated PI with the WI (constant value through the simulation) and the initial phase mobility in each system. This initial phase mobility is the same for all simulation models because the well pressure and fluids saturation are the same. Therefore, as soon as the production starts (first seconds), when the well block pressure and PI have slightly changed, the well block heterogeneity influence represented by the WI can be analyzed on the well's flow rate and BHP (Equation (2.14)).

For the fracture effective permeability, an average value calculated by Equation (4.1) (Rosa et al., 2006) is used to have a representative value in each direction. Equation (4.1) is used for a parallel flow in heterogeneous rock and it considers the same pressure drop in all layers. For the first seconds of production, similar pressure drops in all well layers are expected, allowing the use of Equation (4.1) in comparison (1).

$$\overline{K} = \frac{\sum_{i=1}^{n} k_i A_i}{\sum_{i=1}^{n} A_i} \tag{4.1}$$

where $\overline{K}$ is the average permeability, k_i the well block permeability in layer i, and A_i the well block area opened to the flow in layer i. The equation considers "n" number of layers.

Besides those comparison sets, a deeper analysis of the WI is performed to observe how the WI is impacted by the method change, and how it is related to dynamic data. A sum of WI of all well block layers is used as a representative value for each well.

4.2.5 Well calibration

The objective of this section is to present a methodology to test well representation proposals by calibrating producer and injector wells of a medium-fidelity model aiming to fulfill the third specific objective of this work.

The model selected for calibration is a medium-fidelity model built with the Oda method (CFUX MFM ODA). The MFM is the most used fidelity scale in reservoir simulation studies and Oda is the frequent method adopted by the literature in DFN-permeability upscaling studies.

The reference model is modeled according to the previous results conclusions, with a combination of the least impacted scale of comparison (1) with the least impacted method of comparison (2). However, it is important to mention that the "reference model" is not necessarily a reference, but a model that causes the least variability on flow rate and BHP.

Three calibration methodologies are tested, and they focus on WI modifications, as WI connects the reservoir heterogeneities to the well model (Ribeiro, 2010). The calibration is measured by the flow rate and BHP results for the first registered time step and a relative difference (RD) is used to monitor the results (Equation (4.2)).

$$Relative\ difference\ (\%) = \frac{Value_{CFU1\ MFM\ ODA} - Value_{reference}}{Value_{reference}} x100 \qquad (4.2)$$

The three proposed methodologies are represented in Figure 4.4 and described in the next paragraphs.

Methodology (1) refers to the replacement of the WI of the CFUX MFM ODA by the reference model's WI in the fracture system for each well.

The theoretical explanation for this method can be described by observing the well model equation (Equation (2.14)) for the first-time step. In the first seconds of production, both models tend to have a similar P_{block} for any well, a similar BHP for a producer well, and a similar q for an injector well, considering that the well boundaries for BHP (producer) and q (injector) are the same for all models and are determined previously. Therefore, the differences in q (producers) and in BHP (injectors) are more influenced by the PI parameter. As the phase mobility (Equation (2.16)) does not have a significant variation during the first seconds, the calibration of q and BHP for the wells in the CFUX MFM ODA should be obtained by utilizing the same WI of the reference model. The execution of Methodology (1) has the following workflow:

1) Verification of similar values of P_{block}, BHP (producer), and q (injectors) between the CFUX MFM ODA and the reference model using Equation (4.2)

2) Replacement of the CFUX MFM ODA's WI of the fracture system by the reference model's WI: construction of CFUX MFM ODA1 simulation model

3) Simulation of the new model

4) Analysis of the relative difference for the flux rate and BHP using Equation (4.2)
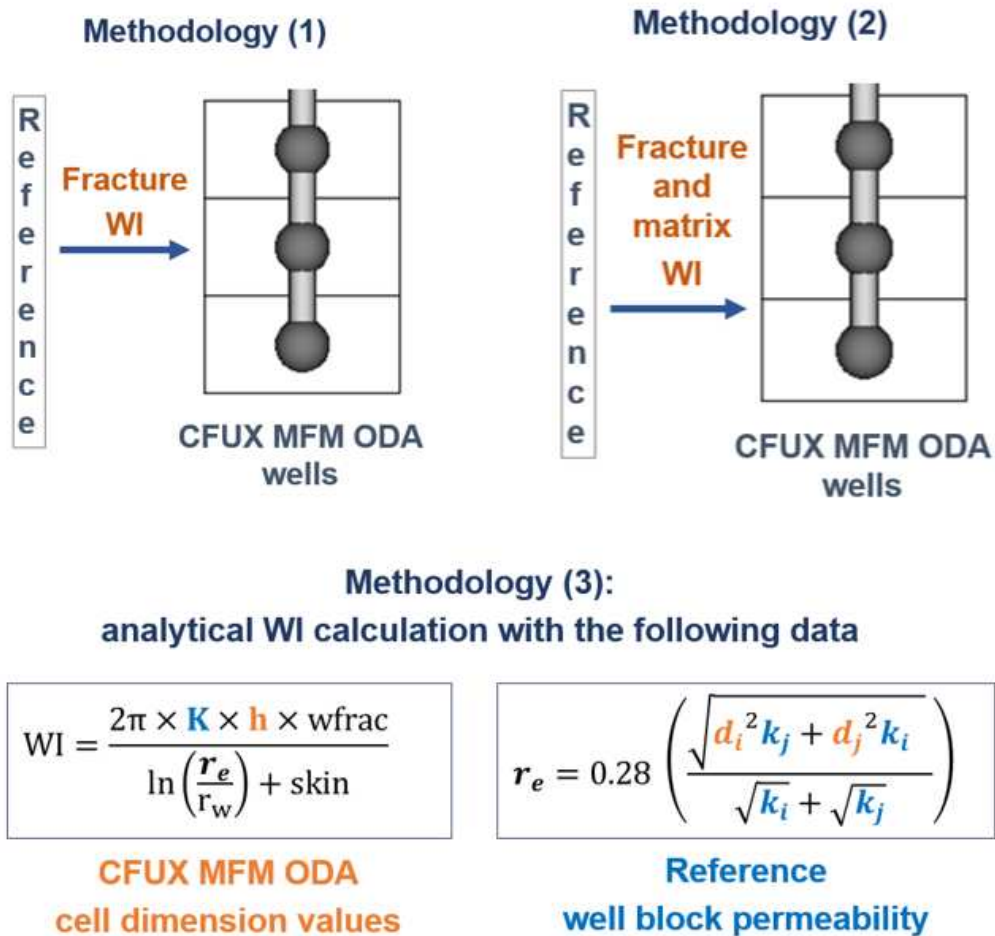
Figure 4.4: illustration of the three calibration methodologies

Methodology (2) refers to the replacement of the WI of the CFUX MFM ODA by the reference model's WI in the fracture and matrix systems. As this methodology is an extension of Methodology (1), it has the same theoretical explanation and workflow. The difference is in step 2, as the WI substitution occurs in the fracture and matrix systems, constructing the CFUX MFM ODA2 simulation model.

Methodology (3) pursues the isolation of well block dimension influence in the WI by calculating analytically the WI for the new MFM model (CFUX MFM ODA3). This methodology considers the WI equation (Equation (2.17)) and the equivalent radius of

Peaceman's (1983) model (Equation (2.18)). The calculation of the WI and r_e considers the cell dimension of the CFUX MFM ODA and the well block permeability of the reference model. Since the matrix permeability is the same for both models, this methodology is already applied in the matrix system; therefore, the matrix's WI is not changed. The execution of Methodology (3) has the following workflow:

1) Verification of similar values of P_{block}, BHP (producer), and q (injectors) between the CFUX MFM ODA and the reference model using Equation (4.2)

2) r_e calculation (Equation (2.18)) using the cell dimension of the CFUX MFM ODA and the well block permeability of the reference model

3) Absolute permeability calculation for each layer (K parameter of Equation (2.17)) according to the reference model data (Equation (4.3))

$$K = \sqrt{k_j * k_i}$$

(4.3)

4) Construction of the CFUX MFM ODA3 simulation model with the WI calculated with the outcomes of steps 2 and 3 utilizing Equation (2.17)

5) Simulation of the new model

6) Analysis of the relative difference for the flux rate and BHP using Equation (4.2)

At the end of the well calibration tests, the methodology which calibrates the flow rate and BHP data for producer and injector wells simultaneously is considered as the well representation proposal for new wells of a medium-fidelity model, and an extrapolation of 20 days of production is performed to observe if the calibration is valid for more time.

4.3   NFR field scale application

The NFR field scale application have the objective to evaluate the impact that the DFN upscaling method cause in the field production, validating the observations of the "well results analysis and comparisons" section (tests performed in a CFU).

The methodology proposed for the NFR field scale application has three steps of the general methodology (Figure 4.1): DFN upscaling, simulation, and simulation results analysis and comparison. However, the focus is not a CFU, but the entire field. The steps before the "DFN upscaling" step described in Figure 4.1, which refers to the characterization and modeling, are not performed and the case study is described in the next section. The matrix

properties are not constant and the CFU of the location of the wells should have the same CFU characteristics as the CFU tests for comparison.

The DFN upscaling step has the same description of sections 4.1.3 and 4.2.3, variating the DFN upscaling methods around the producer wells (until one layer of blocks around the well). The variation of the methods can also be done for injector wells. However, these tests intend to firstly analyze the impact of the DFN upscaling on the field productivity.

The parameters of the "simulation" step are according to the section 4.1.4 (CFU simulation).

The "simulations results analysis and comparison" step does not follow the similar section of the CFU tests (section 4.2.4), since the focus is not the well block results, but the field production data (oil rate and oil cumulative). Moreover, the analysis is not restricted to the first seconds', it considers short, medium, and long terms as defined in Table 4.1.

Table 4.1: production terms definition

Production term	Production time
Short	Until 6 months
Medium	6 months to 5 years
Long	After 5 years

4.4 Application: case studies description

The case studies selected are based on a carbonate Brazilian pre-salt field named Field C. The Brazilian pre-salt fields are located on the southeastern coast of Brazil between the states of Espírito Santo and Santa Catarina situated approximately 250 Km from the coast. They have around 2000 m of water depth with a maximum total depth of 7000 m (Iost, 2015). The proved reserves are in the order of 7.9 billion bbl (ANP, 2019), making the Brazilian pre-salt an auspicious area of exploitation and a study interest of geologists and engineers.

Field C is in Santos Basin, the most productive Basin of the pre-salt with seventeen productive fields which achieved a production mark of 2,487,445 boe/d in June of 2020 (ANP, 2020). The Santos Basin is localized along the coast of the States of Rio de Janeiro, São Paulo, Paraná, and Santa Catarina, covering an area of approximately 350,000 km^2 (ANP, 2017).

The petroleum system which corresponds to the pre-salt section of the Santos Basin is the Piçarras-Itapema/Barra Velha. The source rocks are from a lacustrine environment of Itapema and Piçarras formations, being organic-rich shales interleaved by carbonates. The reservoir rocks correspond to the carbonates of Itapema and Barra Velha formations. The hydrocarbon migration occurred due to the direct contact between the source and the reservoir

rocks in the rift section. The sealing rocks are the salt walls of the Ariri formation (ANP, 2017; Panpaterra, 2010).

4.4.1 CFU tests: Field C sector model

The selected CFU is represented in this work in small dimension models of 600x600x12 m. Thus, a specific region of Field C is selected to perform the CFU characterization; however, the methodology can be done in other areas of the Field C.

The sector model is localized around the most productive well of Field C (well C). This is a highly heterogeneous area with multiscale structures as fractures, vugs, karsts, faults, and build-ups. According to interpretations of the Production Logging Tool (PLT) tests of well C, these heterogeneities should have a significant influence in the flux.

4.4.2 NFR field scale application

For the NFR field scale application, the Field C is modeled in a grid with 2,467,644 cells. The grid scale is divided into two different sections, an upper zone with the grid dimension of 150x150x4 m and lower zone with a grid dimension of 150x150x10 m (Figure 4.5). The matrix porosity and permeability histograms are in Figure 4.6.
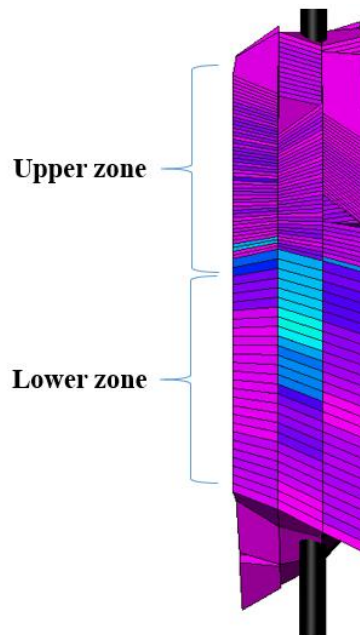
Figure 4.5: grid detail of Field C crossing the well P1
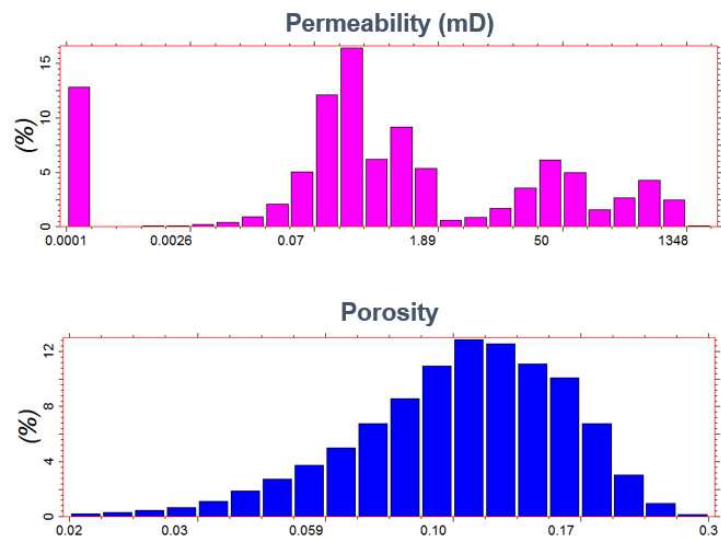
Figure 4.6: matrix permeability and porosity histograms for the Field C

The DFN utilized in the full field was provided for this work, the DFN was calibrated with dynamic properties and upscaled with the Oda method. The DFN utilized for the variation of upscaling methods around the producer wells has more fracture sets and it is not calibrated (a full field illustration of this DFN is in Figure 4.7). All producer wells are perforated in an area with fractures of medium and long size, having a similar characteristic of the CFU selected in the previous tests.

Figure 4.7: DFN utilized in the location of the producer wells

5 RESULTS AND DISCUSSIONS

This chapter covers the main results and discussion of all methodology workflow steps (Figure 4.1), ending with the well representation proposal for new wells in medium-fidelity models and the study in a NFR field.

5.1 CFU characterization

Since the selected reservoir has been recently studied, few data are available. Thus, other necessary information for the CFU characterization is collected from the literature.

5.1.1 CFU1 classification

A Pressure Logging Toll (PLT) test of Well C is used for the CFU selection. Only one CFU is used in this work (CFU1), but further studies can explore different CFUs of Field C. CFU1 represents the PLT most productive interval with fractures as the most flux contributor in a productive geological matrix. Therefore, CFU1 represents a type 3 of NFR according to Nelson's (2001) classification (Figure 2.4).

5.1.2 Geological matrix petrophysics (constant properties)

The selected RRT (RRT A) has the highest porosity and permeability values among the interpreted RRTs present in Filed C. RRT A is oil wet and its histograms are in Figure 5.1. The porosity value of 0.15 and the permeability value of 100 mD are used in this study.
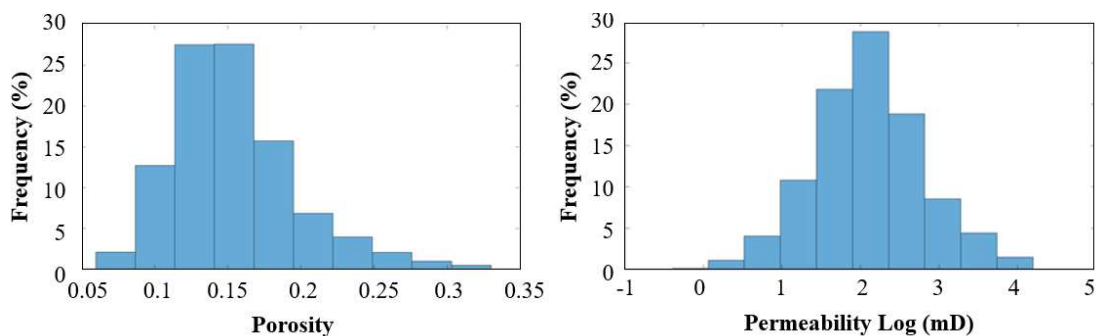
Figure 5.1: porosity and permeability histograms of the RRT A

5.1.3 Heterogeneities characterization

For CFU1, seismic and sub-seismic faults and two fracture sets are characterized. No vugs or karsts are considered in CFU1.

A total of fourteen faults are provided for this study. Their orientation and length were deterministically set using Field C data, the seismic faults were characterized by a geological team and the sub-seismic faults were characterized with the methodology described in De Lima et al. (2019). The main faults properties are in Table 5.1.

The faults aperture and intrinsic permeability are characterized by utilizing data from the literature. The aperture is constant and estimated with Equation (5.1) (Nelson, 2001). The K_f is interpreted from well-test data of Well C having a value of 3,321 mD, and D is estimated from the average of the distance between faults, having a value of 59 m. Therefore, Equation (5.1) yields a fault aperture of 0.0013 m, which is used in the cubic law equation (Equation (2.1)) to estimate the faults intrinsic permeability of 140,000 D.

$$K_f = \frac{(b)^3}{D}(8.35 \times 10^9) \qquad (5.1)$$

where K_f is the measured fracture permeability (mD), b the fracture aperture (cm), and D the fracture spacing (cm).

The fracture sets have many uncertainties in their properties, then, their characterization is done by setting values of mean, max, and min to each property. The fractures density (P32) and orientation are interpreted from BHIs of Well C and are provided for this study. This interpretation classifies two different fracture sets (N180 and N78) according to their orientation (Table 5.1).

The fracture sets apertures are from NFR analogs outcrops of pre-salt (Miranda et al., 2018) and their intrinsic permeability is estimated only in the DFN modeling phase by utilizing the cubic law equation (the mean intrinsic permeability values are in Table 5.3). It is important to mention that fracture intrinsic permeability calculated from literature apertures may result in extremely high permeability values causing numerical problems in the simulation model, more information in Appendix A. Finally, the fracture lengths are synthetic values which correspond to medium length fractures. Table 5.1 has a summary of the main fractures and faults data.

Table 5.1: summary of faults and fractures characterized properties

Fault and fractures	P32 Density (m^{-1})	Mean length (m)	Mean aperture (m)	Intrinsic perm. (x10^3 D)	Orientation	
					Mean dip (°)	Mean dip azi (°)
N78	0.25	20	0.0005	-	63	337
N180	0.25	50	0.0001	-	89	285
Faults	-	2,825	0.0013	140	85	171

5.2 CFU modeling

5.2.1 Model fidelity scales

All models have a total dimension of 600x600x12m and Figure 5.2 has the selected cell dimension for each fidelity scale. The HFM scale was the thinnest cell dimension capable to run a FB upscaling and the MHFM and MFM scale were selected according to a internal project, as the geologic model has the MHFM cell dimension and the simulation models have the MFM cell dimension.
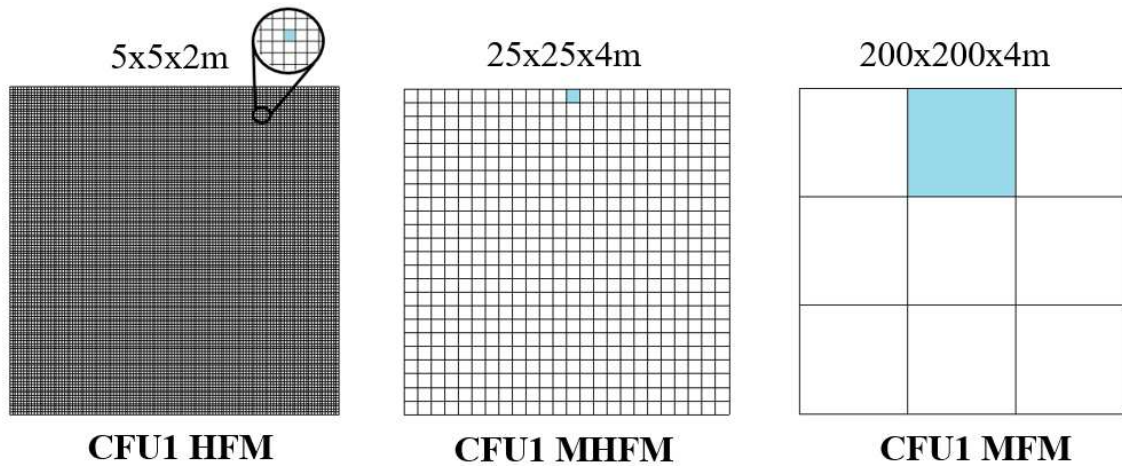
Figure 5.2: all fidelity scales with the cell dimension description

5.2.2 Matrix and DFN construction

The matrix grids for the three fidelity scales are in Figure 5.3 for the porosity property.
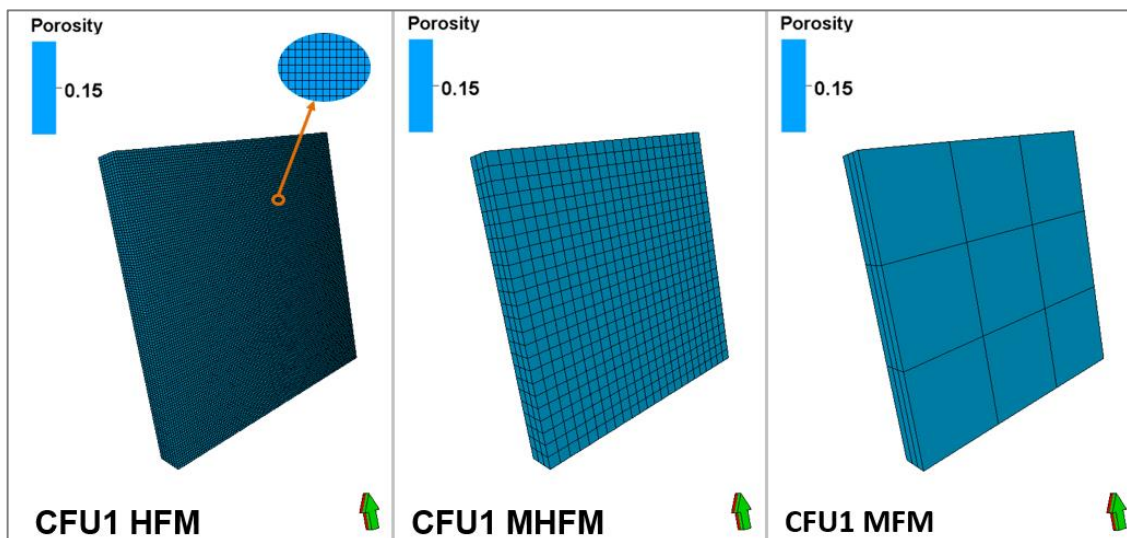
Figure 5.3: matrix grid for the porosity property in all fidelity scales

A unique DFN is built with the two fracture sets and all faults (Figure 5.4). The fractures are modeled stochastically due to their uncertainties and the faults are modeled deterministically. The fracture sets inputs are the same of Table 5.1, the distribution methods used in each property are in Table 5.2, and the output mean values are in Table 5.3.

Seismic and subseismic Faults   **N78 fracture set**   **N180 fracture set**
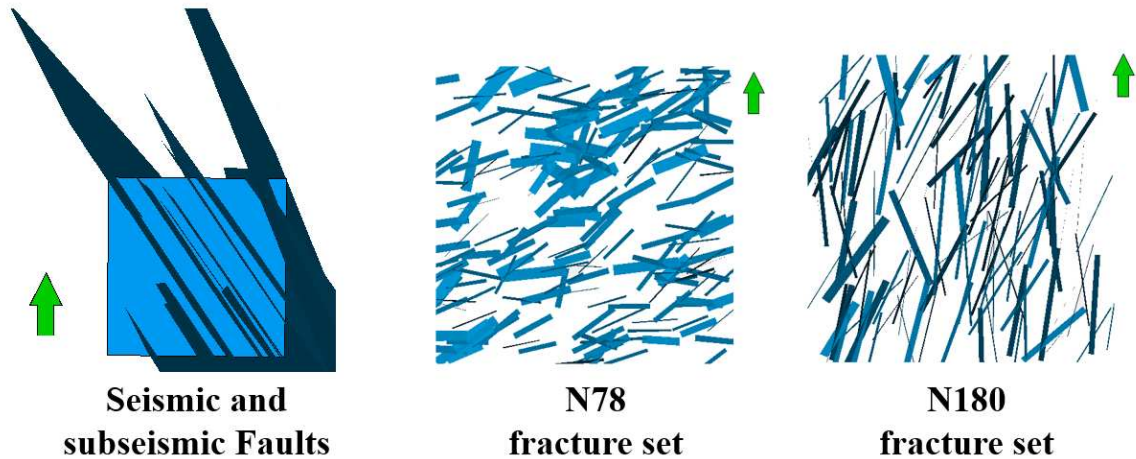
Figure 5.4: DFN illustration of the faults (crossing the model dimension of 600x600 m) and of the two fracture sets (600x600 m)

Table 5.2: distribution methods utilized during the stochastic modeling of the fracture sets

	Property		
	Length	**Aperture**	**Orientation**
Distribution method	Exponential	Normal	Fisher

Table 5.3: fractures properties output mean values after the stochastic modeling

	Mean length (m)	Mean aperture (m)	Mean intrinsic perm. (x10³ D)	Fracture quantity	Orientation	
					Mean dip (°)	Mean dip azi (°)
N78	91	0.003	943	201	63	271
N180	166	0.0009	100	133	75	194

Considering the height (12m) of the DFN, the modeling software has a limitation about the extent of faults in the Z direction, as it considers faults crossing all models vertically. For the fracture sets, they are modeled to cover all vertical extent, as the faults. The fracture sets are in Figure 5.5 where the black lines limit the top and bottom of the model.
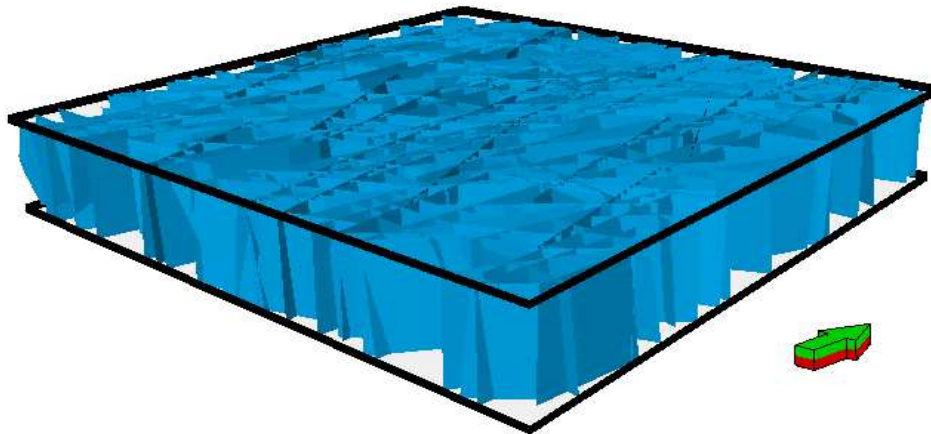
Figure 5.5: N78 and N180 fracture sets extent in all model depth (12m). The black lines represent the top and bottom of the model

5.3 DFN upscaling

The DFN permeability upscaling is performed for all six options described in Chapter 4 (section 4.2.3), but the PD and CP have some observations to be addressed. The CP is not directly included in the next results sections as it has the same results of LP in all scales. The flow-based method with the PD boundary condition is not considered in the analysis due to software limitation in the upscaling execution in the MFM scale; thus, the PD results are considered as not trustful to be used in the other scales, more information in Appendix B.

The well block fracture effective permeability results are further provided and analyzed in section 5.5 (well results analysis and comparisons). Table 5.4 has an example of the results for the fracture spacing for the X direction and Table 5.5 has the porosity distribution values.

Table 5.4: values of min, max, mean and standard deviation (std) of the fracture spacing results for the X direction. A cut-off was applied in the values of this table for better visualization of the values. The maximum value corresponds to the diagonal dimension of the correspondent grid block

Model	Fracture spacing (m) / X direction			
	Min	Max	Mean	Std
CFU1 HFM	1	7	4	1
CFU1 MHFM	4	40	13	6
CFU1 MFM	8	39	19	8

Table 5.5: values of min, max, mean, and standard deviation (std) of the porosity upscaling results

Model	Porosity (x10^{-3})			
	Min	Max	Mean	Std
CFU1 HFM	0	5	0.2	0.4
CFU1 MHFM	0	1.2	0.2	0.2
CFU1 MFM	0.2	0.3	0.2	0

5.4 CFU simulation

Since CFU1 is a type 3 of NFR, all simulation models are DK models since the matrix influence in the flux should be considered. The Gilman-Kazemi formulation (Equation (2.13)) is selected for the sigma factor calculation and all models are run in a black-oil simulator.

The initial conditions and rock-fluid properties are from Field C. Initially the reservoir is 15% saturated with water in an undersaturated condition with a pressure of 592 Kgf/cm^2. The relative permeability curves for fracture and matrix systems are in Figure 5.6.

(a)   **(b)**

Krw x Sw
Kro x Sw
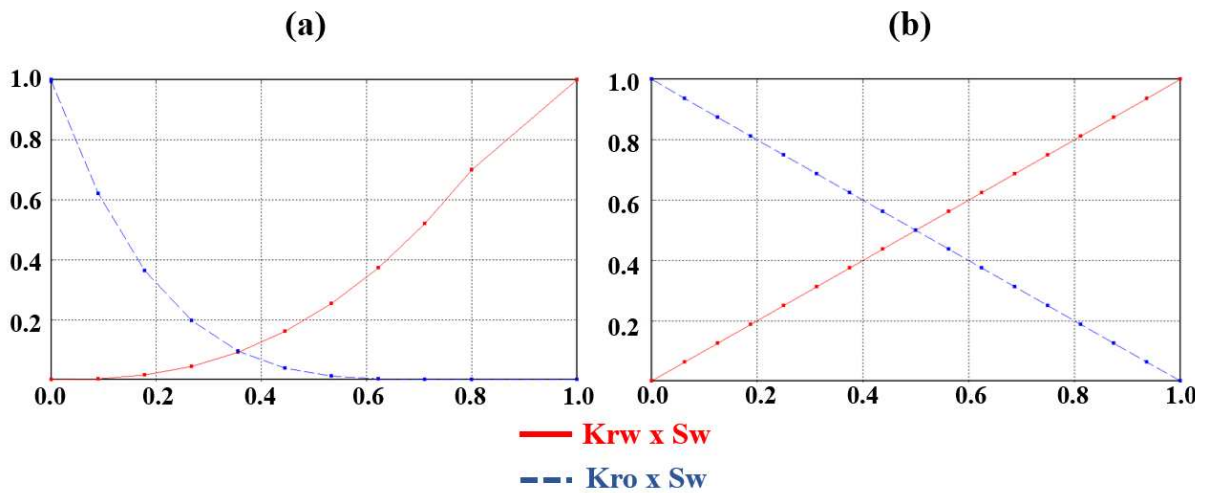
Figure 5.6: matrix (a) and fracture (b) systems relative permeability curves

The production strategy includes one injector and one producer well (Figure 5.7). The injector well has a max surface water rate (STW) of 600 m^3/d and a max BHP of 760 Kgf/cm^2. The producer well has a min BHP of 288 Kgf/cm^2 and no boundary conditions on the liquid rate to better observe the well flow rates differences among cases. The first-time step occurs in 2s of production.

The numerical settings are automatically selected by an automated tune available in the commercial software. For this work, this is important to avoid convergence problems since a small production/injection time is analyzed.

The fracture porosity values are not from the upscaling process due to numerical convergence problems during the simulation. Instead, constant porosity values are selected (Table 5.6) so that all scales have the same pore volume (Table 5.7). There is why the HFM model has a higher porosity value than the other scales, as it has more cells with empty spaces. The modification in the fracture system porosity does not affect the simulation results, as the used pore volume has a small relative difference (RD) to the upscaled values (Table 5.7).
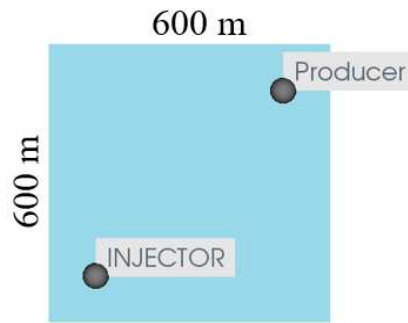
Figure 5.7: producer and injector wells locations inside the model

Table 5.6: porosity constant values selected for each scale

Models	Porosity (%)
CFU1 HFM	1
CFU1 MHFM	0.6
CFU1 MFM	0.6

Table 5.7: initial entire field pore volume (m^3) and its relative difference ((Constant value-Upscaling results)/Upscaling results)*100)

Models	Pore volume (m^3)		Relative difference (%)
	Upscaling results	Constant values	
CFU1 HFM	652	673	3.2%
CFU1 MHFM	652	673	3.2%
CFU1 MFM	655	673	2.8%

5.5 Well results analysis and comparisons

This section is divided into four sub-sections to assess the impact that the DFN permeability upscaling method and the grid-scale cause on wells behavior. They are:

1) Comparison 1: impact of different methods through the same scale

2) Comparison 2: scale-change sensitivity within each method

3) Well index analysis

4) Summary of well static and dynamic data analysis

5.5.1 Comparison 1: impact of different methods through the same scale

This section aims to observe the impact that different DFN upscaling methods cause on well block fracture effective permeability and well dynamic data in each fidelity scale.

5.5.1.1 Well block fracture effective permeability

The fracture effective permeability results for the producer well in all directions are in Figure 5.8, Figure 5.9, and Figure 5.10.

Figure 5.8: CFU1 producer well block fracture effective permeability for the X direction

Figure 5.9: CFU1 producer well block fracture effective permeability for the Y direction

Figure 5.10: CFU1 producer well block fracture effective permeability for the Z direction

Comparing the results in Figure 5.8 and Figure 5.9 for the HFM scale, the CFU1 HFM LP and NF have permeability in the Y direction but not in the X direction. Deeper analysis in the heterogeneities of the CFU1 HFM producer well block (Figure 5.11) reveal no fractures crossing the well block in the X direction, but one fracture connected to one fault crossing the Y direction. Since the FB method calculates the flux in each direction separately, no flux in the X direction is computed, and no fracture permeability in any FB boundary condition is calculated. The Oda method computes permeability in the X direction as it does not account the fractures orientation correctly because of its dependency on grid orientation (Ghahfarokhi, 2017). Moreover, Oda is a method that considers only the fracture geometry, so it always computes positive permeability values if fractures are present in the grid block (Ahmed-Elfeel and Geiger, 2012).

Analyzing Figure 5.10, similar results among all methods are observed for each scale. Figure 5.5 illustrates that all fractures cross the model vertically, consequently, together with the faults, they produce high connectivity in the Z direction. Therefore, the Oda and ODAC methods tend to calculate the permeability with higher precision, being closer to FB results.

The comparison of the LP and NF values in Figure 5.8 and Figure 5.9 yields the FB boundary condition sensitivity for each scale. Considering the permeability ranges in the Y direction, the HFM is the least sensitive scale and the MHFM is the most sensitive scale. These sensitivities differences can occur due to the type of heterogeneities present in each well block. The LP and NF comparison demonstrate that the Flow-based method is boundary condition sensitive, despite no sensitivity are observed between CP and LP.

Figure 5.11: 2D DFN view of the CFU1 HFM producer well block. The N78 represents the fractures in the x direction; and the fault and the N180 fracture set represent the fractures in the y direction. The red dot is the well location inside the block

Comparing FB and Oda results in Figure 5.8 and Figure 5.9, it shows an overestimated permeability in the X and Y directions calculated by the Oda method in all scales. As mentioned, Oda produces an accurate result if the fracture network is dense and well connected. Hence, in the studied wells locations this premise is not fully attended, at least in one direction, as it occurs in the HFM scale.

ODAC in Figure 5.8 and Figure 5.9, and Figure 5.10 show a reduction of Oda`s values in each scale. However, ODAC does not necessarily produce similar values to the FB method, this occurs only in the CFU1 MFM and HFM in the Z direction, where ODA has already closer values to the FB method. ODAC can also underestimate the permeability in cases where Oda is coherent with FB, as it occurs with the CFU1 MHFM ODAC in the Z direction. Moreover, for a methodology that intends to consider the fracture connectivity, ODAC does not have accurate results as it calculates permeability values in the X direction for the CFU1 HFM.

The fracture effective permeability results for the injector well in all directions are in Figure 5.12, Figure 5.13, and Figure 5.14.
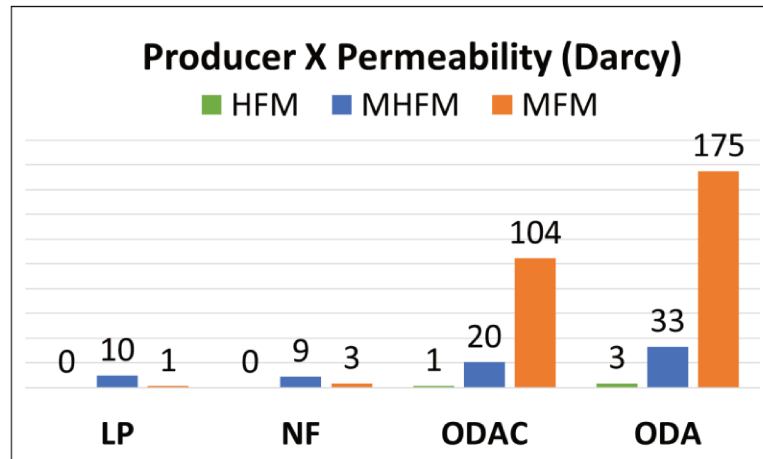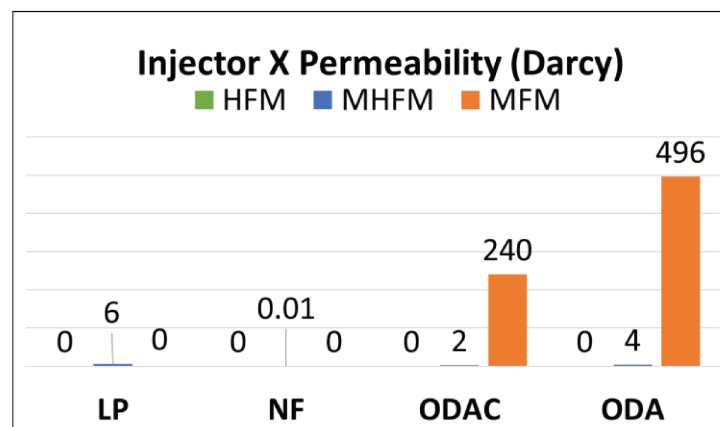

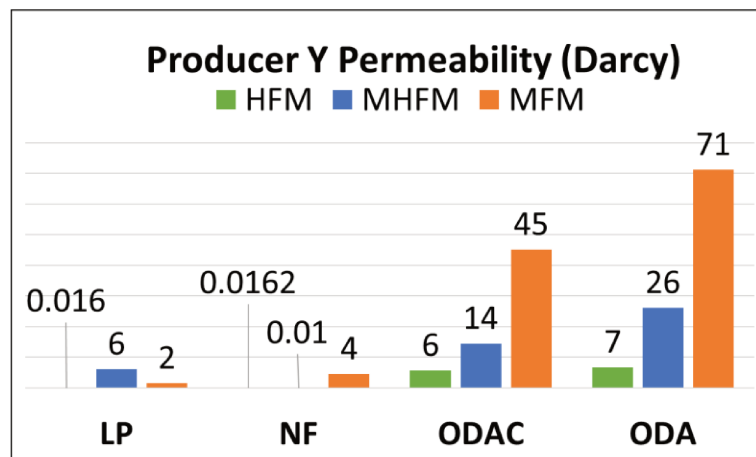Figure 5.12: CFU1 injector well block fracture effective permeability averages for the X direction
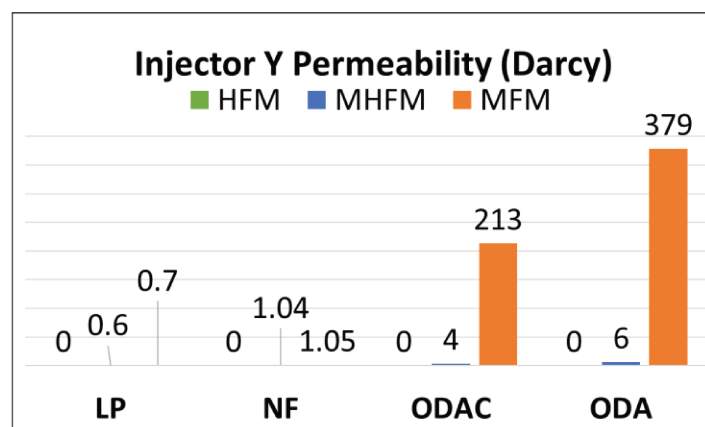
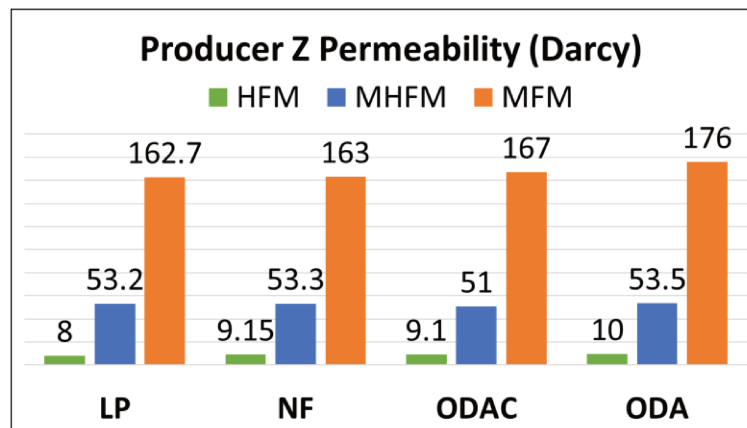Figure 5.13: CFU1 injector well block fracture effective permeability averages for the Y direction
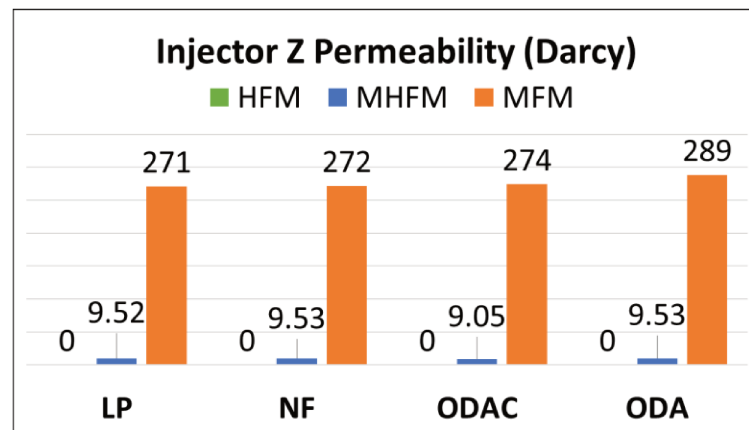
Figure 5.14: CFU1 injector well block fracture effective permeability averages for the Z direction

As can be observed in Figure 5.12, Figure 5.13, and Figure 5.14, the CFU1 HFM injector has zero fracture permeability in all directions. Therefore, it is not possible to perform a method impact analysis for the injector well in this scale. The null values are a consequence of the absence of fractures and faults in the well location.

The CFU1 MFM FB injector has the same CFU1 HFM FB producer issue with zero permeability in the X direction. However, different from the CFU1 HFM producer, the CFU1 MFM injector has fractures in this direction, but they are not connected (Figure 5.15). The absence of connectivity precludes the flux in the X direction, resulting in zero fracture permeability for FB method. On the other hand, Oda returns positive permeability values, as it implicitly considers the fractures` length as infinite (Ahmed-Elfeel and Geiger, 2012), producing non-existing connectivity.
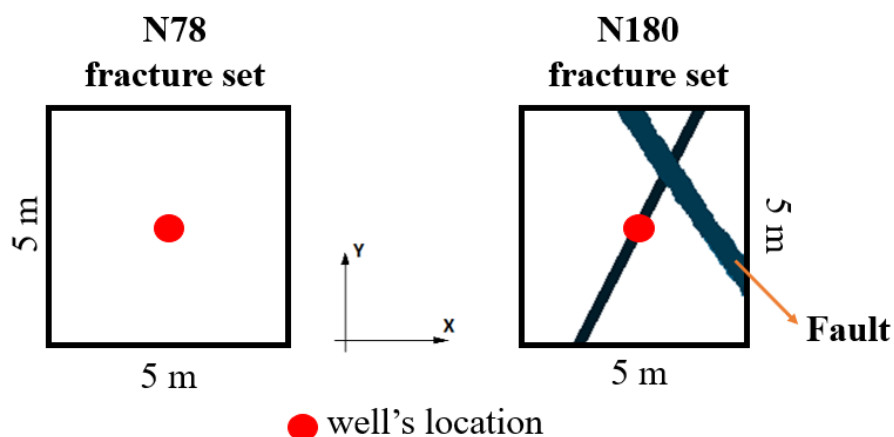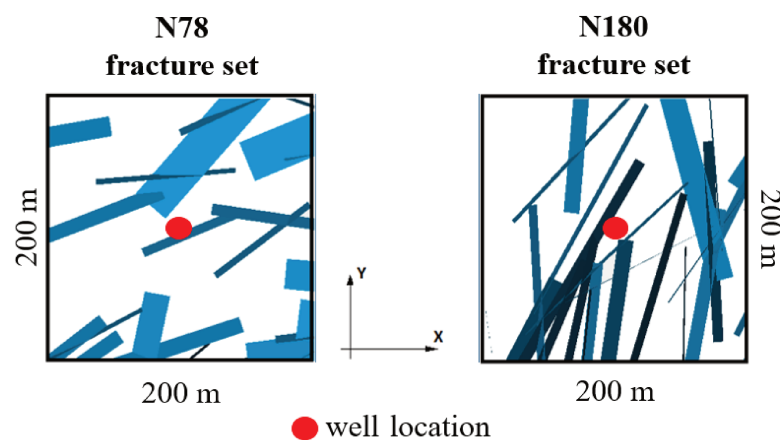

Figure 5.15: 2D DFN view of the N78 and N180 fracture set for the CFU1 MFM injector well block. The N78 represents the fractures in the x direction; and the fault and the N180 fracture set represent the fractures in the y direction. The red dot is the well location inside the block

The injector well is also affected by the connectivity in the Z direction. Consequently, CFU1 MHFM and MFM have similar results among methods in this direction, showing the importance of a dense and connected fracture network to consider Oda an accurate method.

The FB boundary condition comparison among Figure 5.12, Figure 5.13, and Figure 5.14 also yields the conclusion that FB method is boundary condition sensitive between LP and NF, but not between LP and CP. Besides, the same discussion for the producer well about the Oda and the ODAC methods is valid for the CFU1 MFM and MHFM injectors.

For the first comparison, it is concluded that all scales are affected by the upscaling method change.

5.5.1.2 Summary of fracture effective permeability results

This section proposes a summary of the similarities and differences of fracture effective permeability between producer and injector wells.

The main difference is the heterogeneities present in the well block, as they change according to the well`s location. Consequently, in the CFU1 HFM fractures cross only the producer well, and in the CFU1 MFM the injector does not have FB results in the X direction.

Considering the similarities, both wells are impacted by the DFN permeability upscaling method in the three fidelity scales. The FB method is no boundary condition sensitive for LP and CP, Oda overestimates the results, and ODAC does not produce similar permeability values to the FB method for X and Y directions.

The main conclusion for those similarities and differences is that the fracture effective permeability is dependent on the DFN upscaling methodology and the connection of fractures in the well block.

5.5.1.3 Flow rate and BHP

For this section, the flow rate and BHP results for injector and producer wells are discussed. In all models, the producer well has a constant BHP of 288 Kgf/cm^2 and the injector well has a constant water injection rate of 600 m^3/d. Therefore, the impact of the heterogeneities in the dynamic data can be analyzed through the oil flow rates for the producer well and through the BHP for the injector well, since the block pressure (P_{block}) has slightly changed for the first-time step (analysis of Equation (2.17)). Table 5.8 and Table 5.9 have the results for the producer oil rate and injector BHP for the first-time step. Figure 5.16 has examples of oil rate curves for some simulation models in all production time (zero water cut).

Table 5.8: production Oil Rate (m³/d) for the first-time step (2s)

Model	Oil Rate per method (m³/d) x 10³			
	LP	NF	ODAC	ODA
CFU1 HFM	1	1	19	27
CFU1 MHFM	72	4	138	220
CFU1 MFM	10	29	496	786

Table 5.9: injector BHP (Kgf/cm²) for the first-time step (2s)

Model	BHP per method (Kgf/cm²)			
	LP	NF	ODAC	ODA
CFU1 HFM	761	761	761	761
CFU1 MHFM	600	609	597	595
CFU1 MFM	617	610	591.7	591.6
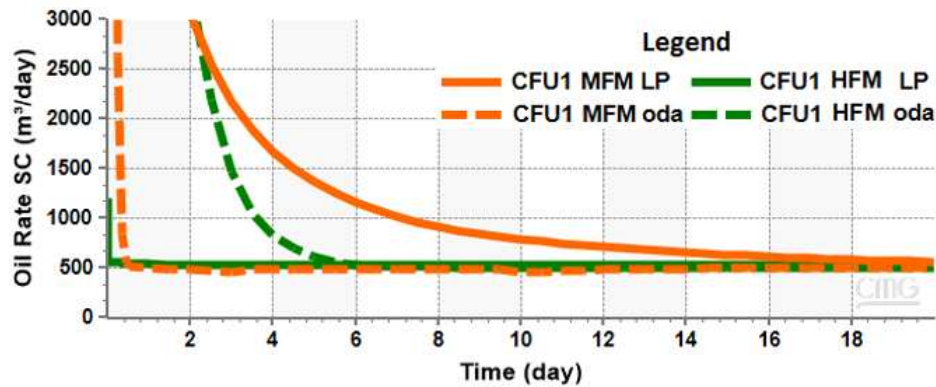
Figure 5.16: production oil rate curves for the CFU1 HFM/MFM LP/ODA simulation models (zero water cut)

As shown in Figure 5.16, the curves are sensitive to the fidelity scale and to the upscaling method. Such sensitivities are also observed in Ahmed-Elfeel and Geiger (2012), the authors discuss that production differences depend on the connectivity of fractures, and this is predicted from the previous section discussions. However, the biggest differences among cases are in the first-time step analysis, where the well production capacity can be observed. The first oil rate values of Figure 5.16 are in Table 5.8, this table may have unreal values of production rate, but they are exclusively used for comparison. Additionally, in Figure 5.16 all models have a production tendency of 500 m³/d, which is coherent with the constant injection rate and the small model dimension that enables the reservoir equilibrium in a short time.

Analyzing the FB boundary condition change in Table 5.8, considering the data range between LP and NF, it is observed a bigger range for the MHFM and a smaller range for the HFM. For the injector well (Table 5.9), the MHFM is also the most impacted.

Overall, in Table 5.8 and Table 5.9, ODAC approximates Oda results of flow rate and BHP to FB data. However, Oda and ODAC still overestimate the producer's flow rate.

To find the most and the least impacted scale, it is considered the range between the biggest and the smallest flow rate/BHP value among all methods in each scale. The most impacted scale for both wells is the MFM with the biggest data range. For the producer well, the least impacted scale with the smallest data range is the HFM (this last analysis could not be done for the injector well). Figure 5.17 has the summary of the oil rate ranges for each scale.
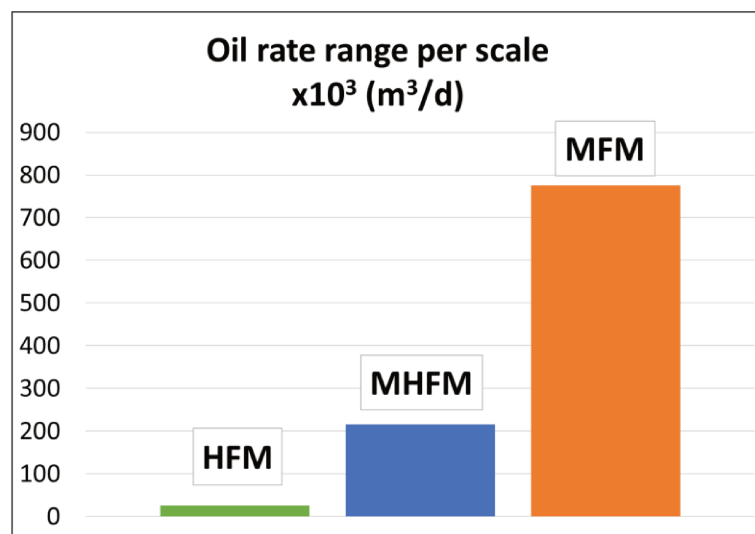
Figure 5.17: range between the biggest and the smallest oil rate values when applying different DFN upscaling methods in each fidelity scale

Comparison (1) suggests a higher variation of the dynamic data as the scale increases, indicating more variability of flow rate and BHP in medium-fidelity models when changing the DFN permeability upscaling method. This higher variability in coarser grids is a consequence of an increase in the number of heterogeneities present in the well block, making the MFM scale more affected by the DFN upscaling methods.

5.5.2 Comparison 2: scale-change sensitivity within each method

As discussed in section 5.5.1.1, differences in the well-block fracture permeability can occur in consequence of the changes in the heterogeneities crossing the well block. Thus, it is expected that the scale variation causes an impact on the results of the DFN upscaling methods. The grid-scale dependency of Oda and FB methods are discussed and affirmed by Wang et al. (2008), Ahmed-Elfeel and Geiger (2012), Decroux (2012), and Correia (2014). For this work, the scale-change sensibilities within methods are evaluated from the well's dynamic properties.

Considering the dynamic data ranges (the difference between the biggest and the lowest values of oil rate and BHP) among all scales for each method (Table 5.8 and Table 5.9), it is analyzed the most and the least impacted method due to the scale change. The producer and injector wells have the same results, Oda has the biggest data variability and NF the smallest. Figure 5.18 has the summary of the oil rate ranges for each DFN upscaling method.
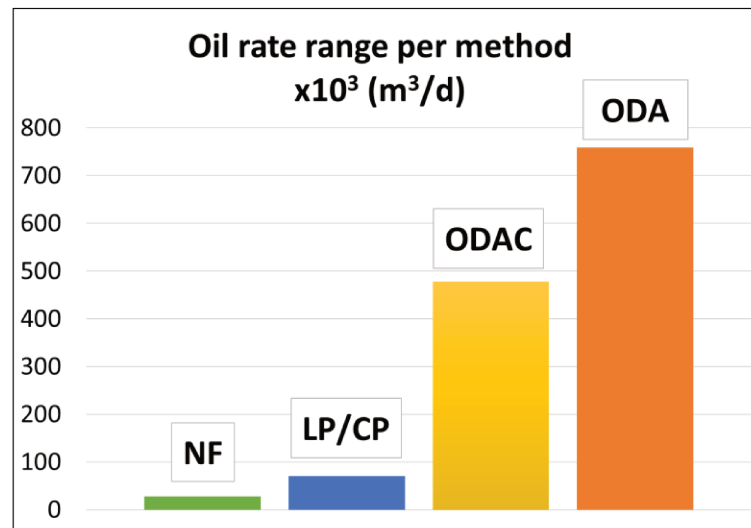
Figure 5.18: range between the biggest and the smallest oil rate values when changing the fidelity scale in each DFN upscaling method

The analysis of comparison (2) concludes that all methods are scale sensitive. Oda produces the most variability in BHP and oil rate, and NF yields the least dynamic data variation. However, LP and CP have the same results, suggesting that for the FB method, these would be the boundary conditions with the least variability.

5.5.3 Well index analysis

Table 5.10 and Table 5.11 have the results for WI for producer and injector wells, respectively. It is important to mention that the matrix WI is constant for each scale, and it decreases the values as the scale increases, which is a consequence of the scale dependency in the WI equation (Equation (2.17)).

Table 5.10: producer well WI (x10³) in mD.m for fracture and matrix systems

Model	Fracture				Matrix
	LP	NF	ODAC	ODA	
CFU1 HFM	0.47	0.475	77	139	3
CFU1 MHFM	137	6	309	530	2
CFU1 MFM	16	46	824	1,340	1

Table 5.11: injector well WI (x10³) in mD.m for fracture and matrix systems

Model	Fracture				Matrix
	LP	NF	ODAC	ODA	
CFU1 HFM	0	0	0	0	3
CFU1 MHFM	34	14	48	85	2
CFU1 MFM	9	13	2,731	5,226	1

Analyzing Table 5.10 and Table 5.11 according to the impact of different methods through the same scale (comparison (1)), they yield the same conclusions of the dynamic data in section 5.5.1.3.

As discussed in the previous section, ODAC tends to reduce Oda values, and the impact of this reduction on WI values are in Table 5.12. Analyzing the relative difference of WI between Oda and ODAC methods, it is noticed an approximate reduction of 40% in Oda values, which it is not enough to correct them to FB results in the studied well locations.

Table 5.12: WI relative difference between ODAC and Oda methods

Well type	WI Relative Difference (ODAC-ODA)/ODA		
	CFU1 HFM	CFU1 MHFM	CFU1 MFM
Producer	-44%	-41%	-38%
Injector	-	-42%	-48%

Comparing WI values in Table 5.10 and Table 5.11 with the dynamic data of Table 5.8 and Table 5.9, it is observed that they have a coherent correlation. The biggest total WI corresponds simultaneously to the biggest total oil rate (producer well) and to the smallest BHP (injector well). This correlation demonstrates the importance of the first-time step analysis, when the well block pressure does not have significant changes among scales, allowing the analysis of the fracture WI impact on wells production and injection behavior.

The correlation between the WI and the well dynamic data is also observed through the contribution that the fracture system provides to the total flux. Equation (5.2) describes the fracture contribution concept and Table 5.13 and Table 5.14 have the results for production oil rate and injection water rate, respectively. Comparing the percentages in Table 5.13 and Table 5.14 with the fracture and matrix WI data (Table 5.10 and Table 5.11), it is observed that if the fracture WI is bigger than the matrix WI, the fracture tends to provide the most flux contribution. Therefore, in Table 5.13 the CFU1 HFM LP and NF have more contribution from the matrix system, demonstrating that the CFU1 HFM ODA and ODAC do not represent well the oil rate flux in this scale, overestimating the production from the fractures.

Table 5.13: fracture contribution in the total production oil rate (%)

Model	Fracture contribution to the production oil rate			
	LP	NF	ODAC	ODA
CFU1 HFM	24%	24%	95.37%	96.78%
CFU1 MHFM	99.21%	87%	99.59%	99.74%
CFU1 MFM	96%	98.70%	99.92%	99.95%

Table 5.14: fracture contribution to the 600 m³/d of injection rate (%)

Model	Fracture contribution to the injection water rate			
	LP	NF	ODAC	ODA
CFU1 HFM	0%	0%	0%	0%
CFU1 MHFM	97%	93%	97.9%	98.7%
CFU1 MFM	94%	95%	99.98%	99.99%

$$Fracture\ contribution\ (\%) = \frac{Flow\ rate\ from\ fracture\ system}{Total\ flow\ rate} \times 100 \qquad (5.2)$$

5.5.4 Summary of well static and dynamic data analysis

The differences and similarities among methods and scales observed in the well block fracture effective permeability in sections 5.5.1.1 and 5.5.1.2 are consistent with the flow rates and BHP results for both wells (section 5.5.1.3). Thus, an analysis of the well fracture effective permeability together with the DFN visualization in the well block can provide highlights in wells production/injection capacity.

Analyzing the scales individually, another conclusion about the fracture contribution described in Table 5.13 and Table 5.14 is the tendency of a flux increase in the matrix medium when the fracture effective permeability reduces (section 5.5.1.1).

Table 5.15 has a summary of the production oil-rate range used in comparisons (1) and (2), considering the maximum and the minimum values obtained among methods for each scale (comparison (1), Figure 5.17) and the maximum and the minimum values obtained among scales for each method (comparison (2), Figure 5.18). The purpose of Table 5.15 is to demonstrate how the values of production can vary when changing the DFN upscaling method and the grid-scale.

Table 5.15: CFU1 production oil-rate range summary for all methods and all scales

	Range among methods for each scale (comparison 1)			Range among scales for each method (comparison 2)			
	HFM	**MHFM**	**MFM**	**LP/CP**	**NF**	**ODAC**	**ODA**
Production oil-rate range in m³/d (x10³)	26	216	775	70	28	477	758

It is concluded that the well static and dynamic data are impacted by the DFN permeability upscaling method and the grid-scale. Consequently, these aspects can affect the reservoir development and management phase or mask the reservoir characterization uncertainties (Correia et al., 2018; Ahmed-Elfeel and Geiger, 2012). Therefore, it is important to carry out a deeper fracture system study when setting new wells in DK simulation models, analyzing the appropriate DFN upscaling method and fidelity scale.

For this study, the least impacted scale and method is the HFM LP/CP. However, it is important to mention that the flow-based method is very time consuming and computationally demanding, and the high-fidelity scale requires more simulation time. Table 5.16 has the approximate upscaling and simulation time for all methods and all scales. All FB time values correspond to an arithmetic mean of all boundary conditions results. The simulations are performed in a cluster with 8 processors with the machine description: Intel Xeon Gold 6244 CPU @ 3.6GHz (architecture x86_64, 16 CPUs, 192 GB of memory, and with the DDR4-2933 memory type). The machine description used for the DFN upscaling is: Intel Xeon Gold 6144 CPU @ 3.50 GHz with 10 processors.

Table 5.16: results for the DFN permeability upscaling and simulation time for all methods and scales

Fidelity scale (total number of cells)	Upscaling time			Simulation time		
	FB	**ODAC**	**ODA**	**FB**	**ODAC**	**ODA**
CFU1 HFM (86,400 cells)	22 h	46 s	16 s	16 min	13 min	11 min
CFU1 MHFM (1,728 cells)	23 min	4 s	2 s	7.5 s	6.9 s	6.9 s
CFU1 MFM (27 cells)	3 min	1 s	1 s	2.2 s	2.3 s	2.3 s

On the other hand, the MFM ODA is the most impacted scale and method. The results show that Oda is not recommended for not dense or not connected fracture networks, despite

its fast processing. However, due to this efficiency, in cases where Oda and FB have similar values, the Oda is the recommended upscaling method.

5.6   Well calibration tests

The calibration tests are performed in the CFU1 MFM ODA and the reference model is the CFU1 HFM LP according to the previous results analysis.

All models have the same dimension of 600x600x12m, the HFM has a cell dimension of 5x5x2m, and the MFM has a cell dimension of 200x200x4m. Since the HFM has 6 layers and the MFM has 3, some treatment in the parameters of the HFM is necessary to execute the calibration methodologies workflow:

- Oil or water rate: sum at each 2 layers of HFM

- BHP: arithmetic average at each 2 layers of HFM

- WI: sum at each 2 layers of HFM

- Well block fracture effective permeability: utilization of Equation (4.1) at each two layers of the HFM in each direction

The result for the first step of all three methodologies workflow is in Table 5.17. It is expected that the P_{block} has a small variation for the first-time step and the BHP and flux rate (q) are the same in both models. The results in Table 5.17 are as expected, making the methodology consistent at this point.

Table 5.17: results for the P_{block}, BHP, and q, and their relative difference between CFU1 HFM LP and CFU1 MFM ODA

	Producer		Injector	
	P_{block} (Kgf/cm^2)	BHP (Kgf/cm^2)	P_{block} (Kgf/cm^2)	q (m^3/d)
CFU1 HFM LP	582	288	592	600
CFU1 MFM ODA	561	288	592	600
Relative difference (%)	-4%	0%	0%	0%

Table 5.18 has the results of WI values for all simulation models used in the well calibration tests (injector and producer wells). Comparing to CFU1 MFM ODA, it is observed that the methodology (1) changes the WI of the fracture system, methodology (2) changes the fracture and matrix systems WI, and methodology (3) changes the WI of the fracture system.

The dynamic data results for both wells together with the RD from the CFU1 HFM LP values are in Table 5.19. The new MFM models have the producer's BHP with 288 Kgf/cm^2, the producer's P_{block} with 1.6% of RD, and the injector's P_{block} with 0.01% of RD.

Table 5.18: results of the WI values for producer and injector wells of all simulation models used in the well calibration tests

	Producer WI (mD.m) x 10^3		Injector WI (mD.m) x 10^3	
	Fracture	**Matrix**	**Fracture**	**Matrix**
CFU1 HFM LP	0.5	2.9	0	2.9
CFU1 MFM ODA	1,340	1.2	5,226	1.2
CFU1 MFM ODA1	0.5	1.2	0	1.2
CFU1 MFM ODA2	0.5	2.9	0	2.9
CFU1 MFM ODA3	0.2	1.2	0	1.2

Table 5.19: well results of dynamic data for all simulation models utilized in the well calibration tests

	Producer		Injector			
	Oil rate (m³/d) x10³	**RD (%)**	**BHP (Kgf/cm²)**	**RD (%)**	**Water rate (m³/d)**	**RD (%)**
CFU1 HFM LP	1.21	-	761	-	600	-
CFU1 MFM ODA	786	64,990	592	-22	600	0
CFU1 MFM ODA1	0.7	-44	760	0	250	-58
CFU1 MFM ODA2	1.23	2	757	-1	600	0
CFU1 MFM ODA3	0.5	-58	760	0	250	-58

According to Table 5.19, the proposed methodologies cause a significant impact on well behavior. Methodology (2) provides the least RD in the dynamic data for producer and injector wells simultaneously. The other methodologies improve the well representation just for the producer well, as the injector does not have a simultaneous match between water rate and BHP. Thus, methodology (2) is selected as the well representation proposal for new wells in medium-fidelity models.

Figure 5.19 has the curves for cumulative oil production and injector BHP during 20 days for the CFU1 HFM LP, CFU1 MFM ODA, and CFU1 MFM ODA2. Figure 5.19 shows that the well representation proposal does not guarantee the fit for more production time, this occurs because the model heterogeneities start to influence the results; however, the calibration of these influences is beyond this work's objective.

The well representation proposal presented in this work can be divided into two main steps. First, there is the calculation of the fracture properties considering the heterogeneities close to the wellbore using the flow-based upscaling method with the linear or constant pressure boundary condition. Second, there is the incorporation of the WI calculated in the previous step in the well model of each MFM well for fracture and matrix systems.
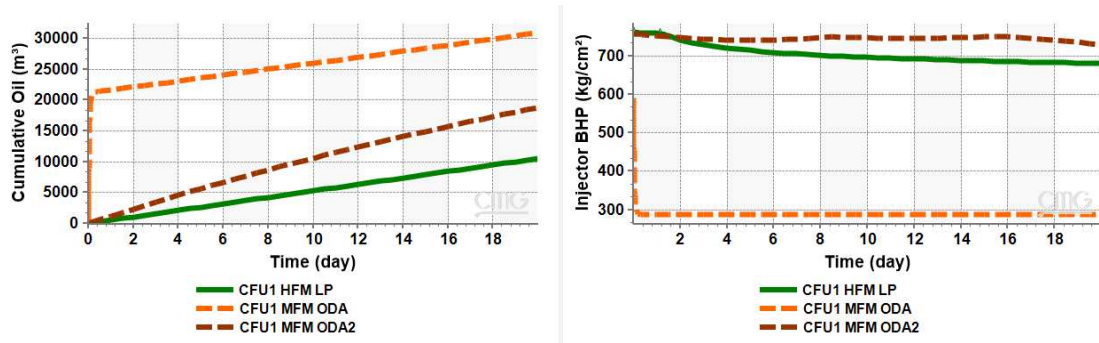
Figure 5.19: cumulative oil production and injector BHP curves for 20 days of production for the for the CFU1 HFM LP, CFU1 MFM ODA, and CFU1 MFM ODA2

5.7 NFR field scale application

5.7.1 DFN upscaling

After the application of the DFN upscaling methods it is observed different fracture permeability in all directions. Figure 5.20 and Figure 5.21 have results for one of the producer wells (well P6). The same considerations about the LP and PD methods cited in section 5.3 are valid for this test (LP=CP results and PD is not considered in the analysis).
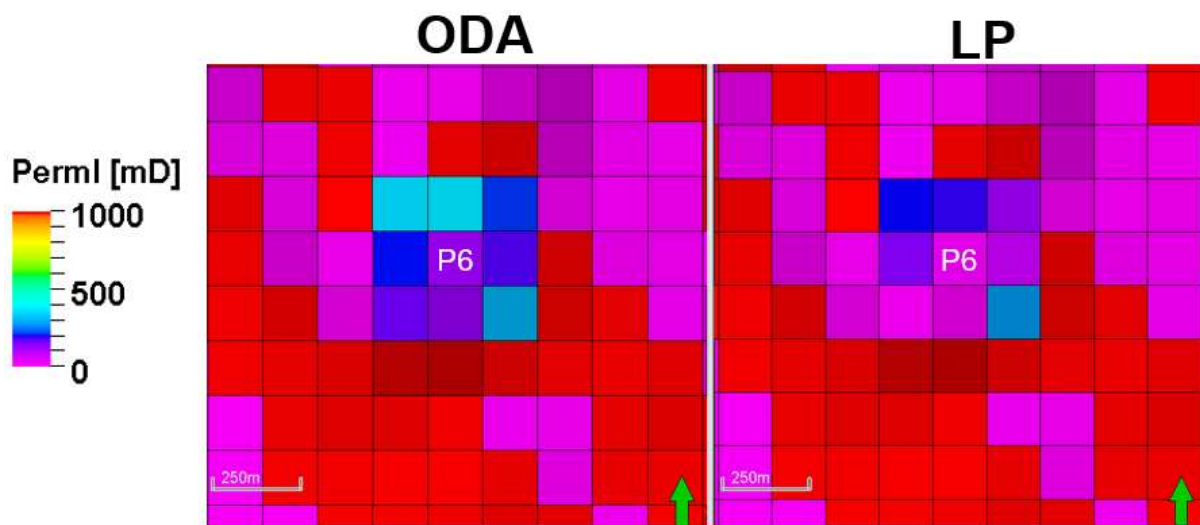
Figure 5.20: fracture permeability (X direction) for the P6 location utilizing the ODA and LP methods (the modification is extended to one layer of blocks around the well)
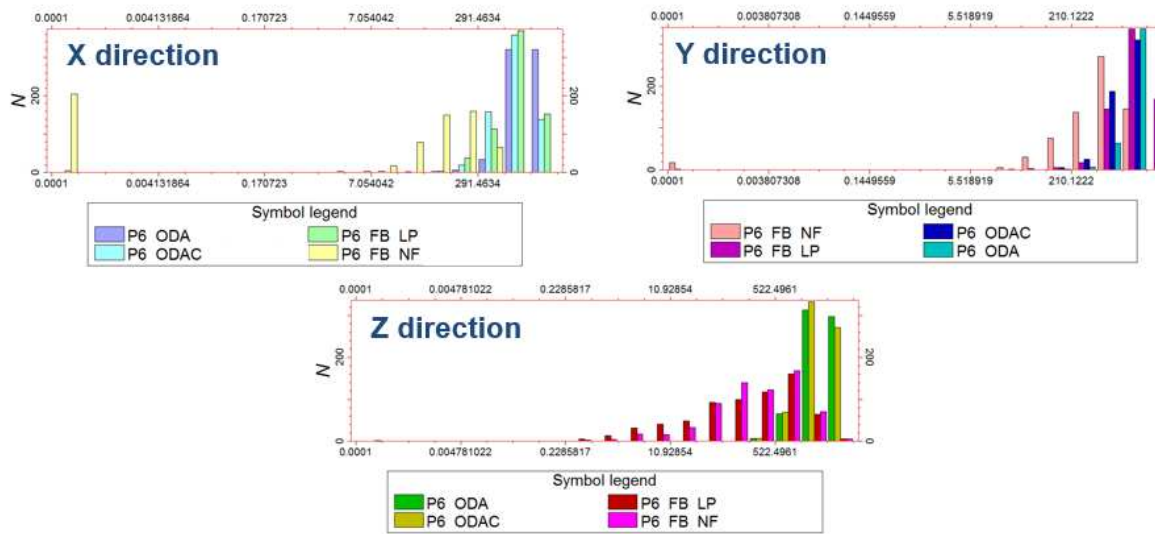
Figure 5.21: histograms for the fracture permeability values around well P6 for all tested DFN upscaling methods in three directions

5.7.2 Simulation settings

The simulation parameters discussed in section 5.4 are the same for the field tests, except for the fracture porosity, production time, wells boundary conditions, and production strategy.

The fracture porosity is set according to the dynamic data calibration in the mass balance equation and it is provided for this work. The total production time is set for 32.6 years. The producer and injector wells boundary conditions are set as follows:

- Producer:
  - Min BHP: 288.3 Kgf/cm^2
  - No flow rate restrictions
- Injector:
  - Max BHP: 750 Kgf/cm^2
  - Max water injection rate: 10016.2 m^3/d

The production strategy is illustrated in Figure 5.22, it has 3 producer wells and 3 injector wells. This is not a real field production strategy, as there are only six wells. However, since the objective is to analyze the field production sensitivity to the DFN upscaling process, this strategy is considered adequate. The proximity of the injector wells I2 and I3 are set close to P6 well to maintain the field pressure during the test.
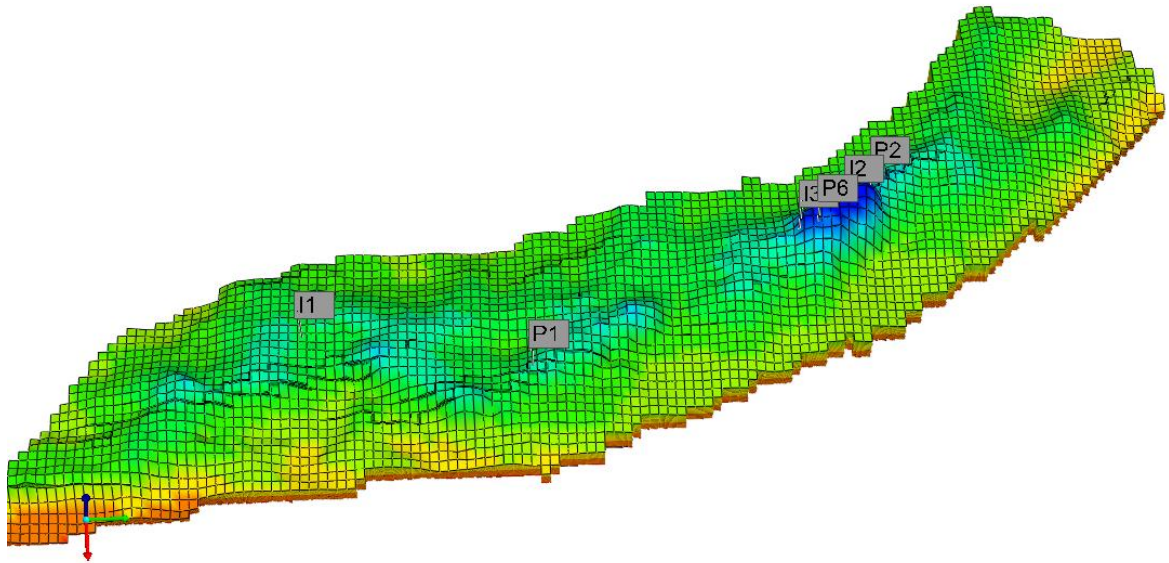
Figure 5.22: production strategy for the Field C

5.7.3 Simulation results analysis and comparisons

To compare the impact of the DFN upscaling methods in the field productivity, the producer wells BHP should be constant, as it is demonstrated in Figure 5.23.
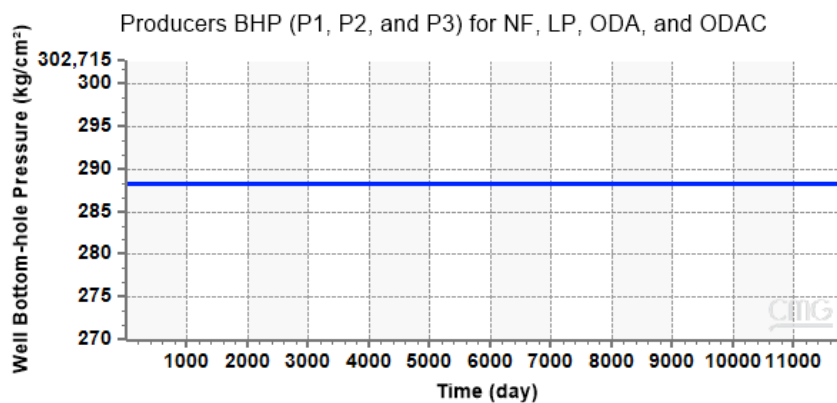
Figure 5.23: producers BHP in the NFR field scale application

The next results are for the oil rate and cumulative production in the first seconds of production and for all production terms. The water production rate is not discussed as it has the same conclusions as the oil production data.

The result for all production term is in Figure 5.24. Since the oil rate has a high variation in a long production time, the results are better analyzed in the separated terms.

Figure 5.24: oil rate and oil cumulative curves for all models of the NFR field scale application during the 32.6 years of production

Figure 5.25 has the results of the oil rate in the first seconds of production. As observed in the previous CFU tests, the well productivity is impacted by the DFN upscaling methods, the NF boundary condition tends to have the lowest oil rate values than the LP, and the Oda method tends to have the highest oil rate. Nevertheless, the LP has a higher similarity with the ODAC method, suggesting a certain connectivity of the fracture network, as discussed by Haridy et al. (2019).
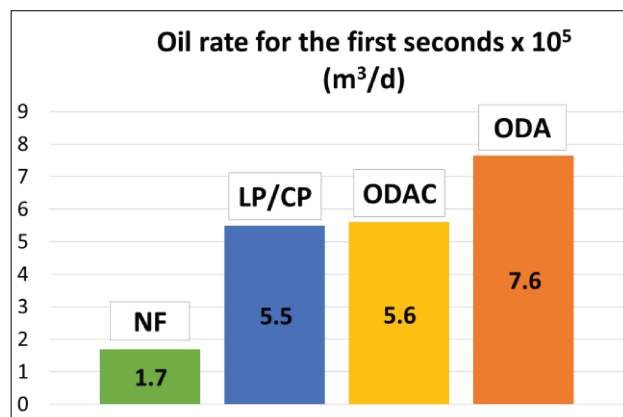
Figure 5.25: oil rate for all models of the NFR field scale application for the first seconds of production

Figure 5.26 has the results for the short production term. For the first six months, there is an impact of the DFN upscaling method in the field production, except for the ODAC and

LP, a tendency of a flow rate equilibrium is observed for all models, and Oda has the highest oil rate and cumulative production values.
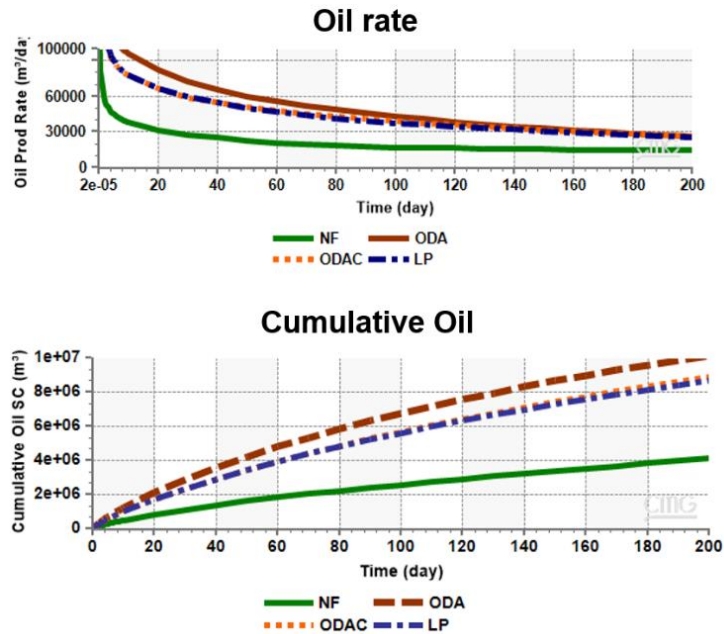
Figure 5.26: oil rate and oil cumulative curves for all models of the NFR field scale application for the short production term (6 months)

Figure 5.27 has the results for the medium production term. It is observed a lower impact of the DFN upscaling methods than the short production time.
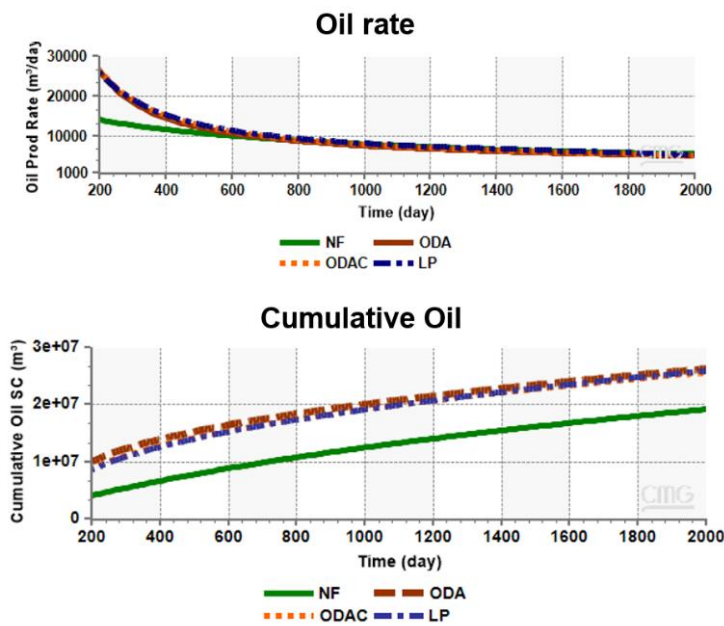
Figure 5.27: oil rate and oil cumulative curves for all models of the NFR field scale application for the medium production term (6 months to 5 years)

Figure 5.28 has the results for the long production term. The impact of the DFN upscaling methods in the field production is the lowest if compared to the other production terms.
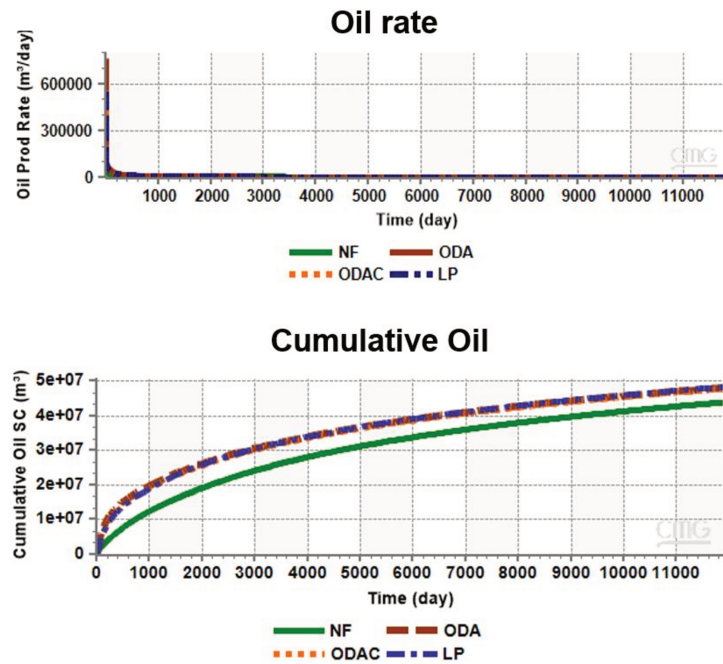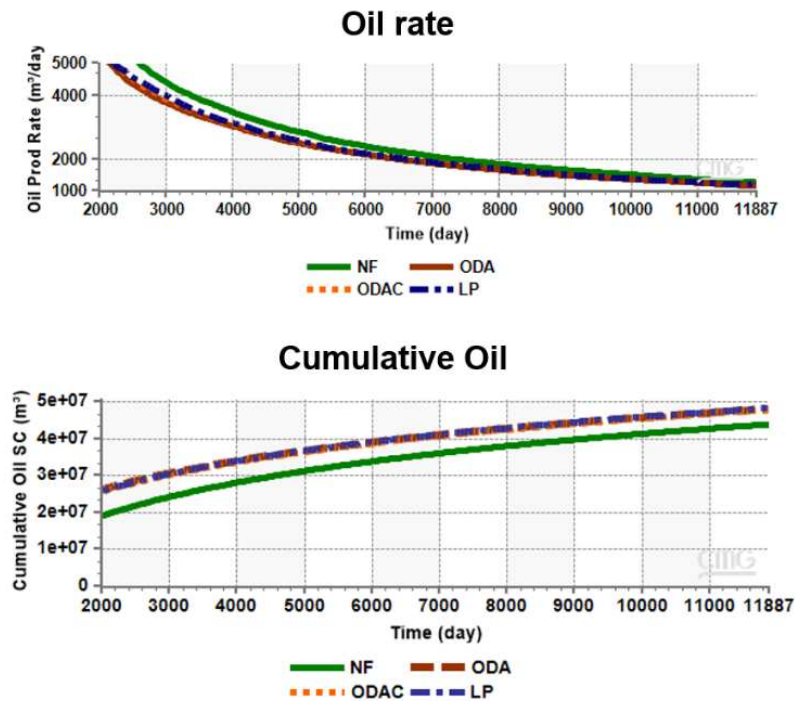

Figure 5.28: oil rate and oil cumulative curves for all models of the NFR field scale application for the long production term (after 5 years)

Finally, Table 5.20 and Table 5.21 has the summary oil rate and oil cumulative values for the end of each production term. It is observed that LP and ODAC have similar values in all terms, the highest impact is in the first seconds and in the short production term, and the lowest impact is in the medium and long term.

Table 5.20: summary of the oil rate values at the end of each production term

	Oil rate x10³ (m³/d)			
	LP	NF	ODAC	ODA
First seconds	549	169	560	765
Short term	28	15	28	29
Medium term	6.0	6.0	5.6	5.5
Long term	1.2	1.3	1.2	1.2

Table 5.21: summary of the oil cumulative values at the end of each production term

	Oil cumulative x10⁷ (m³/d)			
	LP	NF	ODAC	ODA
Short term	0.8	0.4	0.8	1.0
Medium term	2.5	1.8	2.5	2.5
Long term	4.8	4.4	4.8	4.8

6 CONCLUSIONS

Three different DFN permeability-upscaling methodologies in three fidelity scales of DK simulation models were utilized for the tests in a CFU to fulfill the first main objective and the first two specific objectives. The main conclusions are:

- The well behavior is sensitive to the fidelity scale of the model and to the DFN upscaling method used, as the well flow rate and BHP can vary significantly with these two parameters;

- The biggest variability in the well dynamic data (flow rate and BHP) is seen in medium-fidelity models due to the higher difference between the maximum and minimum values of BHP (injector) and oil rate (producers) when changing the DFN upscaling method. This variability tends to be bigger in coarse grids since the number of heterogeneities present in the well block increases as the grid-scale increases, bringing more impact in the DFN upscaling calculation, and consequently in the well productivity/injectivity data;

- The least variability in the well dynamic data is seen in high-fidelity models, therefore, one way to reduce the variability of the upscaling method could be the consideration of the heterogeneities closer to the wellbore in the calculation of the well productivity/injectivity;

- Oda method is the most sensitive to the scale change because it produces more variability in the well dynamic data when changing the grid-scale, and the FB method is the least sensitive because it causes the least variability in the well behavior when comparing different grid-scales. For the FB boundary condition choice, the LP is the most recommended as it yields the same results of CP boundary condition;

- Oda and ODAC methods are not recommended if the DFN is not dense and well connected in at least one direction in the well blocks. This recommendation is based on the fracture permeability computed by the Oda and ODAC method in the HFM producer, a case that does not have connected fractures in the X direction to allow the existence of a fracture permeability in this direction. The fact is that the Oda and ODAC method consider positive fracture permeability if there are fractures inside the grid-block, independently of their connectivity since they assume an infinite fracture length. On the other hand, the FB method did not compute fracture

permeability in the X direction, showing more precision in the fracture permeability calculation.

From the analysis of the previous conclusions, different well calibration methodologies were tested in the same CFU to fulfill the second main objective and the third specific objective. The main conclusion is:

- The well representation proposal is achieved with the utilization of the WI of an HFM LP/CP model in substitution of the WI of the MFM ODA model. This calibration resulted in a better well representation for new producer and injector wells in medium-fidelity models, showing promising results to reduce the well dynamic variability caused by the DFN upscaling methods and the grid-scale;

Honoring the fourth specific objective, the conclusions of the impact that different DFN upscaling methods cause in different terms of a real field scale simulation is:

- The impact of the chosen DFN upscaling methods decrease as the production time increases, showing a significant impact in the short term (first six months) and in the first seconds, but a low impact in the medium (6 months to 5 years) and long terms (after 5 years). This result shows the necessity of a calibrated well model in the reservoir development phase, demonstrating the relevance of the well representation proposal of this work, which allows the application of a calibrated well model from the start of the production;

Overall, the variations in well behavior caused by different DFN upscaling methods can mask the reservoir characterization uncertainties and affect the forward predictions during the reservoir development and management phase. This demonstrates the importance to carry out a deep analysis of the fracture properties in the grid blocks of new wells before starting the production prediction, in order to analyze the connectivity of the fracture system and to evaluate the necessity of the well calibration process utilization.

The well representation proposal of this work can reduce the variability of the well flow rate and BHP when placing new wells in the model during the development and management phase of the reservoir. As such, this work presents a well representation approach for use in simulation models of naturally fractured reservoirs, providing for real field cases, better representation of injection and production forecast related to fault and fracture inclusion utilizing DFN permeability-upscaling methods.

6.1   Recommendations

Some recommendations for future investigation are described below:

- General methodology application:
  - o Test different CFUs in order to analyze if the reported differences among DFN upscaling methods and grid-scale are also observed in different well perforations scenarios;
  - o Consider a DP simulation model and compare to the DK simulation model to understand if a simpler simulation model type can capture the well dynamic behavior variabilities caused by the DFN upscaling methods and grid-scale;
  - o Consider the matrix heterogeneities by varying the matrix porosity and permeability, in order to observe how this can impact the results (as in this study each block had a constant 15% of porosity and 100 mD of permeability);
  - o Consider the grid orientation according to the DFN orientation, as this alignment tends to produce a more precise tensor calculation of the fracture permeability. Analyzing if the orientation of the grid relative to fault/fracture direction has any impact on the results. This analysis could be done by running scenarios of HFM, MHFM, and MFM with a different grid orientation (i.e., oriented NE-SW instead of in this case N-S).
- NFR field scale applications:
  - o Consider the DFN upscaling impact in the injectivity of the field, by modifying the DFN upscaling methods around the injector wells and not around the producer wells, as it was adopted in this dissertation. The injectivity impact analysis should confirm the necessity of a well model calibration in the injector wells, as it was observed for the producer wells during this work;
  - o Utilize an optimized field production strategy, so it represents a real production strategy of Field C, to observe if the productivity impact caused by the DFN upscaling method analyzed in this study are also present in a different production strategy during different production terms;
  - o Test the well representation proposal of this dissertation in a newly drilled well to confirm if the well representation can improve the precision of the well production prediction. This test in the field scale is a way to validate the proposed methodology in real cases.

REFERENCES

Agência Nacional do Petróleo (ANP). 2017. Bacia de Santos: Sumário Geológico e Setores em Oferta. Fifteenth round of concessions.

Agência Nacional do Petróleo (ANP). 2019. Pré-sal brasileiro – Potencial além das 200 milhas náuticas. Oral presentation, Felipe Kury (Director), Brasília, Brazil (Dezember 2019).

Agência Nacional do Petróleo (ANP). 2020. Boletim da Produção de Petróleo e Gás Natural. Number 118 (June 2020).

Ahmed-Elfeel, M., Geiger, S. 2012. Static and Dynamic Assessment of DFN Permeability Upscaling. Paper presented at the SPE Europec/EAGE Annual Conference, 4-7 June, Copenhagen, Denmark. SPE-154369-MS. https://doi.org/10.2118/154369-MS

Allan, J., Qing Sun, S. 2003. Controls on Recovery Factor in Fractured Reservoirs: Lessons Learned from 100Fractured Fields. Paper presented at the SPE Annual Technical Conference and Exhibition, Denver, Colorado, October 2003. https://doi.org/10.2118/84590-MS

Alpay, O. A. 1972. A Practical Approach to Defining Reservoir Heterogeneity. *J Pet Technol* **24**: 841–848. https://doi.org/10.2118/3608-PA

Amiry, M. T. 2014. *Modeling Flow Behavior in Naturally Fractured Reservoirs*. MS thesis, Leoben University, Leoben, Austria (February 2014)

Araújo, R. E. B., La Bruna, V., Rustichelli, A., Bezerra, F. H. R., Junior, M. M. X., Audra, P., Barbosa, J. A., Antonino, A. C. D. 2021. Structural and sedimentary discontinuities control the generation of karst dissolution cavities in a carbonate sequence, Potiguar Basin, Brazil. *Marine and Petroleum Geology* **123**: 104753. https://doi.org/10.1016/j.marpetgeo.2020.104753

Ateeq, B., El Gohary, M., Al Ammari, K., Masoud, R., Noufal, A., Joussineau, G., Weber, M., Agrawal, D. 2017. An Integrated Study to Characterize and Model Natural Fracture Networks of Gas Condensate Carbonate Reservoirs, Onshore Abu Dhabi, UAE. Paper presented at the SPE Reservoir Characterisation and Simulation Conference and Exhibition, Abu Dhabi, UAE, May 2017. https://doi.org/10.2118/186043-MS

Avansi, G., Rios, V., Schiozer, D. 2019. Numerical tuning in reservoir simulation: it is worth the effort in practical petroleum applications. *J Braz. Soc. Mech. Sci. Eng.* **41** (59). https://doi.org/10.1007/s40430-018-1559-9

Avansi, G., von Hohendorff Filho, J. C., Schiozer, D. J. 2020. Simulation Models and Fast Objective Function Estimators Classification for Petroleum Reservoir Studies. *Unisim On-line 138° edition* **15** (3).

Barenblatt, G.I., Zheltov, I.P., Kochina, I.N. 1960. Basic Concepts in the Theory of Seepage of Homogeneous Liquids in Fissured Rocks. *PMM (Soviet Applied Mathematics and Mechanics)* **24** (5): 852-864. https://doi.org/10.1016/0021-8928(60)90107-6

Beicip-Franlab. 2019. FracaFlow Manual, version 2019

Benko, A., Földes, T., Tóth, T. M., Lakos, B. 2012. A Multiscale Approach for Characterizing Fractured Reservoirs, Workflow for Geological Modelling of a Hungarian Reservoir. 74th EAGE Conference and Exhibition incorporating EUROPEC 2012, June 2012. https://doi.org/10.3997/2214-4609.20148505

Berre, I., Doster, F., Keilegavlen, E. 2019. Flow in Fractured Porous Media: A Review of Conceptual Models and Discretization Approaches. *Transp Porous Med* **130**: 215–236. https://doi.org/10.1007/s11242-018-1171-6

Bigi, S., Marchese, M., Meda, M., Nardon, S., Franceschi, M. 2015. Discrete fracture network of the Latemar carbonate platform. *Italian Journal of Geosciences* **134** (3): 474-494. https://doi.org/10.3301/IJG.2014.34

Boro, H., Rosero, E., Bertotti, G. 2014. Fracture-network analysis of the Latemar Platform (northern Italy): integrating outcrop studies to constrain the hydraulic properties of fractures in reservoir models. *Petroleum Geoscience* **20**: 79-92. http://dx.doi.org/10.1144/petgeo2013-007

Bourbiaux, B. 2010. Fractured Reservoir Simulation: a Challenging and Rewarding Issue. *Oil & Gas Science and Technology – Rev. IFP* **65** (2):227-238. https://doi.org/10.2516/ogst/2009063

Cazarin, C. L., Bezerra, F. H., Ennes-Silva., R. A., Balsamo, F., Auler., A. S. 2016. Using Analogue Hypogene Karst Systems to Understand the Pre-Salt Carbonate Reservoirs Offshore Brazil. Poster Presented at AAPG International Conference and Exhibition, Cancun, Mexico, September 6-9

Cazarin, C. L. 2015. *Controle Faciológico do Sistema Cárstico Hipogênico de Campo Formoso, BA: Sistema conduto-barreira*. MS thesis, UFRJ / IGeo, Rio de Janeiro

CMG Ltd. 2019. Imex Manual, version 2019.1

Correia, M. 2014. *Representação de reservatórios carbonáticos naturalmente fraturados em simulação de reservatórios*. PhD dissertation, University of Campinas, Campinas, Sao Paulo (May 2014). http://repositorio.unicamp.br/jspui/handle/REPOSIP/265874

Correia, M. G., Maschio, C., Schiozer, D.J. 2012. A Procedure for Upscaling a Complex Fractured Reservoir using Near-Well Refinement. Paper presented at the SPE Latin American and Caribbean Petroleum Engineering Conference, Mexico City, Mexico, 16–18 April. SPE-153558-MS. https://doi.org/10.2118/153558-MS

Correia, M. G., Maschio, C., von Hohendorff Filho, J. C., Schiozer, D. J. 2016. The impact of time-dependent matrix-fracture fluid transfer in upscaling match procedures. *Journal of Petroleum Science and Engineering* **146**: 752-763 https://doi.org/10.1016/j.petrol.2016.07.039

Correia, M. G., Maschio, C., Schiozer, D.J. 2018. Flow Simulation Using Local Grid Refinements to Model Laminated Reservoirs. *Oil & Gas Science and Technology–Revue d'IFP Energies nouvelles*, **73**: 5. https://doi.org/10.2516/ogst/2017043

De Lima, A, Fourno, A., Noetinger, B., Schiozer, D. J. 2019. Characterization and Modeling of the Fault Network of a Brazilian Pre-Salt Reservoir and Upscaling Results. Paper presented at the SPE Annual Technical Conference and Exhibition, Calgary, Alberta, Canada, September 2019. SPE-195999-MS. https://doi.org/10.2118/195999-MS

Decroux, B. 2012. *Computation of effective dynamic properties of naturally fractured reservoirs: Comparison and validation of methods*. MS Thesis, Imperial College, London. http://hdl.handle.net/10044/1/24177

Dershowitz, B., LaPointe, P., Eiben, T., Wei, L. 2000. Integration of Discrete Feature Network Methods with Conventional Simulator Approaches. *SPE Res Eval & Eng* **3** (2): 165–170. https://doi.org/10.2118/62498-PA

Ding, Y., Basquet, R., Bourbiaux, B. 2006. Upscaling Fracture Networks for Simulation of Horizontal Wells Using a Dual-Porosity Reservoir Simulator. *SPE Res Eval & Eng* **9**: 513–520. https://doi.org/10.2118/92774-PA

Dong, Z., Li, W., Lei, G., Wang, H., Wang, C. 2019. Embedded Discrete Fracture Modeling as a Method to Upscale Permeability for Fractured Reservoirs. *Energies 2019* **12** (5): 812. https://doi.org/10.3390/en12050812

Elsaid, M. E., Al-Jafri, G. M., Mercado, G., Sugawara, Y. 2007. Detecting and Analysing Fractures in the Subsurface: The Critical Steps in Modelling Fractured Carbonate Reservoir. Paper presented at the SPE Middle East Oil and Gas Show and Conference, Manama, Bahrain, March 2007. https://doi.org/10.2118/105707-MS

Fanchi, J. R. 2006. *Principles of Applied Reservoir Simulation*, third edition. Gulf Professional Publishing/Elsevier. https://doi.org/10.1016/B978-0-7506-7933-6.X5000-4

Felici, F., Alemanni, A., Bouacida, D., de Montleau, P. 2016. Fractured reservoir modeling: From well data to dynamic flow. Methodology and application to a real case study in Illizi Basin (Algeria). *Tectonophysics* **690 Part A**: 117-130. https://doi.org/10.1016/j.tecto.2016.06.020

Ghahfarokhi, P. K. 2017. The Structured Gridding Implications for Upscaling Model Discrete Fracture Networks (DFN) Using Corrected Oda's Method. *Journal of Petroleum Science and Engineering* **153:** 70-80. https://doi.org/10.1016/j.petrol.2017.03.027

Gilman, J. R., Kazemi, H. 1983. Improvements in Simulation of Naturally Fractured Reservoirs. *SPE J.* **23**: 695–707. https://doi.org/10.2118/10511-PA

Haridy, M. G., Sedighi, F., Panteha, G., Ussenova, K., Zhiyenkulov, M. 2019. Comprehensive Study of the Oda Corrected Permeability Upscaling Method. Paper presented at the SPE/IATMI Asia Pacific Oil & Gas Conference and Exhibition, Bali, Indonesia, October 2019. https://doi.org/10.2118/196399-MS

Iost, C. S. 2015. *Análise do Pré-Sal Brasileiro Quanto ao Retorno Energético Sobre o Investimento e as Emissões de Gases de Efeito Estufa*. MS thesis, Sao Paulo University (USP), São Paulo, Brazil.

Lamine, S., Richard, P., Steen, E. V., Pattnaik, C., Narhari, R., LeVarlet, X., Dashti, Q. 2017. Integration of Pressure Transient Tests in Fracture Characterization in North Kuwait Carbonate Reservoirs. Paper presented at the Abu Dhabi International Petroleum Exhibition & Conference, Abu Dhabi, UAE (November 2017). https://doi.org/10.2118/188835-MS

Ledsaak, K. 2016. *Geo-modelling of paleokarst reservoirs - from cave-survey to geocellular paleokarst model*. MS Thesis. The University of Bergen (November 2016). https://hdl.handle.net/1956/15419

Lemonnier, P., Bourbiaux B. 2010. Simulation of Naturally Fractured Reservoirs. State of the Art Part 2 – Matrix-Fracture Transfers and Typical Features of Numerical Studies. *Oil & Gas Science and Technology – Rev. IFP* **65** (2): 263-286. https://doi.org/10.2516/ogst/2009067

Lima, B. F. 2013. Simulação de Reservatórios Naturalmente Fraturados. MS thesis. Pontifícia Universidade Católica do Rio de Janeiro, Rio de Janeiro

Lough, M., Lee, S. and Kamath, J. 1997. A New Method to Calculate Effective Permeability of Gridblocks Used in the Simulation of Naturally Fractured Reservoirs. *SPE Res Eng* **12**: 219–224. https://doi.org/10.2118/36730-PA

Mahjour, S. K., Correia, M. G., Santos, A. A. S., Schiozer, D. J. 2019. Developing a workflow to represent fractured carbonate reservoirs for simulation models under uncertainties based on flow unit concept. *Oil & Gas Science and Technology–Revue d'IFP Energies nouvelles*, **74** (15). https://doi.org/10.2516/ogst/2018096

Massaro, L., Corradetti, A., Vinci, F., Tavani, S., Iannace, A., Parente, M., Mazzoli, S. 2018. Multiscale Fracture Analysis in a Reservoir-Scale Carbonate Platform Exposure (Sorrento Peninsula, Italy): Implications for Fluid Flow. *Geofluids 2018.* Article ID 7526425. https://doi.org/10.1155/2018/7526425

Medina, P. L. N. 2012. *Uma Abordagem da Teoria dos Jogos para Ratear os Benefícios Oriundos da Injeção de Gás Rico em Co2 nos Reservatórios do Pré-Sal*. MS Thesis, Universidade Federal do Rio de Janeiro/Coppe, Rio de Janeiro, Rio de Janeiro (June 2012).

Miranda, T. S., Santos, R.F., Barbosa, J.A., Gomes, I.F, Alencar, M.L., Correia, O.J., Falcão, T.C., Gale, J.F.W, Neyman, V.H. 2018. Quantifying aperture, spacing and fracture intensity in a carbonate reservoir analogue: Crato Formation, NE Brazil. *Marine and Petroleum Geology* **97**: 556-567. https://doi.org/10.1016/j.marpetgeo.2018.07.019

Nelson, R. A. 2001. *Geologic analysis of naturally fractured reservoirs*, second edition. Houston, Texas: Gulf Professional Publishing/Butterworth-Heinemann

Oda, M. 1985. Permeability tensor for discontinuous rock masses. *Géotechnique* **35** (4): 483-495

Ouenes, A., Hartley, L. J. 2000. Integrated Fractured Reservoir Modeling Using Both Discrete and Continuum Approaches. Paper presented at the SPE Annual Technical Conference and Exhibition, Dallas, Texas, October 2000. https://doi.org/10.2118/62939-MS

Panja, P., Conner, T., Deo, M. 2013. Grid sensitivity studies in hydraulically fractured low permeability reservoirs. *Journal of Petroleum Science and Engineering* **112**: 78-87. https://doi.org/10.1016/j.petrol.2013.10.009

Panpaterra, G. E. Z. 2010. *Pré-sal: Conceituação Geológica sobre uma Nova Fronteira Exploratória no Brasil*. MS thesis, Federal University of Rio de Janeiro, Rio de Janeiro, Brazil.

Passarela, C. A. 2012. Integração de Dados de Poços e Métodos Geoestatísticos para a Modelagem Geológica do Campo de Namorado. MS Thesis, University of Campinas, Campinas, São Paulo (November 2012). http://repositorio.unicamp.br/jspui/handle/REPOSIP/263080

Peaceman, D. W. 1983. Interpretation of Well-Block Pressures in Numerical Reservoir Simulation with Nonsquare Grid Blocks and Anisotropic Permeability. *SPE J.* **23**: 531–543. https://doi.org/10.2118/10528-PA

Peaceman, D. W. 1978. Interpretation of Well-Block Pressures in Numerical Reservoir Simulation. *SPE J.* **18**: 183–194. https://doi.org/10.2118/6893-PA

Pires, A. L. G. 2016. *Transferência de Escala aplicada ao Modelo Benchmark UNISIM-II.* MS Thesis, Instituto Superior Técnico Lisboa, Lisboa, Portugal

Ribeiro, G. G. 2010. *Implementação e Avaliação de Modelos de Poços em Duas e Três Dimensões para Aplicação em Simuladores de Reservatórios de Petróleo.* MS Thesis, Universidade Federal de Santa Catarina, Florianópolis, Santa Catarina (August, 2010)

Richard, P., Lamine, S., Pattnaik, C., Ajmi, N.A., Kidambi, V., Narhari, R., LeVarlet, X., Swaby, P., Qasem, D. 2017. Integrated Fracture Characterization and Modeling in North Kuwait Carbonate Reservoirs. Paper presented at the Abu Dhabi International Petroleum Exhibition & Conference, 13-16 November, Abu Dhabi, UAE. SPE-188185-MS. https://doi.org/10.2118/188185-MS

Ringrose, P., Bentley, M., 2015. Reservoir Model Design: A Practitioner's Guide. Springer. https://doi.org/10.1007/978-94-007-5497-3

Rosa, A. J., Carvalho, R. S., Xavier, J. A. D. 2006. Engenharia de reservatórios de petróleo. Interciência. Rio de Janeiro

Saalfeld, R. Q. 2016. *Simulação de Reservatórios Naturalmente Fraturados Utilizando Modelos Equivalentes de Porosidade Simples.* MS Thesis. University of Campinas, Campinas, São Paulo (August, 2016). http://repositorio.unicamp.br/jspui/handle/REPOSIP/321241

Sabathier, J., Bourbiaux, B., Cacas, M. C., Sarda, S. 1998. A New Approach of Fractured Reservoirs. Presented at the 1998 SPE International Petroleum Conference and Exhibition of Mexico held in Villahermosa, Mexico, 3-5 March 1998. https://doi.org/10.2118/39825-MS

Sanjombi, B. A. 2004. *Transferência de Escala Aplicada a Blocos com Poços e Reservatórios com Heterogeneidades Fortes*. MS Thesis, University of Campinas, Campinas, Sao Paulo (March 2004). http://repositorio.unicamp.br/jspui/handle/REPOSIP/287267

Schlumberger. 2018. Petrel E&P Software Platform, version 2018.1, Help Center

Singh, S. K., Abu-Habbiel, H., Khan, B., Akbar, M., Etchecopar, A., Montaron, B. 2008. Mapping fracture corridors in naturally fractured reservoirs: An example from Middle East carbonates. *First Break* **26**: 109-113

Snow, D. 1969. Anisotropic permeability of Fractured Media. *Water Resources Research* **5** (6): 1273-1289. https://doi.org/10.1029/WR005i006p01273

Soler, S. A. R. 2019. Wettability and Flow Rate Effects on Mass Transfer for Simulation of Fractured Reservoirs. Paper presented at the SPE Annual Technical Conference and Exhibition, Calgary, Alberta, Canada, September 2019. https://doi.org/10.2118/199905-STU

Trice, R. 2005. Challenges and Insights in Optimising Oil Production Form Middle Eastern Karst Reservoirs. Paper presented at the SPE Middle East Oil and Gas Show and Conference, Kingdom of Bahrain, March 2005. https://doi.org/10.2118/93679-MS

Tueckmantel, C., Lamine, S., Huisman, B., Swaby, P. 2013. Discrete Fracture Network Upscaling Workflows and Tools in SVS Fracture Solutions. Paper presented at the Second EAGE Workshop on Naturally Fractured Reservoirs, Dec 2013. https://doi.org/10.3997/2214-4609.20132027

Wang, H., Forster, C., Deo, M. 2008. Simulating Naturally Fractured Reservoirs: Comparing Discrete Fracture Network Models to the Upscaled Equivalents. Oral Presentation given at the AAPG Annual Convention, San Antonio, Texas, 20-23 April

Warren, J. E., Root, P. J. 1963. The Behavior of Naturally Fractured Reservoirs. SPE Journal, **3** (3): 245–255. SPE-426-PA. https://doi.org/10.2118/426-PA

APPENDIX A – HIGH FRACTURE PERMEABILITY: NUMERICAL CONVERGENCE PROBLEMS

The objective of this appendix is to describe the executed steps to solve some simulation warnings in the first constructed DFN (DFN A). The DFN A settings have the same fault parameters, and the same density, orientation, and length of the fracture sets used in this dissertation (Table 5.1). The different parameters are the aperture and intrinsic permeability of the fracture sets. The inputs for the fracture aperture are the same as Table 5.1. However, for DFN A, the statistic function utilized to generate the aperture distribution is the Power Law. Table A.1 has the fracture sets aperture output for DFN A. Moreover, the intrinsic permeability of the fracture sets is calculated with the cubic law (Equation (2.1)).

Table A.1: aperture output settings for the fracture sets of DFN A

Fracture set	Min aperture (m)	Mean aperture (m)	Max aperture (m)
N78	0.01	0.014	0.029
N180	0.0015	0.0016	0.0036

The issues reported in the simulation models when utilizing DFN A are described in Table A.2 for the Oda method. It is observed a significant quantity of convergence issues mainly in the CFU1 HFM Oda. Avansi et al. (2019) discuss that: "in general, experience shows that a few convergence failures are harmless. On the other hand, higher number of convergence failures announced numerical instabilities, being a first clue concerning the reliability of the results of the numerical model."

Table A.2: main warning types and their quantity for the simulation models built with DFN A

Warning type	CFU1 HFM Oda	CFU1 MHFM Oda	CFU1 MFM Oda
Very large perm values were truncated	3	2	0
The linear solver has not converged	1354	33	0
Pressure or Pb out of PVT table range	44	2	0

Moreover, some models reported backflow in the injector well, having inconsistent oil rates curves in the CFU1 MHFM ODA, as demonstrated in Figure A.1.
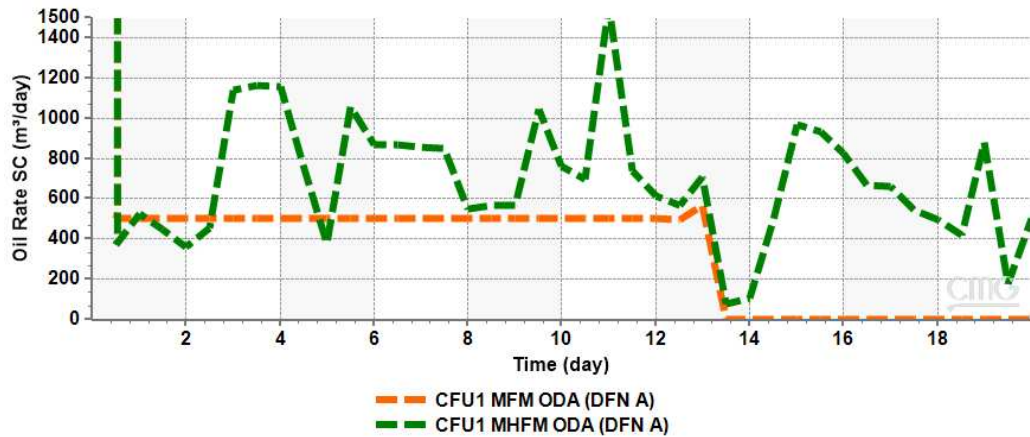
Figure A.1: oil rate curves for the CFU1 MFM Oda and CFU1 MHFM ODA built with DFN A

Considering the simulation issues reported previously, two solutions focused on the improvement of the models are tested, an automatic numerical tuning tool and fracture permeability sensitivity analysis.

Avansi et al. (2019) cite that the "default set of numerical parameters can lead the simulation to serious convergence problems and several time-step cuts." The automatic numerical tuning adapts the time-step size and adjusts numerical parameters, differing from the default numerical set. The utilization of this tool in the tests yields the reduction of some warnings but not completely solved the issues.

CMG (2019) argues that "problems with high permeability and low porosity may suffer from poor solver convergence and poor material balance." Since very high permeability warnings are reported (Table A.2), a fracture permeability sensitivity analysis is tested. Fracture permeability multipliers are applied in each direction to gradually reduce the permeability values, the multipliers vary from 0.7 to 0.005. Table A.3 has a summary of the results of fracture permeability and the considerable reduction of reported warnings after the sensitivity tests.

Table A.3: summary of permeability and type of warnings results for the fracture permeability sensitivity analysis

Models	Mean of Perm J $x10^3$ (Darcy)	Warning type			
		Injector Backflowing	Very High Perm	Linear Solver Convergence	PVT table range
Base Case (BC)	26	297	2	6	2
Perm BC*0.7	18	116	1	0	0
Perm BC*0.1	10	2	0	0	0
Perm BC*0.05	3	2	0	0	0
Perm BC*0.005	1	0	0	0	0

Concluding, an automatic tuning in the numerical settings can reduce the simulation model convergence problems. However, it is necessary to select with careful the fracture aperture values from literature and its corresponding distribution laws. A new fracture permeability values are generated having as parameter the maximum and minimum fracture permeability values of the calibrated DFN of Field C, resulting in the utilization of the distribution laws of Table 5.2 for the construction of the new DFN.

APPENDIX B – PERIODIC BOUNDARY CONDITION

The flow-based method with the periodic boundary condition is not considered in the analysis due to software limitation in the MFM scale execution. This appendix intends to describe the problem to justify the absence of this method in the results.

Figure B.1 has the results of the CFU1 MFM PD fracture permeability for all directions, and only values in the direction K is computed, and no permeability values are shown in the J and I directions. This problem persists in coarse grids, and as the grid is refined, the quantity of active cells increases. The software support team announced that there are some errors in the PD execution, and it will be solved in future versions of the program. Therefore, even if the fracture permeability is fully calculated in the CFU1 MHFM and HFM PD, the values are considered not trustful to be used in this work.
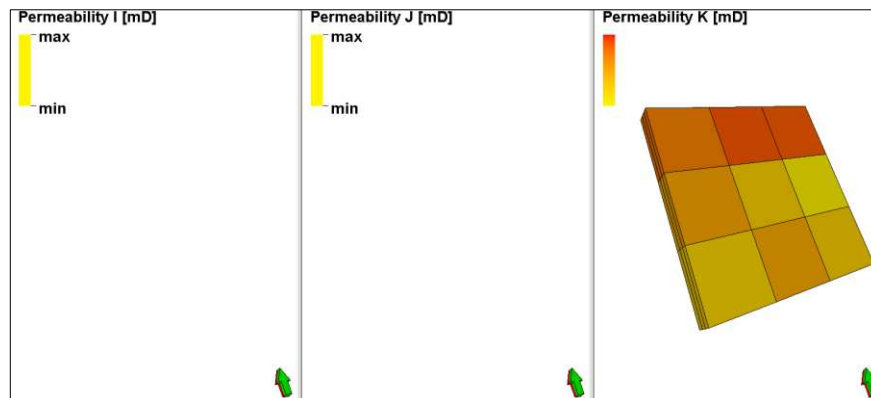

Figure B.1: fracture effective permeability of the CFU1 MFM PD in the directions I, J, and K